BYG·DTU

DANMARKS
TEKNISKE
UNIVERSITET

DTU

Center for ARKTISK TEKNOLOGI

Bæredygtigt arktisk byggeri i det 21. århundrede

Vakuumrørsolfangere – Statusrapport 1 til VILLUM KANN RASMUSSEN FONDEN

Sagsrapport
BYG·DTU SR-04-04
2004
ISSN 1601 - 8605

Bæredygtigt arktisk byggeri i det 21. århundrede

Vakuumrørsolfangere – Statusrapport 1 til
VILLUM KANN RASMUSSEN FONDEN

Louise Jivan Shah

Indholdsfortegnelse

Forskningsindhold

I projektets første år har hovedvægten ligget på udvikling af teoretiske modeller til beregning af termiske ydelser for vakuumrørsolfangere, der udnytter solstrålingen fra alle retninger.

Traditionelle solfangerteorier fra litteraturen er udviklet med henblik på almindelige plane solfangere med plane absorbere. Disse teorier har ikke direkte kunnet anvendes i forbindelse med vakuumrørsolfangerne, da absorberne er cylinderformede.

Derfor er der udviklet en ny teoretisk solfangermodel til vakuumrørsolfangere med cylinderformede absorbere. Modellen tager udgangspunkt i den traditionelle plane solfangerteori, som integreres over den cylinderformede absorber. Derudover udmærker modellen sig ved, at den præcist bestemmer skyggeeffekterne fra rør til rør, ligesom den kan regne på hvordan solfangeren udnytter solstrålingen fra alle kompassets retninger.

Den teoretiske solfangermodel er sammenholdt med målinger på en prototype solfanger, og det viser sig at modellen gengiver "virkeligheden" med stor nøjagtighed. Modellen er herefter videreudviklet så den nu kan indgå i simuleringsprogrammet TRNSYS. Dette amerikanske simuleringsprogram er et komponent baseret program, som er det mest anvendte og anerkendte simuleringsprogram til solvarmeanlæg.

Med modellen er der lavet indledende analyser af, hvilke solfangerydelser man kan forvente i hhv. Danmark og Grønland (Uummannaq).

De foreløbige resultater viser, at vakuumrør-solfangerne kan give en meget større ydelse i Grønland end i Danmark.

Fig. 1. Prototype solfanger

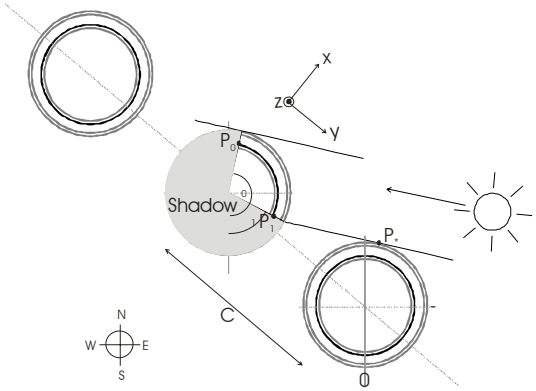

Fig. 2. Rør der skygger for hinanden.

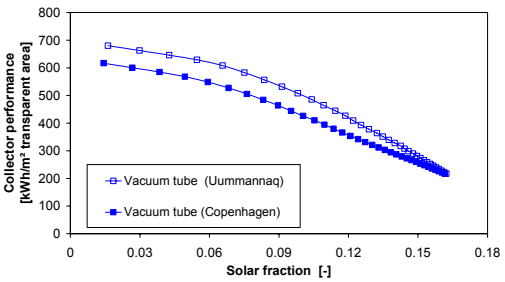

Fig. 3. Solfangerydelser i Grønland og i Danmark.

Publikationer

Shah L.J., Furbo S. (2004)	*New Trnsys Model of Evacuated Tubular Collectors with Cylindrical Absorbers.* In Proceedings of the EuroSun 2004 Congress, Freiburg, Germany, June 20-23, 2004.
Shah L.J. & Furbo, S. (2004)	*Vertical evacuated tubular collectors utilizing solar radiation from all directions.* Applied Energy, Vol. 78/4 pp 371-395, 2004
Shah L.J., Furbo S., Antvorskov S. (2003)	*Thermal Performance of Evacuated Tubular Collectors utilizing Solar Radiation from all Directions.* In Proceedings of the ISES Solar World Congress, Gothenburg, Sweden, June 14-19, 2003.
Shah L.J. & Furbo S. (2003)	*Solvarme i Grønland.* Sletten. Avisen ved DTU. Nr. 7/2003. ISSN 0108-6073.

Foredrag

Shah L.J. (2003)	*Thermal Performance of Evacuated Tubular Collectors utilizing Solar Radiation from all Directions.* Oral presentation, ISES Solar World Congress, Gothenburg, Sweden, June 14-19, 2003.
Shah L.J. (2003)	*Vakuumrørsolfangere.* DANVAK møde: ”Solvarmeforskning på DTU”, 18/9 2003.

Anden formidling

Nyhedsindslag med Simon Furbo og Louise Jivan Shah i TV-avisen d. 24-05-2003 vedr. det nye forskningsprojekt om vakuumrørsolfangere.

Artikel i den grønlandske avis Sermitsiaq, bl.a. vedrørende solvarme om vakuumrør-solfangere.

Regnskab

Indbetalinger	720.000,00
Indtægter i alt	**720.000,00**
Forskertimer	436.688,20
Teknisk/adm. bistand	1.890,90
Rejser	8.286,27
Drift og materialer	403,11
Øvrige	8.656,03
Udgifter i alt	**455.924,51**
Saldo projektkonto	**264.075,49**

Kommentarer til regnskab:

Forbruget har det første år været mindre end budgetteret, idet store dele af de planlagte eksperimenter er flyttet fra foråret 2004 til efteråret 2004/foråret 2005.

Bilag 1: Artikel optaget i proceedings for ISES SOLAR WORLD CONGRESS, June 14-19, 2003.

THERMAL PERFORMANCE OF EVACUATED TUBULAR COLLECTORS UTILIZING SOLAR RADIATION FROM ALL DIRECTIONS

L. J. Shah, S. Furbo & S. Antvorskov
Department of Civil Engineering, Technical University of Denmark
Brovej, Building 118
DK-2800 Kgs. Lyngby
Denmark
E-mail: ljs@byg.dtu.dk
Phone: + 45 25 18 88, Fax: +45 45 93 17 55

Abstract – A prototype collector with parallel-connected evacuated double glass tubes is investigated theoretically and experimentally. The collector has a tubular absorber and can utilize solar radiation coming from all directions.

The collector performance is measured in an outdoor test facility and an efficiency expression for the collector is determined. Further, a theoretical model for calculating the thermal performance is developed. In the model, flat plate collector performance equations are integrated over the whole absorber circumference and the model determines the shades on the tubes as a function of the solar azimuth. Results from calculations with the model are compared with measured results and generally there is a good degree of similarity between the measured and calculated results. However, the comparison shows that the model is suitable only for vertical placed pipes.

The model is used for theoretical investigations on vertically placed pipes at a location in Denmark (Copenhagen, lat. 56°N) and at a location in Greenland (Ummannaq, lat. 71°N). For both locations, the results show that to achieve the highest thermal performance, the tube centre distance must be about 0.2 m and the collector azimuth must be about 45°-60° towards west. Further, the thermal performance of the evacuated solar collector is compared to the thermal performance of the Arcon HT flat plate solar collector. The Arcon collector is the best performing collector under Copenhagen conditions, whereas the performance of the evacuated tubular collector is highest under the Ummannaq conditions. The reason is that the tubular collector is not optimally tilted in Copenhagen but also that there is much more solar radiation "from all directions" in Ummannaq and this radiation can be utilized with the tubular collector. It is concluded that the collector design is very promising – especially for high latitudes.

1 INTRODUCTION

A new collector design based on evacuated tubular collectors is investigated theoretically and experimentally.

The collector is based on a number of parallel-connected double glass tubes, which are open in both ends. The tubes are annuluses with closed ends and the outside of the inner glass wall is treated with an absorbing selective coating. The collector fluid is floating from bottom to top of the inside of the inner tube where also another closed tube is inserted with the purpose to fill out a part of the tube volume so that less collector fluid is needed. Further, it ensures a high heat transfer coefficient from the inner glass tube to the collector fluid. Fig. 1 shows the design of the evacuated tubes and Fig. 2 shows the principle of the tube connection.

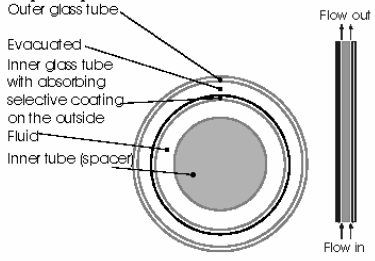

Fig. 1. Design of the evacuated tubes. (Top view: Left. Front view: Right).

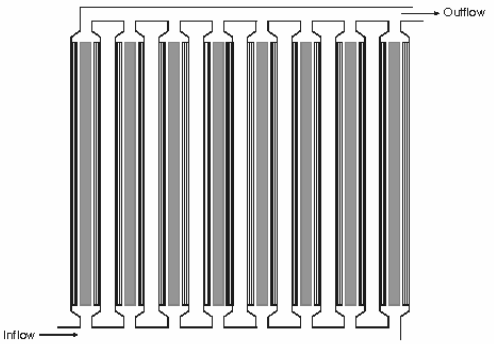

Fig. 2. The tubes connected in a solar collector panel.

The collector is investigated in an outdoor test facility in order to determine the collector performance experimentally.

For the theoretical investigation of this collector principle, traditional collector theory cannot directly be applied, as the absorbers are tubular. Therefore, to theoretically determine the collector performance a number of conditions must be taken into account, including:

- That solar radiation from all directions can be utilized (also from the "back" of the collector).
- Shadow effects from adjacent tubes.
- Special incident angle modifiers.

A collector theory for the collector performance, including the above-mentioned considerations, is developed. The theory is compared with the results from the experiments. Based on the theory, the following points are investigated:

- Optimal distance between tubes.
- Optimal collector azimuth.
- Expected yearly thermal performance for different climates.

Finally, a comparison between the thermal performance of a flat plate collector and of the investigated collector is made.

2 COLLECTOR DESIGN

The solar collector panel consists of 14 evacuated tubes placed with a centre distance of 0.067 m. The tubes are connected to two manifold pipes, which are placed in an insulated box. The tubes are 1.6 m long, however, 2x0.065 m is placed inside the manifold boxes. Thus only 1.47 m is exposed to the sun. The outer diameter of the outer tube is 0.047 m and the outer diameter of the inner tube is 0.037 m. The collector panel is placed on the ground, tilted 45° and facing south. The solar collector areas are described in Table 1 and Fig. 3 shows a photo of the collector. The collector was built by the company SunGain.

Table 1. Solar collector panel areas.

Gross area [m²]	Outer glass tube cross area [m²]	Absorber cross area [m²]	Total absorber area [m²]
1.8	0.97	0.76	2.39

Fig. 3: The evacuated tubular collector.

3 COLLECTOR PERFORMANCE THEORY

Generally, for a solar collector without reflectors and without parts of the collector reflecting solar radiation to other parts of the collector, the performance equation can be written as:

$$P_u = P_b + P_d + P_{gr} - P_{loss} \quad (1)$$

or more detailed described:

$$\begin{aligned} P_u &= A_b \cdot F' \cdot (\tau\alpha)_e \cdot K_\theta \cdot R_b \cdot G_b \\ &+ A_a \cdot F' \cdot (\tau\alpha)_e \cdot K_{\theta,d} \cdot F_{c-s} \cdot G_d \\ &+ A_a \cdot F' \cdot (\tau\alpha)_e \cdot K_{\theta,gr} \cdot F_{c-g} \cdot G_{gr} \\ &- A_a \cdot U_L \cdot (T_{fm} - T_a) \end{aligned} \quad (2)$$

where K_θ is the incident angle modifier defined as:

$$K_\theta = 1 - \tan\left(\frac{\theta}{2}\right)^a \quad (3)$$

The incident angle modifiers for diffuse radiation, $K_{\theta,d}$, and ground reflected radiation, $K_{\theta,gr}$, are evaluated by equation 3 using $\theta = \pi/3$.

For tubular collectors, there are several conditions, which make equation (2) more difficult to evaluate. Amongst others the following can be mentioned:

- In flat plate collector theory, the areas A_a and A_b are typically equal and close to the transparent area. For tubular collectors, however, this is not the case as, depending on the solar azimuth and altitude, only parts of the absorber area are exposed to the beam radiation.
- In flat plate collector theory the incident angle modifier, K_θ, is independent of the longitudinal and transverse component of the incident angle. The cylindrical geometry in tubular collectors makes it necessary to consider both components.
- In the investigated tubular collector, where the absorber covers the whole inner tube circumference, also radiation coming from the "back" of the collector must be evaluated.

To calculate the thermal performance of the evacuated tubes, the general performance equations (1) and (2) have been integrated over the whole absorber circumference. This means that the tube is divided into small "slices", and each slice is treated as if it was a flat plate collector. In this way, the transverse incident angle modifier is eliminated. For describing the solar radiation on a tubular collector, this method has previously been used by Pyrko J. (1984).

Integrating over the absorber area, the performance equation can be described as:

$$P_u = \int_{-\pi}^{\pi} \left(P_b + P_d + P_{gr} - P_{loss}\right) \cdot d\xi \quad (4)$$

In the following each part of equation (4) will be investigated. The investigation is based on a theoretical analysis of a single tube.

Heat loss, P_{loss}:

The heat loss can be described as:

$$P_{loss} = \int_{-\pi}^{\pi} A_a \cdot U_L \cdot (T_{fm} - T_a) \cdot d\xi = \int_{-\pi}^{\pi} L\tau_p \cdot U_L \cdot (T_{fm} - T_a) \cdot d\xi = 2 \cdot \pi \cdot L \cdot \tau_p \cdot U_L \cdot (T_{fm} - T_a) \quad (5)$$

Energy from diffuse radiation on collector/tube, P_d:

The evaluation of the energy contribution from the diffuse radiation is based on an isotropic diffuse model. Thus, the circumsolar diffuse and horizontal brightening contributions are not taken into consideration in this model.

The energy contribution from the diffuse radiation can be written as:

$$P_d = \int_{-\pi}^{\pi} A_a \cdot F' \cdot (\tau\alpha)_e \cdot K_{\theta,d} \cdot F_{c-s} \cdot G_d \cdot d\xi = 2 \cdot \pi \tau_p \cdot L \cdot F' \cdot (\tau\alpha)_e \cdot K_{\theta,d} \cdot G_d \cdot \int_{-\pi}^{\pi} F_{c-s} \cdot d\xi \quad (6)$$

For a flat plate collector, the view factor from the collector to the sky can be described as:

$$F^*_{c-s} = \frac{1+\cos(\beta)}{2} \quad (7)$$

When integrating over the absorber area, the absorber surface tilt, β, and the absorber surface azimuth, ξ, change as illustrated in Fig. 4. This will have an impact on the determination of the incident angle. For instance, when the surface azimuth is 0 (south) the tilt is β_s and when the surface azimuth is $\pm\pi$ (north) the tilt is $\pi - \beta_s$.

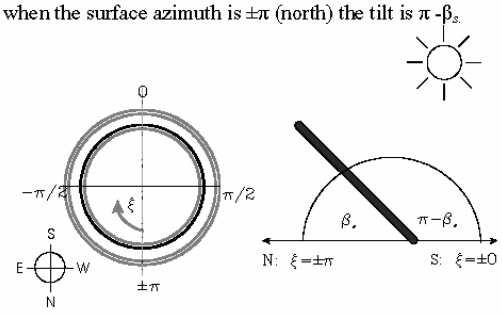

Fig. 4. A tube seen from the top (left) and the side (right). When the performance equation is integrated over the absorber area both the surface azimuth and the surface tilt do change.

The tilt, as a function of the actual absorber azimuth can be written as:

$-\pi \le \xi \le 0$:

$$\beta = \beta_s - (1 - \frac{\beta_s}{\pi/2}) \cdot \xi \quad (8)$$

$0 \ge \xi \ge \pi$:

$$\beta = \beta_s + (1 - \frac{\beta_s}{\pi/2}) \cdot \xi \quad (9)$$

Assuming that there are no adjacent tubes, the view factor from the tube to the sky can be described as:

$$F^*_{c-s} = \frac{1}{2 \cdot \pi} \left[\int_{-\pi}^{0} \frac{1+\cos\left(\beta_s - (1 - \frac{\beta_s}{\pi/2}) \cdot \xi\right)}{2} \cdot d\xi + \int_{0}^{\pi} \frac{1+\cos\left(\beta_s + (1 - \frac{\beta_s}{\pi/2}) \cdot \xi\right)}{2} \cdot d\xi \right] = 0.5 \quad (10)$$

In reality, there will be adjacent tubes, which will reduce the view factors to the ground and the sky respectively. This reduction must be taken into consideration.

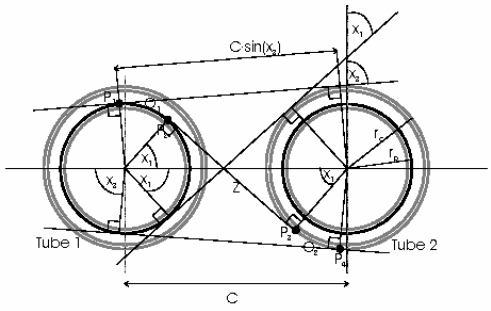

Fig. 5. Determination of view factors between two tubes.

Fig. 5 shows two adjacent tubes. The view factor F_{1-2} between the absorber of tube 1 and tube 2 can be described as:

$$A_1 \cdot F_{1-2} = \frac{1}{2} \sum \textit{length of the crossing curves} - \frac{1}{2} \cdot \sum \textit{length of the non crossing curves} = (O_1 + z + O_2) - C \cdot \sin(x_3) \quad (11)$$

Here A_1 is the absorber perimeter of tube 1. The curves O_1 and O_2 between the points P_1-P_2 and P_3-P_4 respectively can be described by:

$$O_1 = \frac{(\pi/2 - x_1) + (\pi/2 - x_3)}{2 \cdot \pi} \cdot 2 \cdot \pi r_p \quad (12)$$

and

$$O_2 = \frac{(\pi/2 - x_1) - (\pi/2 - x_3)}{2 \cdot \pi} \cdot 2 \cdot \pi r_c \quad (13)$$

Here the angles x_1 and x_3 are defined by:

$$x_1 = a\cos\left(\frac{r_c + r_p}{C}\right) \quad (14)$$

$$x_3 = \mathrm{acos}\left(\frac{r_c - r_p}{C}\right) \quad (15)$$

If the centre of tube 1 has the coordinates (0,0), the coordinates of the points P_2 and P_3 and thus the distance, z, between the two points can be found as:

$$\begin{aligned} P_2 &= \left[r_p \cdot \cos(x_1), r_p \cdot \sin(x_1)\right] \\ P_3 &= \left[C + r_c \cdot \cos(\pi + x_1), r_c \cdot \sin(\pi + x_1)\right] \end{aligned} \quad (16)$$

$$z = \sqrt{\left(C + r_c \cdot \cos(\pi + x_1) - r_p \cdot \cos(x_1)\right)^2 + \left(r_c \cdot \sin(\pi + x_1) - r_p \cdot \sin(x_1)\right)^2} \quad (17)$$

By inserting equations (12), (13) and (17) into equation (11), the view factor from tube 1 to tube 2 can be written as:

$$F_{1-2} = \frac{1}{2 \cdot \pi r_p} \cdot \left[\begin{array}{l} (\pi - x_1 - x_3) r_p \\ + \sqrt{\left(C + r_c \cdot \cos(\pi + x_1) - r_p \cdot \cos(x_1)\right)^2 + \left(r_c \cdot \sin(\pi + x_1) - r_p \cdot \sin(x_1)\right)^2} \\ + (x_3 - x_1) r_c \\ - C \cdot \sin(x_3) \end{array} \right] \quad (18)$$

The final view factor from tube to sky, including shading adjacent tubes can thus be described as:

$$F_{c-s} = F^*_{c-s} - F_{1-2} \quad (19)$$

Energy from ground reflected radiation on collector/tube, P_{gr}:

The energy contribution from the ground reflected radiation can be written as:

$$\begin{aligned} P_{gr} &= \int_{-\pi}^{\pi} A_a \cdot F' \cdot (\tau\alpha)_e \cdot K_{\theta,gr} \cdot F_{c-g} \cdot G_{gr} \cdot d\xi \\ &= 2 \cdot \pi r_p \cdot L \cdot F' \cdot (\tau\alpha)_e \cdot K_{\theta,gr} \cdot G_{gr} \cdot \int_{-\pi}^{\pi} F_{c-g} \cdot d\xi \end{aligned} \quad (20)$$

with

$$G_{gr} = \rho_{gr} \cdot (G_b + G_d) \quad (21)$$

For a flat plate collector, the view factor from the collector to the ground can be described as:

$$F^*_{c-g} = \frac{1 - \cos(\beta)}{2} \quad (22)$$

In a similar way as for the diffuse radiation, the view factor from the tube to the ground, assuming that there are no neighbouring tubes, can be described as:

$$F^*_{c-g} = \frac{1}{2 \cdot \pi} \cdot \left[\begin{array}{l} \int_{-\pi}^{0} \frac{1 - \cos\left(\beta_s - (1 - \frac{\beta_s}{\pi/2}) \cdot \xi\right)}{2} \cdot d\xi + \\ \int_{0}^{\pi} \frac{1 - \cos\left(\beta_s - (1 + \frac{\beta_s}{\pi/2}) \cdot \xi\right)}{2} \cdot d\xi \end{array} \right] \quad (23)$$

$$= 0.5$$

Including the adjacent shading tubes, the view factor from tube to ground becomes:

$$F_{c-g} = F^*_{c-g} - F_{1-2} \quad (24)$$

Energy from beam radiation on collector/tube, P_b:

The energy contribution from the beam radiation can be written as:

$$\begin{aligned} P_b &= \int_{\xi_{strat}}^{\xi_{stop}} F' \cdot (\tau\alpha)_e \cdot G_b \cdot A_b \cdot K_\theta \cdot R_b \cdot d\xi \\ &= F' \cdot (\tau\alpha)_e \cdot G_b \cdot L \cdot r_p \cdot \int_{\xi_{strat}}^{\xi_{stop}} K_\theta \cdot R_b \cdot d\xi \end{aligned} \quad (25)$$

Notice that there is now integrated over only a part of the circumference. This is because only part of the absorber surface is exposed to the beam radiation. Assuming that the pipes are placed vertically, Fig. 6 shows the three critical angles, when the solar azimuth, γ_s, is between 0 and $\pi/2$ (Lart S. (2000)).

When the solar azimuth is smaller than the angle x_1, there is no shading on the tubes. If the solar azimuth is larger than x_3, the tubes are fully shaded and if the solar azimuth is between x_1 and x_3 the tubes are partly shaded. If the solar azimuth is equal x_2, the tubes are half shaded. In Table 2 the critical angles are defined for all four quadrants of the circle.

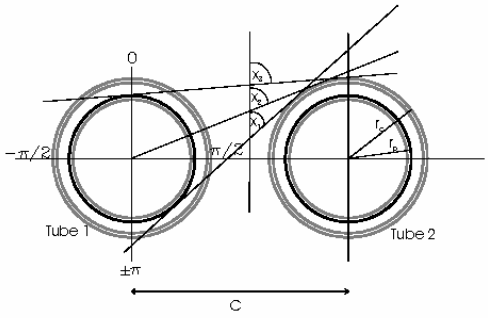

Fig. 6. Critical angles determining the exposed area, when the pipes are placed vertically.

Table 2. Critical angles determining the exposed area, when the pipes are placed vertically.

Quadrant:	x_1	x_2	x_3
$-\pi \le \gamma_s < -\pi/2$	$\arccos\left(\frac{r_c+r_p}{C}\right)-\pi$	$\arccos\left(\frac{r_c}{C}\right)-\pi$	$\arccos\left(\frac{r_c-r_p}{C}\right)-\pi$
$-\pi/2 \le \gamma_s < 0$	$-\arccos\left(\frac{r_c+r_p}{C}\right)$	$-\arccos\left(\frac{r_c}{C}\right)$	$-\arccos\left(\frac{r_c-r_p}{C}\right)$
$0 \le \gamma_s < \pi/2$	$\arccos\left(\frac{r_c+r_p}{C}\right)$	$\arccos\left(\frac{r_c}{C}\right)$	$\arccos\left(\frac{r_c-r_p}{C}\right)$
$\pi/2 \le \gamma_s < \pi$	$-\arccos\left(\frac{r_c+r_p}{C}\right)+\pi$	$-\arccos\left(\frac{r_c}{C}\right)+\pi$	$-\arccos\left(\frac{r_c-r_p}{C}\right)+\pi$

In Fig. 7 - Fig. 10, the angle 'q_{ys}' represents the tube area exposed to beam radiation, for different solar azimuths. Further, the angles ξ_{start} and ξ_{stop} used in equation (25), are shown.

As a function of the solar azimuth, the angle, q_{ys}, and the integration borders, ξ_{start} and ξ_{stop}, are described in Table 3.

Table 3. Angles determining the exposed area, when the pipes are placed vertically and the collector panel azimuth is 0°.

$-\pi \le \gamma_s < -\pi/2$	$\lvert q_{ys}\rvert$	ξ_{start}	ξ_{stop}
$\gamma_s \le x_1$	π	$3/2\cdot\pi-\lvert\gamma_s\rvert$	$\lvert q_{ys}\rvert+3/2\cdot\pi-\lvert\gamma_s\rvert$
$x_1 < \gamma_s < x_2$	$\pi-\arccos\left(\frac{C\cdot\cos(\gamma_s+\pi)-r_c}{r_p}\right)$	$3/2\cdot\pi-\lvert\gamma_s\rvert$	$\lvert q_{ys}\rvert+3/2\cdot\pi-\lvert\gamma_s\rvert$
$\gamma_s = x_2$	$\pi/2$	$3/2\cdot\pi-\lvert\gamma_s\rvert$	$\lvert q_{ys}\rvert+3/2\cdot\pi-\lvert\gamma_s\rvert$
$x_2 < \gamma_s < x_3$	$\arccos\left(\frac{r_c-C\cdot\cos(\gamma_s+\pi)}{r_p}\right)$	$3/2\cdot\pi-\lvert\gamma_s\rvert$	$\lvert q_{ys}\rvert+3/2\cdot\pi-\lvert\gamma_s\rvert$
$\gamma_s \ge x_3$	0	-	-
$-\pi/2 \le \gamma_s < 0$	$\lvert q_{ys}\rvert$	ξ_{start}	ξ_{stop}
$\gamma_s \le x_1$	π	$\pi/2-\lvert\gamma_s\rvert-\lvert q_{ys}\rvert$	$\pi/2-\lvert\gamma_s\rvert$
$x_1 < \gamma_s < x_2$	$\pi-\arccos\left(\frac{C\cdot\cos(\lvert\gamma_s\rvert)-r_c}{r_p}\right)$	$\pi/2-\lvert\gamma_s\rvert-\lvert q_{ys}\rvert$	$\pi/2-\lvert\gamma_s\rvert$
$\gamma_s = x_2$	$\pi/2$	$\pi/2-\lvert\gamma_s\rvert-\lvert q_{ys}\rvert$	$\pi/2-\lvert\gamma_s\rvert$
$x_2 < \gamma_s < x_3$	$\arccos\left(\frac{r_c-C\cdot\cos(\lvert\gamma_s\rvert)}{r_p}\right)$	$\pi/2-\lvert\gamma_s\rvert-\lvert q_{ys}\rvert$	$\pi/2-\lvert\gamma_s\rvert$
$\gamma_s \ge x_3$	0	-	-
$0 \le \gamma_s < \pi/2$	$\lvert q_{ys}\rvert$	ξ_{start}	ξ_{stop}
$\gamma_s \le x_1$	π	$\lvert\gamma_s\rvert-\pi/2$	$\lvert q_{ys}\rvert+\lvert\gamma_s\rvert-\pi/2$
$x_1 < \gamma_s < x_2$	$\pi-\arccos\left(\frac{C\cdot\cos(\gamma_s)-r_c}{r_p}\right)$	$\lvert\gamma_s\rvert-\pi/2$	$\lvert q_{ys}\rvert+\lvert\gamma_s\rvert-\pi/2$
$\gamma_s = x_2$	$\pi/2$	$\lvert\gamma_s\rvert-\pi/2$	$\lvert q_{ys}\rvert+\lvert\gamma_s\rvert-\pi/2$
$x_2 < \gamma_s < x_3$	$\arccos\left(\frac{r_c-C\cdot\cos(\gamma_s)}{r_p}\right)$	$\lvert\gamma_s\rvert-\pi/2$	$\lvert q_{ys}\rvert+\lvert\gamma_s\rvert-\pi/2$
$\gamma_s \ge x_3$	0	-	-
$\pi/2 \le \gamma_s < \pi$	$\lvert q_{ys}\rvert$		
$\gamma_s \le x_1$	π	$-3/2\cdot\pi+\lvert\gamma_s\rvert-\lvert q_{ys}\rvert$	$-3/2\cdot\pi+\lvert\gamma_s\rvert$
$x_1 > \gamma_s > x_2$	$\pi-\arccos\left(\frac{C\cdot\cos(\gamma_s-\pi)-r_c}{r_p}\right)$	$-3/2\cdot\pi+\lvert\gamma_s\rvert-\lvert q_{ys}\rvert$	$-3/2\cdot\pi+\lvert\gamma_s\rvert$
$\gamma_s = x_2$	$\pi/2$	$-3/2\cdot\pi+\lvert\gamma_s\rvert-\lvert q_{ys}\rvert$	$-3/2\cdot\pi+\lvert\gamma_s\rvert$
$x_2 > \gamma_s > x_3$	$\arccos\left(\frac{r_c-C\cdot\cos(\gamma_s-\pi)}{r_p}\right)$	$-3/2\cdot\pi+\lvert\gamma_s\rvert-\lvert q_{ys}\rvert$	$-3/2\cdot\pi+\lvert\gamma_s\rvert$
$\gamma_s \le x_3$	0	-	-

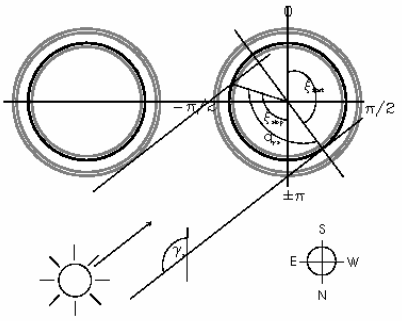

Fig. 7. Relationship between the solar azimuth, γ_s, the beam exposure angle, q_{ys}, and the integration borders ξ_{start} and ξ_{stop}, for $-\pi \le \gamma_s < -\pi/2$, when the pipes are placed vertically.

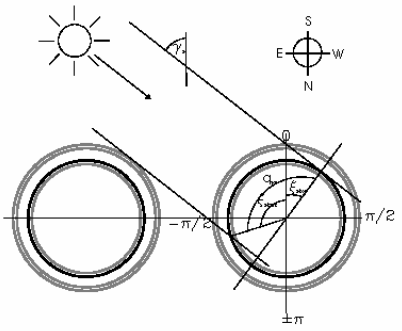

Fig. 8. Relationship between the solar azimuth, γ_s, the beam exposure angle, q_{ys}, and the integration borders ξ_{start} and ξ_{stop}, for $-\pi/2 \le \gamma_s < 0$, when the pipes are placed vertically.

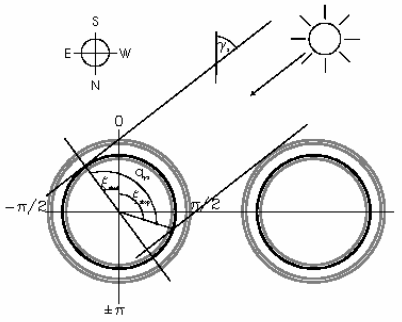

Fig. 9. Relationship between the solar azimuth, γ_s, the beam exposure angle, q_{ys}, and the integration borders ξ_{start} and ξ_{stop}, for $0 \le \gamma_s < \pi/2$, when the pipes are placed vertically.

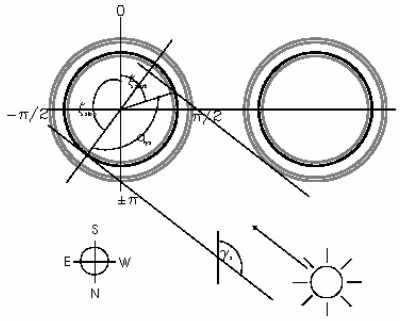

Fig. 10. Relationship between the solar azimuth, γ_s, the beam exposure angle, q_{hs}, and the integration borders ξ_{start} and ξ_{stop}, for $\pi/2 \leq \gamma_s < \pi$, when the pipes are placed vertically.

The theory above is developed for vertical placed pipes, that is for $\beta_s = \pi/2$. If the pipes are not placed vertically, the angle determining the exposed area will be different.

An illustration of this can be seen in Fig. 11. The figure shows two pipes placed horizontally and with the solar azimuth, $\gamma_s = -\pi/2$. Comparing Fig. 6 and Fig. 11 makes it clear that the exposed area, q_{hs}, for an collector facing south is not equal 0 if the solar altitude, h_s, is larger than $\pi/2-x_3$. The angle determining the exposed area, q_{hs}, when the solar azimuth, γ_s, is $\pm\pi/2$ and with horizontal pipes, is given by the formulas in Table 4.

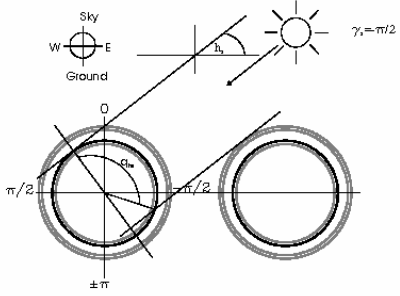

Fig. 11. Relationship between the solar altitude, h_s, the beam exposure angle, q_{hs}, when the pipes are placed horizontally.

Table 4. Angles determining the exposed area with the solar azimuth, $\gamma_s = \pm\pi/2$ for horizontally placed pipes.

$0 \leq h_s < \pi/2$	$\lvert q_{hs} \rvert$	ξ_{start}	ξ_{stop}
$\gamma_s \leq x_1$	π	$\lvert q_{hs} \rvert + h_s$	h_s
$x_1 < \pi/2 - h_s < x_2$	$\pi - a\cos\left(\frac{C\cos\left(\frac{\pi}{2}-h_s\right)-r_c}{r_p}\right)$	$\lvert q_{hs} \rvert + h_s$	h_s
$\pi/2 - h_s = x_2$	$\pi/2$	$\lvert q_{hs} \rvert + h_s$	h_s
$x_2 < \pi/2 - h_s < x_3$	$a\cos\left(\frac{r_c - C\cdot\cos\left(\frac{\pi}{2}-h_s\right)}{r_p}\right)$	$\lvert q_{hs} \rvert + h_s$	h_s
$\pi/2 - h_s \geq x_3$	0	-	-

The incident angle, θ, and the geometric factor, R_b:

In equation (25), the incident angle, θ, and the geometric factor, R_b, still need to be addressed. As earlier mentioned, when integrating over the absorber area, both the surface tilt and the surface azimuth change will have an impact on both K_θ and R_b.

The incident angle, θ, can be described as (Duffie J.A. and Beckman W.A. (1991)):

$$\begin{aligned}\cos(\theta) = &\sin(\delta)\cdot\sin(\phi)\cdot\cos(\beta)\\ &-\sin(\delta)\cdot\cos(\phi)\cdot\sin(\beta)\cdot\cos(\xi)\\ &+\cos(\delta)\cdot\cos(\phi)\cdot\cos(\omega)\cdot\cos(\beta)\\ &+\cos(\delta)\cdot\sin(\phi)\cdot\cos(\omega)\cdot\cos(\xi)\cdot\sin(\beta)\\ &+\cos(\delta)\cdot\sin(\omega)\cdot\sin(\xi)\cdot\sin(\beta)\end{aligned} \quad (26)$$

Here the tilt, β, is described in equation 8 and 9 as a function of the absorber surface azimuth, ξ.

The geometric factor, R_b, can be described as(Duffie J.A. and Beckman W.A. (1991)):

$$\begin{aligned}R_b &= \frac{\cos(\theta)}{\cos(\theta_{horizontal})}\\ &= \frac{\cos(\theta)}{\cos(\delta)\cdot\cos(\phi)\cdot\cos(\omega)+\sin(\delta)\cdot\sin(\phi)}\end{aligned} \quad (27)$$

Solving the performance equation:

All the parameters involved in the performance equation (1) and (2) have now been described in the equations (3)-(27).

In order to evaluate the performance of the tubular collector on a yearly basis, the above theory was implemented into a numerical program. All the integrals could be solved analytically, except the integral in equation (25), which was solved by using the trapezoidal formula for solving integrals numerically. 360 integration steps were used in the numerical integration.

The program is based on weather data with hourly data for global radiation, diffuse radiation on horizontal and outdoor temperature. However, the incident angle and thus the collector performance were calculated every half hour.

4 MEASUREMENTS

The performance of the collector was measured in an outdoor test facility where the inlet temperature, the outlet temperature and the volume flow rate was measured. The temperatures were measured with copper-constantan thermocouples (Type TT) and the volume flow rate was measured with a HGQ1 flow meter. A 31% glycol/water mixture was used in the solar collector loop. Further, the global radiation and the diffuse radiation on horizontal were measured with two Kipp&Zonen CM5 pyranometers.

The power from the solar collector was determined from the measurements by:

$$P_u = \dot{V}\cdot\rho\cdot C_p\cdot\left(T_{in,hot} - T_{out,cold}\right) \quad (28)$$

Further, an efficiency expression for the solar collector panel was determined from the measurements. Only

measurements where the below mentioned conditions were fulfilled were used by determination of the efficiency expression:

- G_{total} was larger than 800 W/m²
- The incidence angle on a south facing 45° tilted surface was smaller than 20°
- The diffuse radiation was less than 22% of the global radiation
- Stationary conditions during at least 15 min.

The solar collector efficiency, based on the absorber area and on the tube cross section area, could thus be determined by:

Absorber area :

$$\eta = \frac{P_u}{G_{total} \cdot A_a} \qquad (29)$$

Tube cross section area :

$$\eta = \frac{P_u}{G_{total} \cdot A_{cross,tube}}$$

Fig. 12 shows the measured efficiency expressions based on the absorber area and the tube cross section area, respectively.

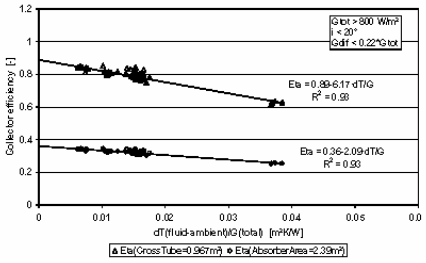

Fig. 12. Measured efficiency expressions based on the absorber area and the tube cross section area.

5 COMPARING THE MODEL WITH MEASUREMENTS

A period of 13 days (17/5-30/5 2003) has been selected for validating the computer model of the collector. In Fig. 13 the total solar irradiance on the collector plane, the ambient temperature, the inlet temperature to the collector and the volume flow rate in the collector are shown. These values are used as input data to the model.

The necessary data for describing the collector are shown in Table 5. The heat loss coefficient, k_0, was determined from the efficiency measurements (Fig. 12) and split into two parts for the evacuated tubes and the manifold pipes respectively. F' was calculated from theory (Duffie J.A. and Beckman W.A. (1991)), (Incropera F.P. and de Witt D.P. (1990)) and $\tau\alpha_e$ and a were calculated with a simulation program for determining optical properties (Svendsen S. and Jensen F.F. (1994)).

In Fig. 14 the measured and calculated collector outlet temperature are compared. Generally, it can be seen that there is a good degree of similarity between the measured and calculated temperatures. However, it can also be seen that the model has a tendency to calculate too low outlet temperatures in the morning and in the evening. This tendency is especially clear for the last 3-4 days in Fig. 14. The reason for this problem is that the collector is tilted 45°, whereas the model is developed only for horizontally or vertically placed pipes. As earlier described, with a tilted collector both the solar azimuth and the solar altitude will influence the size of the shadowed area of the pipes. The larger differences between the calculated and the measured outlet temperature occur especially when the solar altitude is dominating the size of the area exposed to beam radiation. In the model the shadow calculations are based on only the solar azimuth (for vertical pipes) or on only the solar altitude (for horizontal pipes).

Table 5. Data describing the collector in the model.

No. of pipes	L [m]	r_o [m]	r_p [m]	C [m]	k_0 [W/m²K]	F` [-]	$\tau\alpha_e$ [-]	a [-]
14	1.47	0.0235	0.0185	0.067	2.09	0.98	0.856	3.8

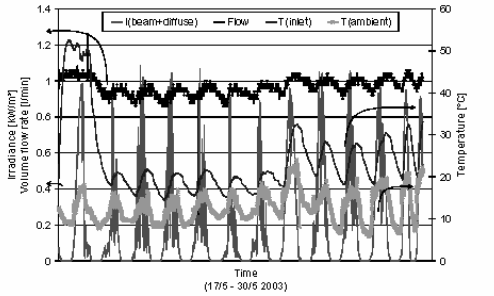

Fig. 13. Total solar irradiance on the collector plane, ambient temperature, collector inlet temperature and collector volume flow rate during the test period.

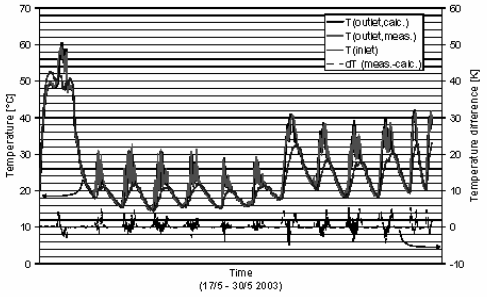

Fig. 14. Measured and calculated outlet temperature for the test period.

6 THEORETICAL INVESTIGATIONS

In this section, the model will be used for theoretical investigations. Only vertically placed pipes will be analysed, as the model is yet unfit to calculate on tilted pipes. The collector performance is investigated for two locations:

- Copenhagen, Denmark, lat. 56°N, yearly average ambient temperature: 7.8°C. Weather data: DRY (Lund H. (1995)).
- Ummannaq, Greenland, lat. 71°N, yearly average ambient temperature: -4.2°C. Weather data: TRY (Kragh J. et al (2002)).

Fig. 15 shows the sum of the solar radiation on the front and the back of vertical planes with different orientations. For Copenhagen, there is symmetry around 0° (south) whereas for Ummannaq the minimum solar radiation on the plane is around –30° (towards east). The reason for this asymmetrical behaviour is that there is a mountain east of Ummannaq, which reduces the radiation coming from east.

As a function of the collector azimuth, Fig. 16 shows the utilized solar energy per tube in a panel assuming a tube centre distance of 0.067m and a constant solar collector fluid temperature throughout the year of 50°C. For both Ummannaq and Copenhagen, there is an optimum at a collector azimuth of about 45°-60°. The results are caused both by the distribution of solar radiation and by higher afternoon temperatures.

Fig. 17 shows the utilized solar energy per tube as a function of the tube centre distance for a collector fluid temperature of 50°C. For both locations, the utilized energy increases for tube centre distances up to 0.2 m, which is due to reduced shaded areas. For larger distances the utilized energy decreases again, due to the increasing heat loss from the manifold pipes.

For the two locations, Fig. 18 and Fig. 19 show the utilized solar energy per tube as a function of the collector azimuth and the tube centre distance for a collector fluid mean temperature of 50°C. Here it can be seen that the tendencies in Fig. 16 are true for tube distances in the range of 0.047 m - 0.3 m.

Finally Fig. 20 and Fig. 21 show the utilized solar energy per m^2 as a function of the collector fluid mean temperature assuming a tube centre distance of 0.047 m and a collector azimuth of 50°. Further, the thermal performance of the newest (Vejen N.K. (2003)) Arcon HT collector is shown. The Arcon HT collector is facing south and tilted 45° in Copenhagen. In Ummannaq the Arcon HT collector is facing south and tilted 60°.

It is interesting that the Arcon collector is the best performing collector under Copenhagen conditions, whereas the thermal performance of the evacuated tubular collector based on the outer tube cross section area, is the highest under the Ummannaq conditions. The reason for the change in the ranking of the collectors is that the tubular collector is not optimally tilted in Copenhagen but also that there is much more solar radiation "from all directions" in Ummannaq and this radiation can be utilized with the tubular collector.

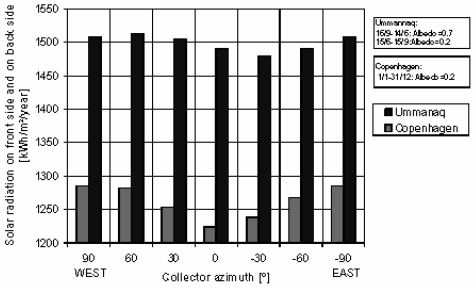

Fig. 15. Solar radiation on the front and the back of vertical planes with different orientations.

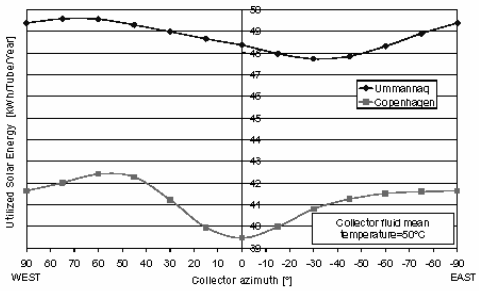

Fig. 16. Utilized solar energy per tube as a function of the collector azimuth. Tube centre distance=0.067 m.

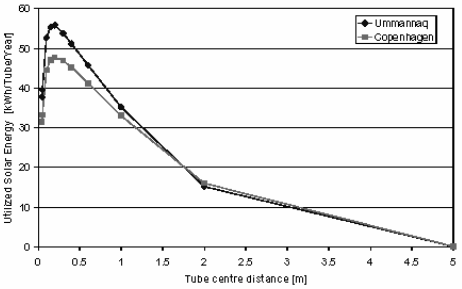

Fig. 17. Utilized solar energy per tube as a function of the tube centre distance for a collector fluid mean temperature of 50°C.

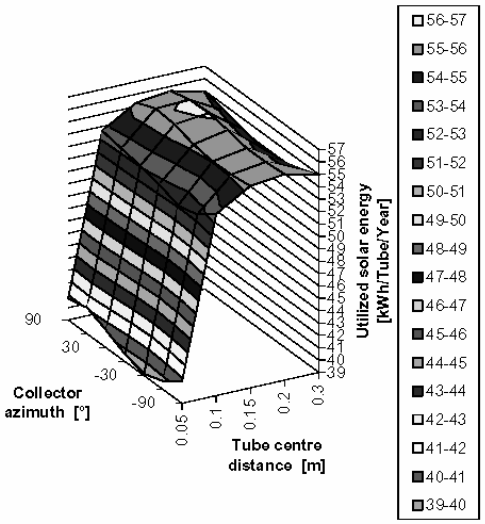

Fig. 18. **Ummannaq**: Utilized solar energy per tube as a function of the collector azimuth and the tube centre distance. Collector fluid mean temperature: 50°C.

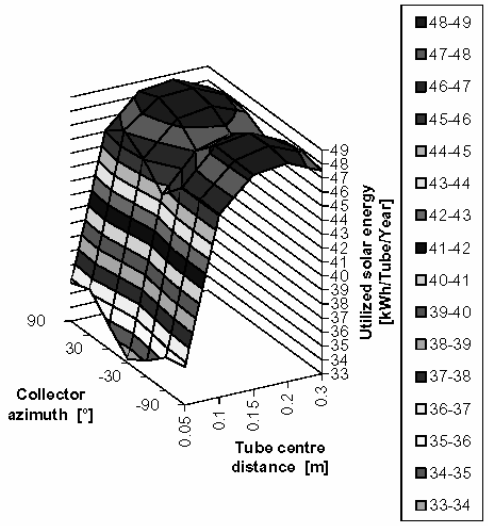

Fig. 19. **Copenhagen**: Utilized solar energy per tube as a function of the collector azimuth and the tube centre distance. Collector fluid mean temperature: 50°C.

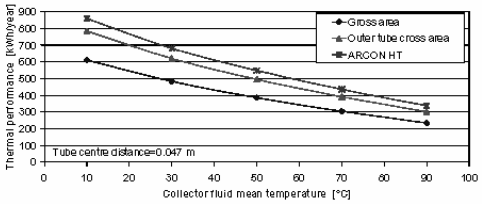

Fig. 20. **Copenhagen**: Utilized solar energy per m^2 as a function of the collector fluid mean temperature at a tube distance of 0.047m.

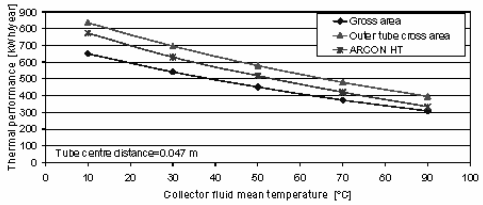

Fig. 21. **Ummannaq**: Utilized solar energy per m^2 as a function of the collector fluid mean temperature at a tube distance of 0.047m.

7 DISCUSSION AND CONCLUSION

A prototype collector with parallel-connected evacuated double glass tubes is investigated theoretically and experimentally. The collector has a tubular absorber and can thus utilize solar radiation coming from all directions.

The collector performance is measured in an outdoor test facility and an efficiency expression for the collector is determined from the measurements.

Further, a theoretical model for calculating the thermal performance is developed. In the model, the flat plate collector performance equations have been integrated over the whole absorber circumference. In this way, the transverse incident angle modifier is eliminated. Also, the model determines the shades on the tubes as a function of the solar azimuth in order to calculate the energy from the beam radiation correctly. The calculation of the energy from the diffuse and ground reflected radiation is based on an isotropic diffuse sky model.

The calculations with the model is compared with measured results and generally, there is a good degree of similarity between the measured and calculated results. However, the comparison also shows that the model is suitable only for vertical placed pipes.

The model is used for theoretical investigations on vertically placed pipes placed in Copenhagen, Denmark and in Ummannaq, Greenland. For both locations, the results show that to achieve the highest thermal performance the tube distance should be about 0.2 m and the collector azimuth should be about 45°-60° towards west. The thermal performance of the evacuated solar collector is also compared to the thermal performance of the Arcon HT flat plate solar collector. These results

show that Arcon collector is the best performing collector under Copenhagen conditions, whereas the performance of the evacuated tubular collector is the highest under the Ummannaq conditions. The reason is that the tubular collector is not optimally tilted in Copenhagen but also that there is much more solar radiation "from all directions" in Ummannaq and this radiation can be utilized with the tubular collector. It is therefore concluded that the collector design is very promising – especially for high latitudes.

The theoretical results presented in this paper are based on a collector model, which needs to be further developed. First of all, the model must be able to calculate on tilted pipes. The reflections between the pipes must be included in the model and also an anisotropic diffuse sky model should be included. This extended model must of course be thoroughly validated with measurements.

Finally, though the collector design seems very promising the collector reliability and durability must be examined before any final conclusions can be drawn.

AKNOWLEDGEMENT

The study is financed by VILLUM KANN RASMUSSEN FOUNDATION.

NOMENCLATURE

LATIN SYMBOLS:

a	Incident angle modifier constant	[-]
A_l	Absorber perimeter length	[m]
A_a	Absorber area	[m²]
A_b	Absorber area exposed to beam radiation	[m²]
A_d	Absorber area exposed to diffuse radiation	[m²]
A_{gr}	Absorber area exposed to ground reflected radiation	[m²]
$A_{cross,tube}$	Tube cross section area	[m²]
C	Cylinder centre distance	[m]
C_p	Collector fluid heat capacity	[J/(kg·K)]
F`	Collector efficiency factor	[-]
F_{1-2}	View factor from tube 1 to tube 2	[-]
F_{c-g}	View factor from tube to ground	[-]
F_{c-s}	View factor from tube to sky	[-]
F^*_{c-g}	View factor from tube to ground without adjacent tubes	[-]
F^*_{c-s}	View factor from tube to sky without adjacent tubes	[-]
G_b	Beam radiation on horizontal	[W/m²]
G_d	Diffuse radiation on horizontal	[W/m²]
G_{gr}	Ground reflected radiation on horizontal	[W/m²]
G_{global}	Global radiation	[W/m²]
G_{total}	Total radiation on collector plane	[W/m²]
h_s	Solar altitude	[rad]
k_0	Collector heat loss coefficient	[W/m²K]
K_θ	Incident angle modifier for beam radiation	[-]
$K_{\theta,d}$	Incident angle modifier for diffuse radiation	[-]
$K_{\theta,gr}$	Incident angle modifier for ground reflected radiation	[-]
L	Pipe length	[m]
O_1	Help length	[m]
O_2	Help length	[m]
P_b	Energy from beam radiation on collector/tube	[W]
P_d	Energy from diffuse radiation on collector/tube	[W]
P_{gr}	Energy from ground reflected radiation on collector/tube	[W]
P_{loss}	Heat loss from collector/tube	[W]
P_u	Useful energy from collector/tube	[W]
q_{hs}	Angle determining the area exposed to beam radiation as a function of h_s	[rad]
q_{ys}	Angle determining the area exposed to beam radiation as a function of γ_s	[rad]
R_b	Geometric factor; irradiance on a tilted surface divided by irradiance on a horizontal surface	[-]
r_o	Outer glass tube radius	[m]
r_p	Absorber radius	[m]
T_a	Ambient temperature	[°C]
T_{fm}	Fluid mean temperature	[°C]
$T_{in,hot}$	Hot inlet temperature	[°C]
$T_{out,cold}$	Cold outlet temperature	[°C]
U_L	Heat loss coefficient based on absorber area	[W/(m²K)]
$\dot{V}$	Collector volume flow rate	[m³/s]
x_1	Help angle	[rad]
x_2	Help angle	[rad]
x_3	Help angle	[rad]
z	Help length	[m]

GREEK SYMBOLS:

β	Collector tilt	[rad]
β_s	Absorber surface tilt when absorber surface azimuth is zero	[rad]
η	Solar collector efficiency	[-]
γ_s	Solar azimuth	[rad]
δ	Declination	[rad]
ρ	Collector fluid density	[kg/m³]
θ	Incident angle	[rad]
$\tau\alpha_e$	Effective transmittance-absorptance product	[-]
ξ	Absorber surface azimuth	[rad]
ξ_{start}	Integration border	[rad]
ξ_{stop}	Integration border	[rad]
Φ	Latitude	[rad]
ω	Solar time	[rad]

REFERENCES

Duffie J.A. and Beckman W.A. (1991) *Solar Engineering of Thermal Processes,* 2nd edn. pp. 268-283 & pp 13-31. Wiley Interscience, New York.

Incropera F.P. and de Witt D.P. (1990) pp. 428-467. *Introduction to heat transfer*, John Wiley & Sons, Singapore.

Lund H. (1995) *The Design Reference Year user manual.* Report of IEA-SHC Task 9. Report 274. Thermal Insulation Laboratory. Technical University of Denmark.

Kragh J. et al (2002) *Grønlandske vejrdata. Nuuk. Uummannaq*. Department of Civil Engineering, Technical University of Denmark . November 2002.

Lart S. (2000) *Development of a thermal performance test for an Integrated Collector-Storage solar water heating system.* pp. 90-100. Ph.D. thesis. Division of Mechanical Engineering and Energy studies. University of Wales Cardiff.

Pyrko J. (1984) A model of the average solar radiation for the tubular collector. *Int. J. Solar Energy.* 32, 563-565.

Vejen N.K. (2003) Development of 12.5 m2 solar collector panel for solar heating plants. *Proceedings of ISES Solar World Congress*, 16-19 June, Gothenburg, Sweden. In Press.

Svendsen S. and Jensen F.F. (1994) *Soltransmittans.* Lecture note. Thermal Insulation Laboratory, Technical University of Denmark.

Bilag 2: Artikel optaget i proceedings for EuroSun 2004 Congress, 20-23 juni 2004.

NEW TRNSYS MODEL OF EVACUATED TUBULAR COLLECTOR WITH CYLINDRICAL ABSORBER

Louise Jivan Shah & Simon Furbo
Department of Civil Engineering, Technical University of Denmark
Building 118
DK-2800 Kgs. Lyngby
Denmark
E-mail: ljs@byg.dtu.dk

Introduction

A new collector design based on parallel-connected double glass evacuated tubes has previously been investigated theoretically and experimentally (Shah, L.J. & Furbo, S. (2004)). The tubes were annuluses with closed ends and the outside of the inner glass wall was treated with a selective coating. The collector fluid was floating inside the inner tube where also another closed tube was inserted so less collector fluid was needed. The collector design made utilization of solar radiations from all directions possible. Fig. 4 shows the design of the evacuated tubes and the principle of the tube connection.

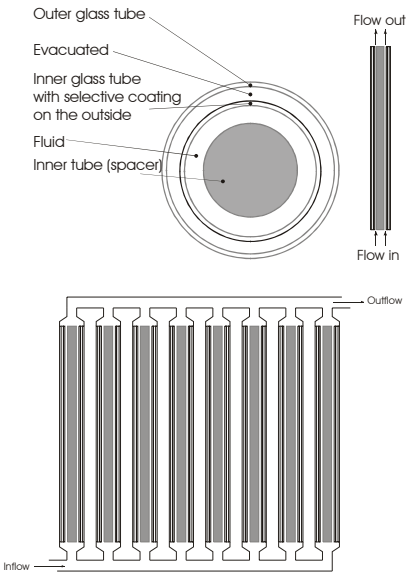

Fig. 4: Design of the evacuated tubes (top) and the tubes connected to a solar panel (bottom).

The investigations resulted in a validated collector model that could calculate the yearly thermal performance of the collector based on hourly weather data. The advantages of the model were that shadows, the solar radiation and the incidence angle modifier for each tube were precisely determined for all solar positions, including solar positions on the "back" of the collector. However, the model could be improved further as the model was only valid for vertically tilted pipes and as the model was not developed for a commonly used simulation program.

In the present paper, the theory is further developed so it can simulate solar collector panels of any tilt and based on the theory a new TRNSYS (Klein, S.A. et al. (1996).) collector type is developed. This model is validated with the measurements from outdoor experiments.

TRNSYS simulations of the yearly thermal performance of a solar heating plant based on the evacuated solar collectors are carried out and among other things it is investigated how the distance between tubes and the collector tilt influences the yearly thermal performance. The calculations are carried out for two locations: Copenhagen, Denmark, lat. 56°N, and Uummannaq, Greenland, lat. 71°N.

Further, the results are compared to the calculated thermal performance of the solar heating plant based on traditional flat plate collectors.

Collector performance theory for tubular absorbers

In Shah, L.J. & Furbo, S. (2003) and Shah, L.J. & Furbo, S. (2004), a theoretical model for calculating the thermal performance of evacuated collectors with tubular absorbers was developed. The principle in the model was that flat plate collector performance equations were integrated over the whole absorber circumference. In this way, the transverse incident angle modifier was eliminated. The model was valid only for vertically tilted pipes.

In this section, the principle of the model will shortly be summarized. Further, the newest development that improves the model to be able to also take tilted pipes into calculation will be described.

Generally, for a solar collector without reflectors and without parts of the collector reflecting solar radiation to other parts of the collector, the performance equation can be written as:

$$P_u = P_b + P_d + P_{gr} - P_{loss} \quad (1)$$

or more detailed described:

$$P_u = A_b \cdot F' \cdot (\tau\alpha)_e \cdot K_\theta \cdot R_b \cdot G_b + A_a \cdot F' \cdot (\tau\alpha)_e \cdot K_{\theta,d} \cdot F_{c-s} \cdot G_d + A_a \cdot F' \cdot (\tau\alpha)_e \cdot K_{\theta,gr} \cdot F_{c-g} \cdot G_{gr} - A_a \cdot U_L \cdot (T_{fm} - T_a) \quad (2)$$

where K_θ is the incident angle modifier defined as:

$$K_\theta = 1 - \tan^a\left(\frac{\theta}{2}\right) \quad (3)$$

The incident angle modifiers for diffuse radiation, $K_{\theta,d}$, and ground reflected radiation, $K_{\theta,gr}$, are evaluated by equation 3 using $\theta=\pi/3$.

To calculate the thermal performance of the evacuated tubes, the general performance equations (1) and (2) have been integrated over the whole absorber circumference. This means that the tube is divided into small “slices”, and each slice is treated as if it was a flat plate collector. In this way, the transverse incident angle modifier is eliminated. For describing the solar radiation on a tubular geometry, this method has previously been used by Pyrko J. (1984). .

Integrating over the absorber area, the performance equation can be described as:

$$P_u = \int_{-\pi}^{\pi} \left(P_b + P_d + P_{gr} - P_{loss}\right) \cdot d\xi \quad (4)$$

where,

$$P_{loss} = \int_{-\pi}^{\pi} A_a \cdot U_L \cdot (T_{fm} - T_a) \cdot d\xi = \int_{-\pi}^{\pi} L \cdot r_p \cdot U_L \cdot (T_{fm} - T_a) \cdot d\xi = 2 \cdot \pi \cdot L \cdot r_p \cdot U_L \cdot (T_{fm} - T_a) \quad (5)$$

$$P_d = \int_{-\pi}^{\pi} A_a \cdot F' \cdot (\tau\alpha)_e \cdot K_{\theta,d} \cdot F_{c-s} \cdot G_d \cdot d\xi = 2 \cdot \pi \cdot r_p \cdot L \cdot F' \cdot (\tau\alpha)_e \cdot K_{\theta,d} \cdot G_d \cdot \int_{-\pi}^{\pi} F_{c-s} \cdot d\xi \quad (6)$$

$$P_{gr} = \int_{-\pi}^{\pi} A_a \cdot F' \cdot (\tau\alpha)_e \cdot K_{\theta,gr} \cdot F_{c-g} \cdot G_{gr} \cdot d\xi = 2 \cdot \pi \cdot r_p \cdot L \cdot F' \cdot (\tau\alpha)_e \cdot K_{\theta,gr} \cdot G_{gr} \cdot \int_{-\pi}^{\pi} F_{c-g} \cdot d\xi \quad (7)$$

$$G_{gr} = \rho_{gr} \cdot (G_b + G_d) \quad (8)$$

$$F_{c-s} = 0.5 - F_{1-2} \quad (9)$$

$$F_{c-g} = 0.5 - F_{1-2} \quad (10)$$

Power from beam radiation on collector/tube, P_b:
The power contribution from the beam radiation can be written as:

$$\begin{aligned} 0 < \gamma_1 - \gamma_0 \le \pi: \quad P_b &= \int_{\gamma_0}^{\gamma_1} F' \cdot (\tau\alpha)_e \cdot G_b \cdot A_b \cdot K_\theta \cdot R_b \cdot d\xi \quad = F' \cdot (\tau\alpha)_e \cdot G_b \cdot L \cdot r_p \cdot \int_{\gamma_0}^{\gamma_1} K_\theta \cdot R_b \cdot d\xi \\ 0 \le \gamma_0 - \gamma_1 < \pi: \quad P_b &= \int_{\gamma_1}^{\gamma_0} F' \cdot (\tau\alpha)_e \cdot G_b \cdot A_b \cdot K_\theta \cdot R_b \cdot d\xi \quad = F' \cdot (\tau\alpha)_e \cdot G_b \cdot L \cdot r_p \cdot \int_{\gamma_1}^{\gamma_0} K_\theta \cdot R_b \cdot d\xi \end{aligned} \tag{11}$$

Notice that there is now integrated over only a part of the circumference. This is because only part of the absorber surface is exposed to the beam radiation due to shadows from the neighbour tube. The task is now to determine the size of this area, thus determining the size and position of the shadowed area. In vector notation, the position of the sun can be described by:

$$\vec{S} = \begin{pmatrix} \sin\theta_z \cdot \cos\gamma_s \\ \sin\theta_z \cdot \sin\gamma_s \\ \cos\theta_z \end{pmatrix} \tag{12}$$

and a "cross section circle" (see Fig. 5) on the absorber of one tube can be described by:

$$\vec{N} = r_p \cdot \begin{pmatrix} \cos\left(\frac{\pi}{2} - \beta_s\right) \cdot \cos\gamma_0 \\ \sin\gamma_t \\ \sin\left(\frac{\pi}{2} - \beta_s\right) \cdot \sin\gamma_0 \end{pmatrix} \tag{13}$$

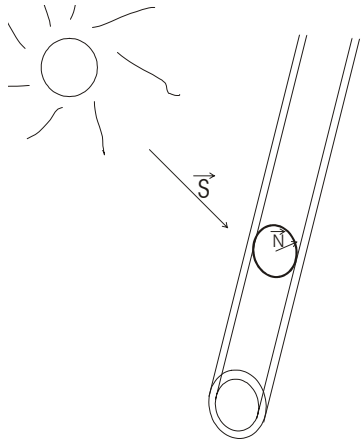

Fig. 5: The solar vector, $\vec{S}$, and the tube vector, $\vec{N}$.

Fig. 6 shows an example where a part of one tube is shaded and a part is exposed to beam radiation. In order to determine the size of the area exposed to beam radiation, the points P_0 and P_1 must be determined.

Since P_0 is located where the solar vector and the tube vector are at right angles to each other, P_0, described by the angle γ_0, can be determined by the scalar product of the two vectors:

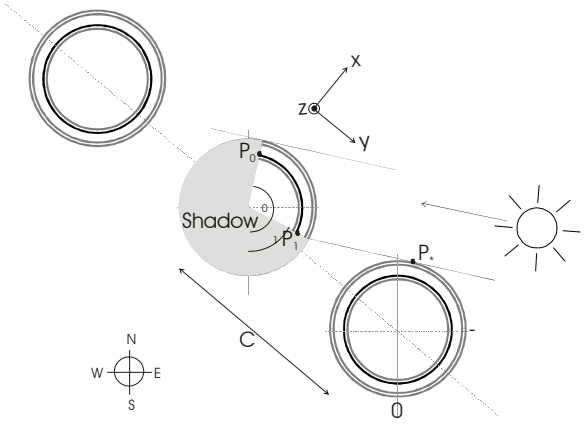

Fig. 6: Illustration of the shaded area and the area exposed to beam radiation.

$$\vec{S} \cdot \vec{N} = |S| \cdot |N| \cdot \cos\left(\frac{\pi}{2}\right) = 0 \Rightarrow \sin\theta_z \cdot \cos\gamma_s \cdot \cos\left(\frac{\pi}{2} - \beta_s\right) \cdot \cos\gamma_0 + \sin\theta_z \cdot \sin\gamma_s \cdot \sin\gamma_0 + \cos\theta_z \cdot \sin\left(\frac{\pi}{2} - \beta_s\right) \cdot \sin\gamma_0 = 0 \Rightarrow$$

$$\gamma_0 = -\arctan\left(\frac{\sin(\theta_z) \cdot \cos(\gamma_s) \cdot \cos(\frac{\pi}{2} - \beta_s) + \cos(\theta_z) \cdot \sin(\frac{\pi}{2} - \beta_s)}{\sin(\theta_z) \cdot \sin(\gamma_s)} \right) \tag{14}$$

Since the equation for γ_0 involves the tangens function, the equation will return two solutions. Based on information on the position of the sun, the correct solution is found.

The point P_1, described by the angle γ_1, can be determined from the following equations (15), (16) and (17). A graphical illustration of symbols used in the equations can be seen in Fig. 6 and Fig. 7.

$$P_1 = \begin{pmatrix} x_1 \\ y_1 \\ z_1 \end{pmatrix} = \begin{pmatrix} x_* \\ y_* \\ z_* \end{pmatrix} + \begin{pmatrix} \sin\theta_z \cdot \cos\gamma_s \\ \sin\theta_z \cdot \sin\gamma_s \\ \cos\theta_z \end{pmatrix} \cdot T \qquad (15)$$

$$P_1 = \begin{pmatrix} x_1 \\ y_1 \\ z_1 \end{pmatrix} = \begin{pmatrix} x_n \\ 0 \\ z_n \end{pmatrix} + r_p \cdot \begin{pmatrix} \cos\left(\frac{\pi}{2} - \beta_s\right) \cdot \cos\gamma_1 \\ \sin\gamma_1 \\ \sin\left(\frac{\pi}{2} - \beta_s\right) \cdot \sin\gamma_1 \end{pmatrix} \qquad (16)$$

$$x_n = -z_n \cdot \tan\left(\frac{\pi}{2} - \beta_s\right) \qquad (17)$$

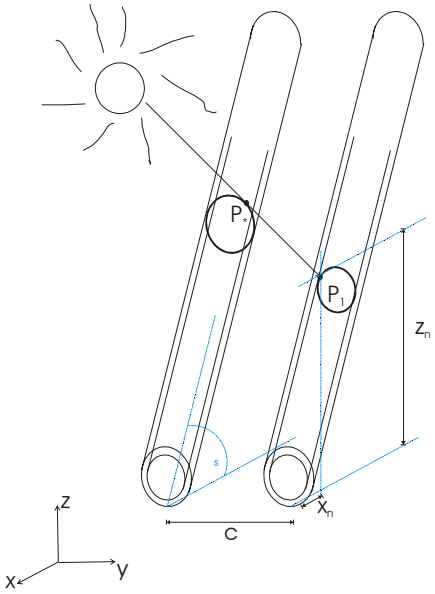

Fig. 7: Illustration of the shaded area and the area exposed to beam radiation.

Equations(15) (16) and (17) together give four equations to the four unknowns: T, γ_1, x_n and z_n. Solving for γ_1 gives:

$$\gamma_1 = \arctan 2\left[\frac{K_1 + 0.5 \cdot \frac{K_2}{K_2^2 + K_3^2} \cdot \left(-2 \cdot K_1 \cdot K_2 + 2 \cdot K_4^{0.5}\right)}{K_3}, \frac{0.5}{K_2^2 + K_3^2} \cdot \left(-2 \cdot K_1 \cdot K_2 + 2 \cdot K_4^{0.5}\right) \right]$$

or (18)

$$\gamma_1 = \arctan 2\left[\frac{K_1 + 0.5 \cdot \frac{K_2}{K_2^2 + K_3^2} \cdot \left(-2 \cdot K_1 \cdot K_2 - 2 \cdot K_4^{0.5}\right)}{K_3}, \frac{0.5}{K_2^2 + K_3^2} \cdot \left(-2 \cdot K_1 \cdot K_2 - 2 \cdot K_4^{0.5}\right) \right]$$

where

$$K_1 = \frac{x_*}{\tan\left(\frac{\pi}{2} - \beta_s\right)} - \frac{y_*}{\tan\left(\frac{\pi}{2} - \beta_s\right) \cdot \tan\left(\gamma_s - \gamma_f\right)} - \frac{y_*}{\tan\left(\theta_z\right) \cdot \sin\left(\gamma_s - \gamma_f\right)} + z_*$$

$$K_2 = \frac{C}{\tan\left(\frac{\pi}{2} - \beta_s\right) \cdot \tan\left(\gamma_s - \gamma_f\right)} + \frac{C}{\tan\left(\theta_z\right) \cdot \sin\left(\gamma_s - \gamma_f\right)} \qquad (19)$$

$$K_3 = C \cdot \left(\cos^2\left(\frac{\pi}{2} - \beta_s\right) + \frac{1}{\tan\left(\theta_z\right) \cdot \sin\left(\gamma_s - \gamma_f\right)} \right)$$

$$K_4 = K_3^4 - K_1^2 \cdot K_3^2 + K_2^2 \cdot K_3^2$$

From equation (18) it appears that there are two solutions for γ_1. Based on information on the position of γ_0, the correct solution is found.

The incident angle, θ, and the geometric factor, R_b:

The incident angle, θ, can be described as:

$$\cos(\theta) = \sin(\theta_z)\cdot\cos(\gamma_s - \gamma_f)\cdot\cos\left(\frac{\pi}{2} - \beta_s\right)\cdot\cos(\gamma_{actual}) + \sin(\theta_z)\cdot\sin(\gamma_s - \gamma_f)\cdot\sin(\gamma_{actual}) + \cos(\theta_z)\cdot\sin\left(\frac{\pi}{2} - \beta_s\right)\cdot\cos(\gamma_{actual}) \quad (20)$$

The geometric factor, R_b, can be described as (Duffie J.A. and Beckman W.A. (1991).):

$$R_b = \frac{\cos(\theta)}{\cos(\theta_{zl})} \quad (21)$$

Solving the performance equation:

In order to evaluate the performance of the tubular collector on a yearly basis, the above theory is implemented into a Trnsys type. All the integrals can be solved analytically, except the integral in equation (11), which is solved by using the trapezoidal formula for solving integrals numerically. 360 integration steps are used in the numerical integration. Taking the collector capacity into account, the collector outlet temperature is evaluated by:

$$P_u = \dot{V}\cdot\rho\cdot C_p\cdot\left(T_{out,hot} - T_{in,cold}\right) + \frac{C_{p,col}\cdot(T_{fm}^{t} - T_{fm}^{t-\Delta t})}{\Delta t} \quad (22)$$

Measurements and model validation

The thermal performance of the collector described in Table 1 was measured in an outdoor test facility where the inlet temperature, the outlet temperature and the volume flow rate was measured. The temperatures were measured with copper-constantan thermocouples (Type TT) and the volume flow rate was measured with a HGQ1 flow meter. A 31% glycol/water mixture was used in the solar collector loop. Further, the global radiation and the diffuse radiation on horizontal were measured with two Kipp&Zonen CM5 pyranometers.

No. of pipes	[-]	14
L	[m]	1.47
r_c	[m]	0.0235
r_p	[m]	0.0185
C	[m]	0.067
k_0	[W/m²K]	2.09
F'	[-]	0.98
$(\tau\alpha)_e$	[-]	0.856
a	[-]	3.8
$C_{collector}$	[kJ/K/tube]	1.9

Table 1: Data describing the collector in the model.

The collector performance was measured for two different tilts: 45° and 90° (both facing south). A period of 11 days (17/5-28/5 2003) has been selected for validating the Trnsys model for the collector at 45° and a period of 7 days (12/8-19/8 2003) has been selected for validating the Trnsys model for the collector at 90°.

The necessary data for describing the collector are shown in Table 1. The heat loss coefficient, k_0, was determined from efficiency measurements (Shah, L.J. & Furbo, S. (2004)) and split into two parts for the evacuated tubes and the manifold pipes respectively. F' was calculated from theory (Duffie J.A. and Beckman W.A. (1991)), (Incropera F.P. and de Witt D.P. (1990)) and $(\tau\alpha)_e$ and *a* were calculated with a simulation program for determining optical properties (Svendsen S. and Jensen F.F. (1994)).

In Fig. 9 the measured and calculated collector outlet temperatures are compared. It can be seen that there is a good degree of similarity between the measured and calculated temperatures. Further Fig. 8 shows the measured and calculated collector performance for the two periods. The difference between the measured and calculated performance lies within the measuring inaccuracy of 4%.

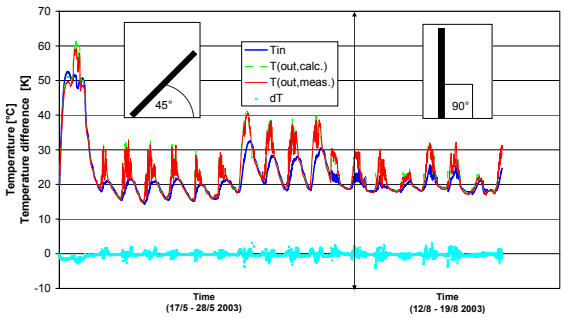

Fig. 9: Measured and calculated outlet temperature for the test periods

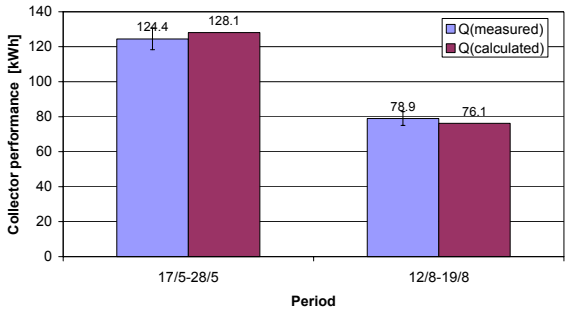

Fig. 8: Measured and calculated collector performance for the test periods.

Simulation of solar heating plants

Model description:

A model of a solar heating plant is built in TRNSYS. The collector array consists of 100 rows where the distance between the rows is assumed to be so large that the shadows between the rows have negligible influence on the collector performance. The energy consumption of a town is defined by a water mass flow rate, a return temperature and a flow temperature of 80°C.

If the temperature from the solar heat exchanger is above 80°C the temperature is mixed down to 80°C with at three-way valve.

If the temperature from the solar heat exchanger is below 80°C, an auxiliary boiler plant heats up the district heating water to 80°C.

An illustration of the TRNSYS model can be seen in Fig. 10 and Fig. 11 shows the mass flow rate and a flow and return temperature through out the year for the district heating net of the town. The annual heat consumption of the town is about 32500 MWh.

The collector performance is investigated for two locations:

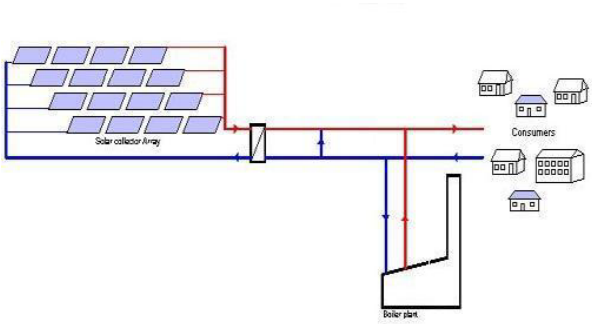

Fig. 10: Schematic illustration of the TRNSYS model.

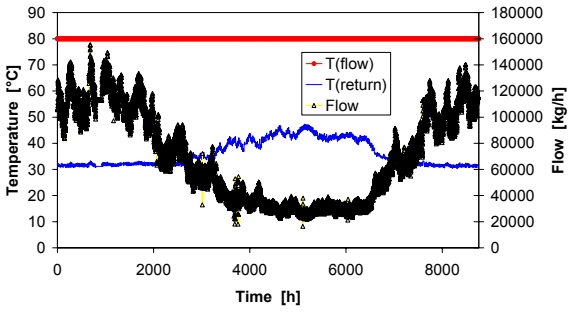

Fig. 11: Assumed flow rate and temperatures in the district heating net.

- Copenhagen, Denmark, lat. 56°N, yearly average ambient temperature: 7.8°C. Weather data: DRY (Lund H. (1995).).

- Uummannaq, Greenland, lat. 71°N, yearly average ambient temperature: -4.2°C. Weather data: TRY (Kragh J. et al (2002).).

Tube distance, collector tilt and collector orientation

The optimum tube centre distance, collector tilt and orientation with respect the thermal performance per tube is investigated for the two locations. The gross collector area is assumed to be constant in the solar heating plant. Consequently, there are more tubes in the collector area when the tube distance is small than when the tube distance is large. Table 2 shows how the collector orientation, the tilt and the tube distance are varied.

Collector azimuth [°]	-90 (east), 75, 60, 45, 30, 15, 0, 15, 30, 45, 60, 75, 90 (west)
Collector tilt [°]	15, 30, 45, 60, 75, 89
Tube centre distance [m]	0.048, 0.077, 0.107, 0.137, 0.167, 0.197 (corresponds to 1mm – 150 mm of air gap between the tubes)

Table 2: Overview of the parameter variations performed with the model.

Fig. 12 and Fig. 13 show the thermal performance per tube for Copenhagen and Uummannaq respectively. The figures clearly show how the thermal performance increases with increasing tube centre distance. The increase is mainly caused by less shadow from the adjacent tubes but also by the differences in the average temperature level of the collector.

The figures also show that the optimum tilt and orientation is about 45° south for Copenhagen and about 60° south for Uummannaq.

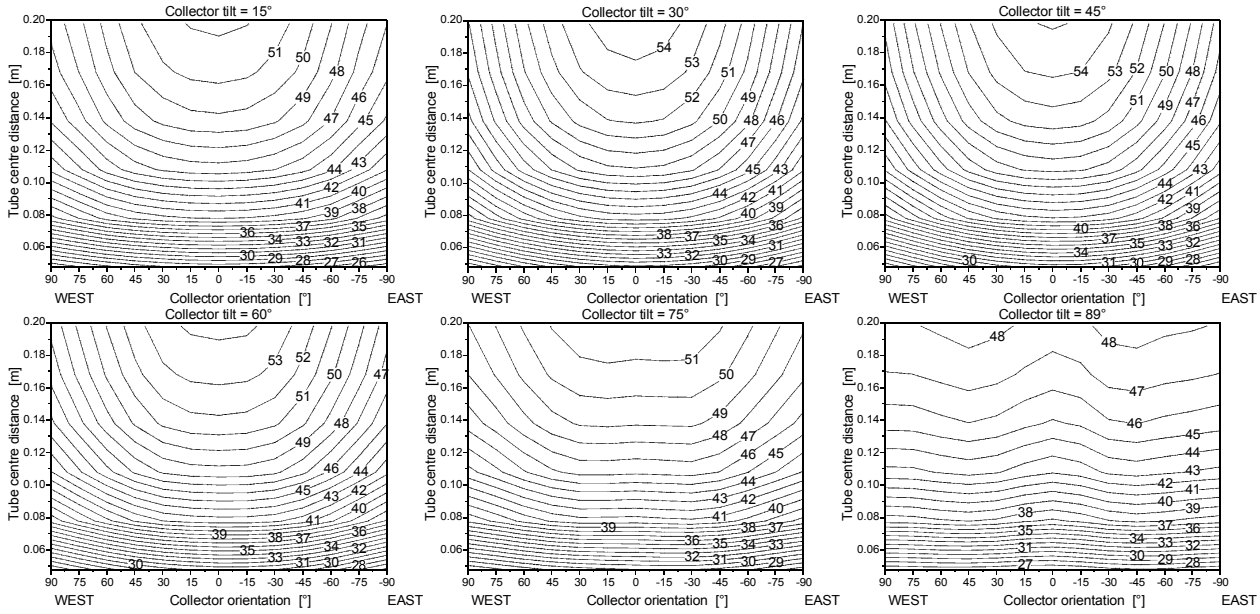

Fig. 12: The thermal performance per tube as a function of the tube centre distance, collector tilt and orientation (Copenhagen).

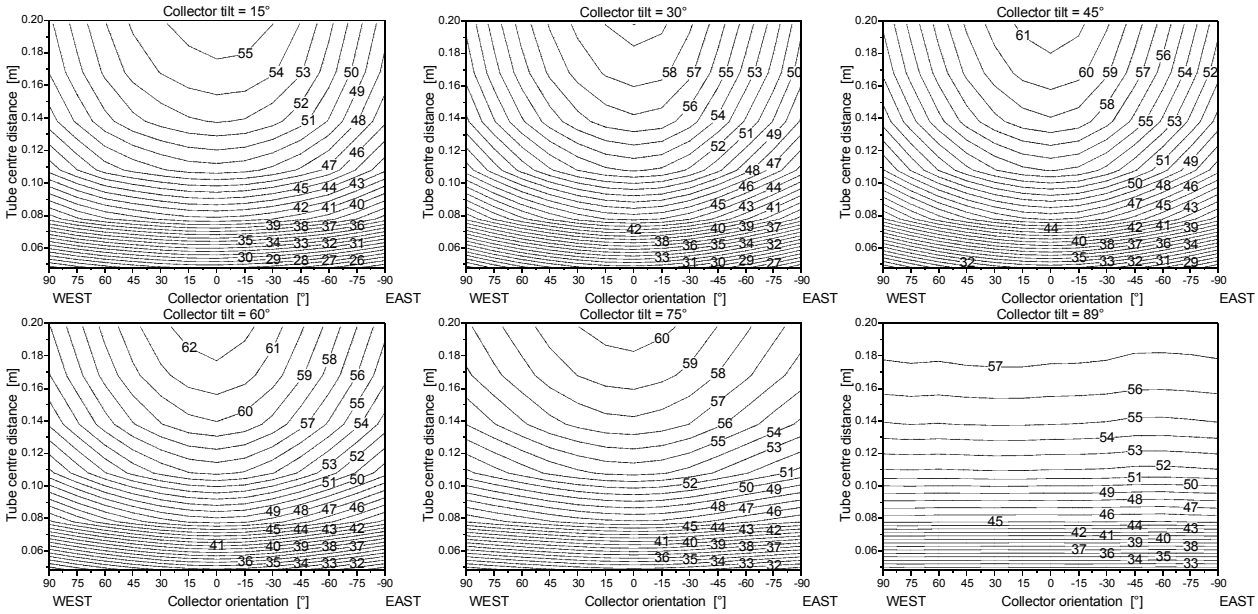

Fig. 13: The thermal performance per tube as a function of the tube centre distance, collector tilt and orientation (Uummannaq).

Comparison with a flat-plate collector

Still considering the solar heating plant, the thermal performance of the evacuated tubular collector is compared to the thermal performance of the newest (Vejen N.K., Furbo S., Shah L.J. (2004).) Arcon HT collector. The collectors are facing south and tilted 45° in Copenhagen. In Ummannaq the collectors are facing south and tilted 60°.

It can be difficult to compare the thermal performances of flat-plate collectors and tubular collectors as the effective area of a flat plate collector typically is defined as the transparent area of the glass cover and the effective area of a tubular collector can be defined in many ways. In the present comparison, the tubes are placed close together so that there is no air-gap between the tubes and the outer tube cross-section area ($=L\cdot 2\cdot r_c\cdot N$) directly corresponds to the transparent area of a flat-plate collector.

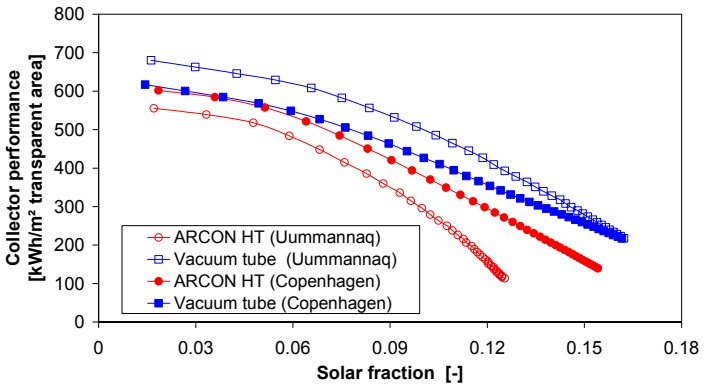

Fig. 14: Thermal performance pr. m² collector as a function of the solar fraction of the solar heating plant.

Fig. 14 shows the thermal performance per m² collector as a function of the solar fraction of the solar heating plant for the two collector types. Here, the solar fraction is defined as:

$$\text{Solar fraction} \quad 1 - \frac{Q_{\text{auxiliar}}}{Q_{\text{town}}} \tag{23}$$

First of all, the figure shows that the tubular collector has the highest thermal performance for both locations. Further, it can be seen that the Uummannaq curves decreases more

rapidly with increasing solar fractions. This is due to the lower air temperature in Uummannaq.
The figure also shows that the ARCON HT collector has a better thermal performance in Copenhagen than in Uummannaq, whereas the tubular collector performs best in Uummannaq. The main reason for the result is that there is much more solar radiation ‘‘from all directions’’ in Uummannaq and this radiation can better be utilized with the tubular collector.

Conclusions

A new TRNSYS collector model for evacuated tubular collectors with tubular absorbers is developed. The model is based on traditional flat plate collector theory, where the performance equations have been integrated over the whole absorber circumference. On each tube the model determines the size and position of the shadows caused by the neighbour tube as a function of the solar azimuth and zenith. This makes it possible to calculate the energy from the beam radiation.
The thermal performance of an all glass tubular collector with 14 tubes connected in parallel is investigated theoretically with the model and experimentally in an outdoor collector test facility. Calculations with the new model of the tubular collector vertically placed and tilted 45° is compared with measured results and a good degree of similarity between the measured and calculated results is found.
Further, the collector model is used in a model of a solar heating plant and a sensitivity analysis of the tube centre distance, collector tilt and orientation with respect the thermal performance per tube is investigated for the two locations Copenhagen (Denmark) and Uummannaq (Greenland). The results show that the optimum tilt and orientation is about 45° south for Copenhagen and about 60° south for Uummannaq.
Finally, the thermal performance of the evacuated tubular collector is compared to the thermal performance of the newest Arcon HT collector. Here, the results show that the tubular collector has the highest thermal performance for both Uummannaq and Copenhagen. This analysis also illustrates the differences in the thermal behaviour of the two collector types: The ARCON HT collector has a higher thermal performance in Copenhagen than in Uummannaq, whereas the tubular collector performs best in Uummannaq compared to Copenhagen. The main reason for the result is that there is much more solar radiation ‘‘from all directions’’ in Uummannaq and this radiation can better be utilized with the tubular collector than with the flat plate collector.

References

Shah, L.J. & Furbo, S. (2004). *Vertical evacuated tubular collectors utilizing solar radiation from all directions.* Applied Energy, Vol 78/4 pp 371-395.
Klein, S.A. et al. (1996). TRNSYS 14.2, User Manual. University of Wisconsin Solar Energy Laboratory.
Pyrko J. (1984). *A model of the average solar radiation for the tubular collector.* Int. J. Solar Energy. 32, 563-565.
Duffie J.A. and Beckman W.A. (1991). *Solar Engineering of Thermal Processes,* 2nd edn. Wiley Interscience, New York.
Shah, L.J. & Furbo, S. (2003). *Thermal performance of evacuated tubular collectors utilizing solar radiation from all directions*. Proceedings, ISES World Sun Congress, Gothenburg

Svendsen S. and Jensen F.F. (1994). *Soltransmittans.* Lecture note. Thermal Insulation Laboratory, Technical University of Denmark.
Incropera F.P. and de Witt D.P. (1990). *Introduction to heat transfer*, pp. 428-467, John Wiley & Sons, Singapore.
Lund H. (1995). *The Design Reference Year user manual.* Report of IEA-SHC Task 9. Report 274. Thermal Insulation Laboratory. Technical University of Denmark.
Kragh J. et al (2002). *Grønlandske vejrdata. Nuuk. Uummannaq*. Department of Civil Engineering, Technical University of Denmark . November 2002.
Vejen N.K., Furbo S., Shah L.J. (2004). *Development of 12.5 m² Solar Collector Panel for Solar Heating Plants.* Solar Energy Materials and Solar Cells. *In press.*

Nomenclature

LATIN SYMBOLS:

a	Incident angle modifier constant	[-]
A_a	Absorber area	[m²]
A_b	Absorber area exposed to beam radiation	[m²]
C	Tube centre distance	[m]
C_p	Collector fluid heat capacity	[J/(kg·K)]
$C_{collector}$	Collector panel heat capacity incl. fluid	[kJ/K/Tube)]
F'	Collector efficiency factor	[-]
F_{1-2}	View factor from tube 1 to tube 2	[-]
F_{c-g}	View factor from tube to ground	[-]
F_{c-s}	View factor from tube to sky	[-]
G_b	Beam radiation on horizontal	[W/m²]
G_d	Diffuse radiation on horizontal	[W/m²]
G_{gr}	Ground reflected radiation on horizontal	[W/m²]
k_0	Collector heat loss coefficient	[W/m²K]
K_1	Help variable	[-]
K_2	Help variable	[-]
K_3	Help variable	[-]
K_4	Help variable	[-]
K_θ	Incident angle modifier for beam radiation	[-]
$K_{\theta,d}$	Incident angle modifier for diffuse radiation	[-]
$K_{\theta,gr}$	Incident angle modifier for ground reflected radiation	[-]
$\vec{N}$	Tube vector	[-]
N	Number of tubes	[-]
L	Pipe length	[m]
P_b	Energy from beam radiation on collector/tube	[W]
P_d	Energy from diffuse radiation on collector/tube	[W]
P_{gr}	Energy from ground reflected radiation on collector/tube	[W]
P_{loss}	Heat loss from collector/tube	[W]
P_u	Useful energy from collector/tube	[W]
$Q_{auxiliar}$	Energy supplied from the boiler plant	[kWh]
Q_{town}	Energy supplied to the town	[kWh]
R_b	Geometric factor; irradiance on a tilted surface divided by irradiance on a horizontal surface	[-]
r_c	Outer glass tube radius	[m]
r_p	Absorber radius	[m]
$\vec{S}$	Solar vector	[-]
T_a	Ambient temperature	[°C]
T_{fm}	Fluid mean temperature	[°C]
$T_{in,hot}$	Hot inlet temperature	[°C]
$T_{out,cold}$	Cold outlet temperature	[°C]
T	Help parameter	[-]
U_L	Heat loss coefficient based on absorber area	[W/(m²K)]
$\dot{V}$	Collector volume flow rate	[m³/s]
x_1	x coordinate for P_1	[m]
x_n	Help length	[m]
x_*	x coordinate for P_*	[m]
y_1	y coordinate for P_1	[m]
y_*	y coordinate for P_*	[m]
z_1	z coordinate for P_1	[m]
z_n	Help length	[m]
z_*	z coordinate for P_*	[m]

GREEK SYMBOLS:

β_s	Collector panel tilt	[rad]
γ_s	Solar azimuth	[rad]
ρ	Collector fluid density	[kg/m³]
θ	Incident angle	[rad]
θ_z	Solar zenith	[rad]
$\tau\alpha_e$	Effective transmittance-absorptance product	[-]
ξ	Integration variable	[rad]
γ_0	Integration border	[rad]
γ_1	Integration border	[rad]
γ_f	Collector panel azimuth	[rad]
γ_{actual}	Actual absorber azimuth	[rad]

Bilag 3: Artikel optaget i det videnskabelige tidsskrift APPLIED ENERGY.

Available online at www.sciencedirect.com
SCIENCE DIRECT®
ELSEVIER
Applied Energy 78 (2004) 371–395
APPLIED ENERGY
www.elsevier.com/locate/apenergy

Vertical evacuated tubular-collectors utilizing solar radiation from all directions

L.J. Shah*, S. Furbo

Department of Civil Engineering, Technical University of Denmark, Brovej, Building 118, DK-2800 Kgs. Lyngby, Denmark

Received 16 September 2003; received in revised form 8 October 2003; accepted 11 October 2003

Abstract

A prototype collector with parallel-connected evacuated double glass tubes is investigated theoretically and experimentally. The collector has a tubular absorber and can utilize solar radiation coming from all directions. The collector performance is measured in an outdoor test facility. Further, a theoretical model for calculating the thermal performance is developed. In the model, flat-plate collector's performance equations are integrated over the whole absorber circumference and the model determines the shading on the tubes as a function of the solar azimuth. Results from calculations with the model are compared with measured results and there is a good degree of similarity between the measured and calculated results. The model is used for theoretical investigations on vertically-placed pipes at a location in Denmark (Copenhagen, lat. 56°N) and at a location in Greenland (Uummannaq, lat. 71°N). For both locations, the results show that to achieve the highest thermal performance, the tube centre distance must be about 0.2 m and the collector azimuth must be about 45–60° towards the west. Further, the thermal performance of the evacuated solar-collector is compared to the thermal performance of the Arcon HT flat-plate solar-collector with an optimum tilt and orientation. The Arcon collector is the best performing collector under Copenhagen conditions, whereas the performance of the evacuated tubular collector is highest under the Uummannaq conditions. The reason is that the tubular collector is not optimally tilted in Copenhagen but also that there is much more solar radiation "from all directions" in Uummannaq and this radiation can be utilized with the tubular collector. It is concluded that the collector design is very promising—especially for high latitudes.

Keywords: Evacuated tubular solar collectors; Collector modelling; Solar heating

* Corresponding author. Tel.: +45-25-18-88; fax: +45-45-93-44-30.
E-mail address: ljs@byg.dtu.dk (L.J. Shah).

0306-2619/$ - see front matter © 2003 Elsevier Ltd. All rights reserved.
doi:10.1016/j.apenergy.2003.10.004

Nomenclature

a	Incident angle modifier constant [ ]
A_l	Absorber perimeter length [m]
A_a	Absorber area [m^2]
A_b	Absorber area exposed to beam radiation [m^2]
$A_{cross,tube}$	Tube's cross-section area [m^2]
A_d	Absorber area exposed to diffuse radiation [m^2]
A_{gr}	Absorber area exposed to ground reflected radiation [m^2]
C	Cylinder centre distance [m]
C_p	Collector-fluid's heat-capacity [J/(kg K)]
$C_{p,col}$	Collector-panel's heat-capacity [J/K]
F_{1-2}	View factor from tube 1 to tube 2 [ ]
F_{c-g}	View factor from tube to ground [ ]
F_{c-s}	View factor from tube to sky [ ]
F'	Collector's efficiency-factor [ ]
F^*_{c-g}	View factor from tube to ground without adjacent tubes [ ]
F^*_{c-s}	View factor from tube to sky without adjacent tubes [ ]
G_b	Beam radiation on horizontal [W/m^2]
G_d	Diffuse radiation on horizontal [W/m^2]
G_{global}	Global radiation [W/m^2]
G_{gr}	Ground reflected radiation on horizontal [W/m^2]
G_{total}	Total radiation on collector plane [W/m^2]
h_s	Solar altitude [rad]
k_0	Collector's heat-loss coefficient [W/m^2K]
K_θ	Incident angle modifier for beam radiation [ ]
$K_{\theta,d}$	Incident angle modifier for diffuse radiation [ ]
$K_{\theta,gr}$	Incident angle modifier for ground reflected radiation [ ]
L	Pipe length [m]
N	Number of pipes [ ]
O_1	Help length [m]
O_2	Help length [m]
P_b	Power from beam radiation on collector/tube [W]
P_d	Power from diffuse radiation on collector/tube [W]
P_{gr}	Power from ground-reflected radiation on collector/tube [W]
P_{loss}	Heat loss from collector/tube [W]
P_u	Useful power from collector/tube [W]
$q_{\gamma s}$	Angle determining the area exposed to beam radiation as a function of γ_s [rad]
R_b	Geometric factor; irradiance on a tilted surface divided by irradiance on a horizontal surface [ ]
r_c	Outer glass tube radius [m]
r_p	Absorber radius [m]

t	Time [s]
T_a	Ambient temperature [°C]
T_{fm}	Fluid's mean temperature [°C]
$T_{in,cold}$	Cold-inlet temperature [°C]
$T_{out,hot}$	Hot-outlet temperature [°C]
U_L	Heat-loss coefficient based on absorber area [W/(m^{2}K)]
$\dot{V}$	Collector volume flow rate [m^3/s]
x_1	Help angle [rad]
x_2	Help angle [rad]
x_3	Help angle [rad]
z	Help length [m]

Greek symbols:

β	Collector's tilt [rad]
δ	Declination [rad]
Δt	Time step [s]
η	Solar-collector's efficiency [ ]
θ	Incident angle [rad]
γ_c	Collector's azimuth [rad]
γ_s	Solar azimuth [rad]
ξ	Absorber surface azimuth [rad]
ξ_{start}	Integration border [rad]
ξ_{stop}	Integration border [rad]
ρ	Collector's fluid-density [kg/m^3]
$\tau\alpha_e$	Effective transmittance-absorptance product [ ]
Φ	Latitude [rad]
ω	Solar time [rad]

1. Introduction

A new collector design, based on evacuated tubular collectors, is investigated theoretically and experimentally. The collector is based on a number of parallel-connected double glass tubes, which are open at both ends. The tubes are annuli with closed ends and the outside of the inner glass wall is treated with an absorbing selective coating. The collector fluid is floating from bottom to top of the inside of the inner tube where also another closed tube is inserted with the purpose of filling a part of the tube volume so that less collector fluid is needed. Further, it ensures a high heat-transfer coefficient from the inner glass tube to the collector fluid. Fig. 1 shows the design of the evacuated tubes and Fig. 2 shows the principle of the tube connection.

For the theoretical investigation of this collector principle, traditional collector theory cannot be applied directly, as the absorbers are tubular. Therefore, to

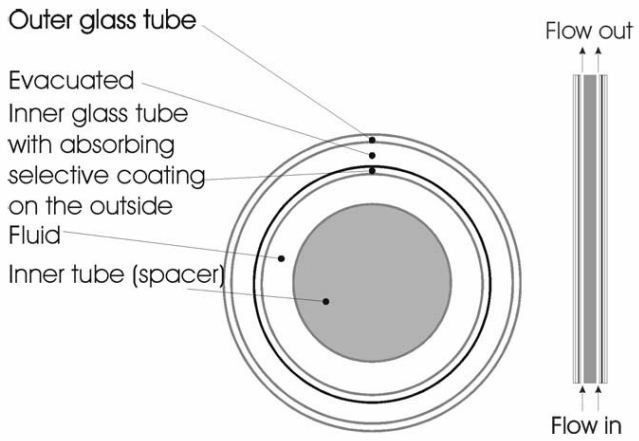

Fig. 1. Design of the evacuated tubes. (Top view: Left. Front view: Right).

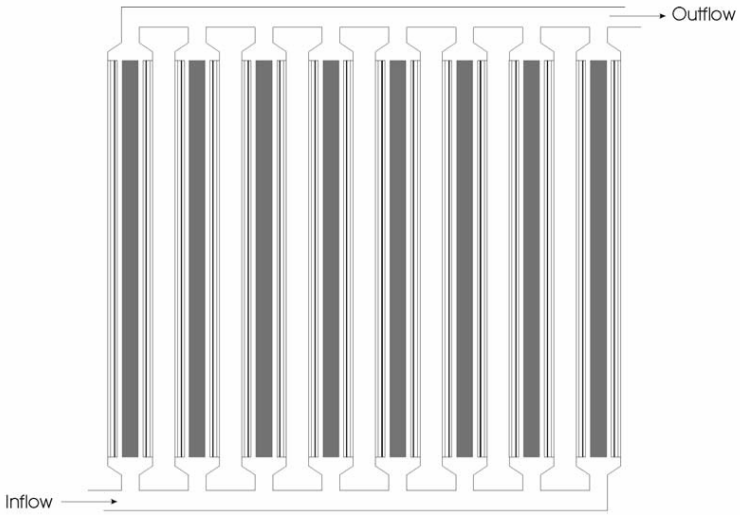

Fig. 2. The tubes connected in a solar-collector panel.

theoretically determine the collector performance a number of conditions must be taken into account, including:

- That solar radiation from all directions can be utilized (also from the "back" of the collector).
- Shadow effects from adjacent tubes.
- Special incident-angle modifiers.

Thermal modelling of evacuated tubular collectors has previously been addressed. Barrett et al. [1] developed an evacuated tubular collector model that included two

incidence-angle modifiers for the longitudinal and the transverse directions. This model has widely been used, among others, by Qin and Furbo [2] who investigated the performance of differently designed evacuated solar-collectors. Based on the tube geometry and panel design, the model cannot be used to find the efficiency expression and the incidence angle modifiers since the model does not take into account directly shadow effects from adjacent tubes or solar radiation received from the back of the collector.

Perez et al. [3] developed a radiation model for evacuated tubular collectors with tubular absorbers. The model was based on the theory of a single-axis tracking solar collector and did take into account solar radiation received from the back of the collector. Further, the model gave an estimation of the size of the shadowed area of the total collector panel. However, the model did not determine the position of the shadows on each tube.

Lart [4] developed a geometrical method to determine the size and position of the shadowed area on each tube. This information was used to modify the transverse incidence-angle modifier so that the effective absorber area was taken into account.

In the present work, a collector theory for the collector's performance is developed. In the model, flat-plate collector performance equations are integrated over the absorber circumference and the model determines the shading on the tubes as a function of the solar azimuth. In this way, the determination of the transverse incident-angle modifier is not necessary.

Further, the collector is investigated in an outdoor test facility in order to determine the collector's performance experimentally. The theory is compared with the results from experiments. Based on the theory, the following points are investigated:

- Distance between tubes.
- Optimal collector-azimuth.
- Expected yearly thermal performances for different climates.

Finally, a comparison between the thermal performance of a flat-plate collector and of the investigated collector is made.

2. Collector design

The solar collector panel consists of 14 evacuated-tubes placed with a centre distance of 0.067 m. The tubes are connected to two manifold pipes, which are placed in an insulated box. The tubes are 1.6 m long, however, 2×0.065 m is placed inside the manifold boxes. Thus only 1.47 m is exposed to the Sun. The outer diameter of the outer tube is 0.047 m and the outer diameter of the inner tube is 0.037 m. The collector panel is vertically placed on the ground and faces south. The solar collector areas are described in Table 1 and Fig. 3 shows a photo of the collector.

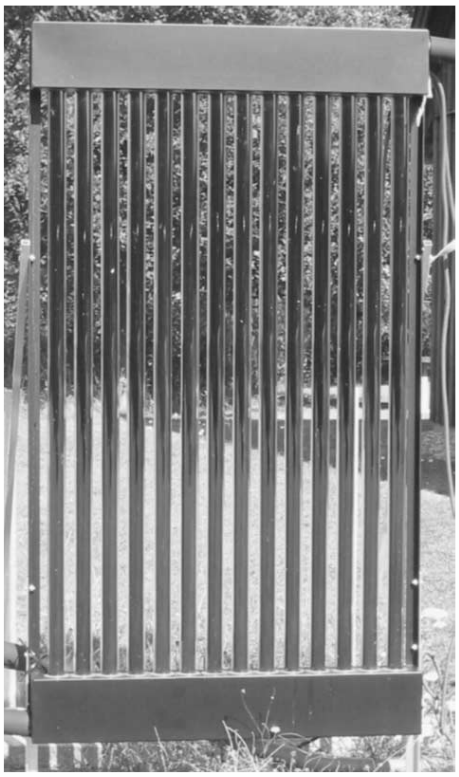

Fig. 3. The evacuated tubular-collector.

Table 1
Solar collector panel's areas

Gross area (m^2)	Outer glass tube cross area (m^2)	Absorber cross area (m^2)	Total absorber area (m^2)
1.8	0.97	0.76	2.39

3. Collector performance theory

Generally, for a solar collector without reflectors and without parts of the collector reflecting solar radiation to other parts of the collector, the performance equation can be written as:

$$P_u = P_b + P_d + P_{gr} - P_{loss} \quad (1)$$

or in more detail described by Shah et al. [5]:

$$P_u = A_b F'(\tau\alpha)_e K_\theta R_b G_b + A_a F'(\tau\alpha)_e K_{\theta,d} F_{c-s} G_d + A_a F'(\tau\alpha)_e K_{\theta,gr} F_{c-g} G_{gr} - A_a U_L (T_{fm} - T_a) \quad (2)$$

where K_θ is the incident angle modifier defined as:

$$K_\theta = 1 - \tan\left(\frac{\theta}{2}\right)^a \quad (3)$$

The incident-angle modifiers for diffuse radiation, $K_{\theta,d}$, and ground reflected radiation, $K_{\theta,gr}$, are evaluated by Eq. (3) using $\theta = \pi/3$.

For tubular collectors, there are several conditions, which make Eq. (2) more difficult to evaluate. Amongst others, the following can be mentioned:

- In flat-plate collector theory, the areas A_a and A_b are typically equal and close to the transparent area. For tubular collectors, however, this is not the case as, depending on the solar azimuth and altitude, only parts of the absorber area are exposed to the beam radiation.
- In flat-plate collector theory the incident angle modifier, K_θ, is independent of the longitudinal and transverse component of the incident angle. The cylindrical geometry in tubular collectors makes it necessary to consider both components.
- In the investigated tubular collector, where the absorber covers the whole inner-tube circumference, also radiation coming from the "back" of the collector must be evaluated.

To calculate the thermal performance of the evacuated tubes, the general performance Eqs. (1) and (2) have been integrated over the whole absorber circumference. This means that the tube is divided into small "slices", and each slice is treated as if it was a flat-plate collector. In this way, the transverse incident-angle modifier is eliminated. For describing the solar radiation on a tubular geometry, this method has previously been used by Pyrko [6].

Integrating over the absorber area, the performance equation can be described as:

$$P_u = \int_{-\pi}^{\pi} (P_b + P_d + P_{gr} - P_{loss}) d\xi \quad (4)$$

In the following, each part of Eq. (4) will be investigated. The investigation is based on a theoretical analysis of a single tube.

3.1. Heat loss, P_{loss}

The heat loss can be described as:

$$\begin{aligned} P_{loss} &= \int_{-\pi}^{\pi} A_a U_L (T_{fm} - T_a) d\xi \\ &= \int_{-\pi}^{\pi} L r_p U_L (T_{fm} - T_a) d\xi \\ &= 2\pi L r_p U_L (T_{fm} - T_a) \end{aligned} \tag{5}$$

3.2. Power from diffuse radiation on collector/tube, P_d:

The evaluation of the power contribution from the diffuse radiation is based on an isotropic diffuse model. Thus, the circumsolar diffuse and horizontal brightening contributions are not taken into consideration in this model.

The power contribution from the diffuse radiation can be written as (Shah et al. [5]):

$$\begin{aligned} P_d &= \int_{-\pi}^{\pi} A_a F'(\tau\alpha)_e K_{\theta,d} F_{c-s} G_d d\xi \\ &= 2\pi r_p L F'(\tau\alpha)_e K_{\theta,d} G_d \int_{-\pi}^{\pi} F_{c-s} d\xi \end{aligned} \tag{6}$$

Assuming that there are no adjacent tubes, the view factor from the tube to the sky can be described as:

$$F^*_{c-s} = \int_{-\pi}^{\pi} \frac{1 + \cos(\beta)}{2} = 0.5 \tag{7}$$

In reality, there will be adjacent tubes, which will reduce the view factors to the ground and the sky respectively. This reduction must be taken into consideration.

Fig. 4 shows two adjacent tubes. The view factor F_{1-2} between the absorber of tube 1 and tube 2 can be described as:

$$\begin{aligned} A_1 \cdot F_{1-2} &= \frac{1}{2} \sum (\text{length of the crossing curves}) \\ &\quad - \frac{1}{2} \sum \text{length of the non crossing curves} \\ &= (O_1 + z + O_2) - C\sin(x_3) \end{aligned} \tag{8}$$

Here A_1 is the absorber perimeter of tube 1. The curves O_1 and O_2 between the points P_1 P_2 and P_3 P_4 respectively can be described by:

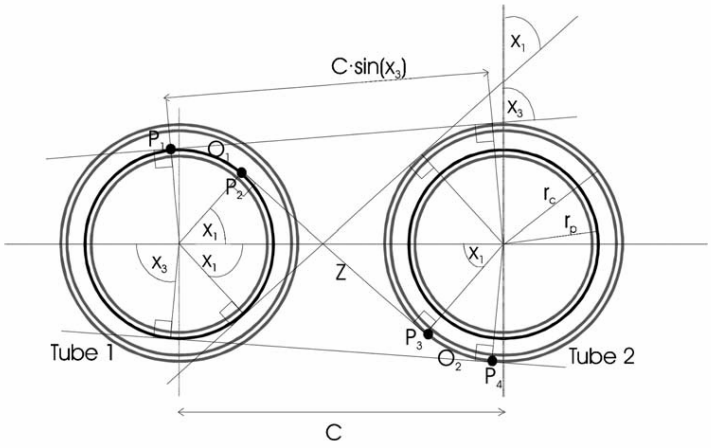

Fig. 4. Determination of view factors between the two tubes.

$$O_1 = \frac{(\pi/2 - x_1) + (\pi/2 - x_3)}{2\pi} 2\pi r_p \tag{9}$$

and

$$O_2 = \frac{(\pi/2 - x_1) - (\pi/2 - x_3)}{2\pi} 2\pi r_c \tag{10}$$

Here the angles x_1 and x_3 are defined by:

$$x_1 = \operatorname{acos}\left(\frac{r_c + r_p}{C}\right) \tag{11}$$

$$x_3 = \operatorname{acos}\left(\frac{r_c - r_p}{C}\right) \tag{12}$$

If the centre of tube 1 has the coordinates (0,0), the coordinates of the points P_2 and P_3 and thus the distance, z, between the two points can be found as:

$$\begin{aligned} P_2 &= \left[r_p\cos(x_1), r_p\sin(x_1)\right] \\ P_3 &= \left[C + r_c\cos(\pi + x_1), r_c\sin(\pi + x_1)\right] \end{aligned} \tag{13}$$

$$z = \sqrt{\left(C + r_c\cos(\pi + x_1) - r_p\cos(x_1)\right)^2 + \left(r_c\sin(\pi + x_1) - r_p\sin(x_1)\right)^2} \tag{14}$$

By inserting Eqs. (9), (10) and (14) into Eq. (8), the view factor from tube 1 to tube 2 can be written as:

$$F_{1-2} = \frac{1}{2\pi r_p}\left[(\pi - x_1 - x_3)r_p + \sqrt{\left(C + r_c\cos(\pi + x_1) - r_p\cos(x_1)\right)^2 + \left(r_c\sin(\pi + x_1) - r_p\sin(x_1)\right)^2} + (x_3 - x_1)r_c - C\sin(x_3)\right] \quad (15)$$

The final view factor from tube to sky, including shading adjacent tubes can thus be described as:

$$F_{c-s} = F^*_{c-s} - F_{1-2} \quad (16)$$

3.3. Power from ground-reflected radiation on collector tube, P_{gr}:

The power contribution from the ground reflected radiation is described by (Shah et al. [5]):

$$\mathbf{P}_{gr} = \int_{-\pi}^{\pi} A_a F'(\tau\alpha)_e K_{\theta,gr} F_{c-g} G_{gr} d\xi \quad (17)$$

$$= 2\pi r_p L F'(\tau\alpha)_e K_{\theta,gr} G_{gr} \int_{-\pi}^{\pi} F_{c-g} d\xi$$

with

$$G_{gr} = \rho_{gr}(G_b + G_d) \quad (18)$$

In a similar way as for the diffuse radiation, the view factor from the tube to the ground, assuming that there are no neighbouring tubes, can be described as:

$$F^*_{c-g} = \int_{-\pi}^{\pi} \frac{1 - \cos(\beta)}{2} = 0.5 \quad (19)$$

Including the adjacent shading tubes, the view factor from tube to ground becomes:

$$F_{c-g} = F^*_{c-g} - F_{1-2} \quad (20)$$

3.4. Power from beam radiation on the collector tube, P_b:

The power contribution from the beam radiation can be written as (Shah et al. [5]):

$$\begin{aligned} P_b &= \int_{\xi_{start}}^{\xi_{stop}} F'(\tau\alpha)_e G_b A_b K_\theta R_b d\xi \\ &= F'(\tau\alpha)_e G_b L r_p \int_{\xi_{start}}^{\xi_{stop}} K_\theta R_b d\xi \end{aligned} \tag{21}$$

Notice that there is now integration over only a part of the circumference. This is because only part of the absorber surface is exposed to the beam radiation.

Assuming that the tubes are placed vertically and that the collector panel azimuth is 0°, Fig. 5 shows the three critical angles, when the solar azimuth, γ_s, is between 0 and $\pi/2$ (Lart [4]). When the solar azimuth is smaller than the angle x_1, there is no shading of the tubes. If the solar azimuth is larger than x_3, the tubes are fully shaded and if the solar azimuth is between x_1 and x_3 the tubes are partly shaded. If the solar azimuth is equal x_2, the tubes are half shaded.

For the analysis of the critical angles as well as the area that is exposed to beam radiation when the collector azimuth is not 0°, the tubes are divided into six parts. These parts are illustrated in Fig. 6 for a collector-panel orientation towards the east ($\gamma_c \leqslant 0°$) and towards the west ($\gamma_c \geqslant 0°$) and in Table 2 the critical angles are defined for all six parts of the circle.

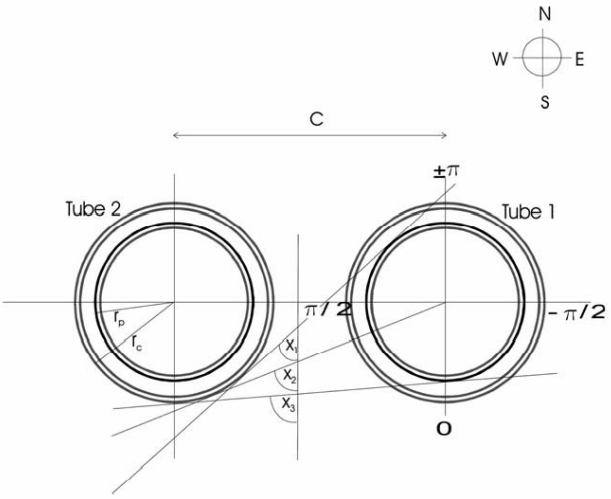

Fig. 5. An illustration of the critical angles determining the exposed area, when the pipes are placed vertically and when the collector panel azimuth is 0°.

Table 2
Critical angles determining the exposed area, when the pipes are placed vertically

Part of the tube	$\gamma_c \leqslant 0°$			$\gamma_c \geqslant 0°$		
	x_1	x_2	x_3	x_1	x_2	x_3
1	$\operatorname{acos}\left(\frac{r_c + r_p}{C}\right) - \pi$	$\operatorname{acos}\left(\frac{r_c}{C}\right) - \pi$	$\operatorname{acos}\left(\frac{r_c - r_p}{C}\right) - \pi$	$\operatorname{acos}\left(\frac{r_c + r_p}{C}\right) - \pi$	$\operatorname{acos}\left(\frac{r_c}{C}\right) - \pi$	$\operatorname{acos}\left(\frac{r_c - r_p}{C}\right) - \pi$
2	$\operatorname{acos}\left(\frac{r_c + r_p}{C}\right) - \pi$	$\operatorname{acos}\left(\frac{r_c}{C}\right) - \pi$	$\operatorname{acos}\left(\frac{r_c - r_p}{C}\right) - \pi$	$-\operatorname{acos}\left(\frac{r_c + r_p}{C}\right)$	$-\operatorname{acos}\left(\frac{r_c}{C}\right)$	$-\operatorname{acos}\left(\frac{r_c - r_p}{C}\right)$
3	$-\operatorname{acos}\left(\frac{r_c + r_p}{C}\right)$	$-\operatorname{acos}\left(\frac{r_c}{C}\right)$	$-\operatorname{acos}\left(\frac{r_c - r_p}{C}\right)$	$-\operatorname{acos}\left(\frac{r_c + r_p}{C}\right)$	$-\operatorname{acos}\left(\frac{r_c}{C}\right)$	$-\operatorname{acos}\left(\frac{r_c - r_p}{C}\right)$
4	$\operatorname{acos}\left(\frac{r_c + r_p}{C}\right)$	$\operatorname{acos}\left(\frac{r_c}{C}\right)$	$\operatorname{acos}\left(\frac{r_c - r_p}{C}\right)$	$\operatorname{acos}\left(\frac{r_c + r_p}{C}\right)$	$\operatorname{acos}\left(\frac{r_c}{C}\right)$	$\operatorname{acos}\left(\frac{r_c - r_p}{C}\right)$
5	$\operatorname{acos}\left(\frac{r_c + r_p}{C}\right)$	$\operatorname{acos}\left(\frac{r_c}{C}\right)$	$\operatorname{acos}\left(\frac{r_c - r_p}{C}\right)$	$-\operatorname{acos}\left(\frac{r_c + r_p}{C}\right) + \pi$	$-\operatorname{acos}\left(\frac{r_c}{C}\right) + \pi$	$-\operatorname{acos}\left(\frac{r_c - r_p}{C}\right) + \pi$
6	$-\operatorname{acos}\left(\frac{r_c + r_p}{C}\right) + \pi$	$-\operatorname{acos}\left(\frac{r_c}{C}\right) + \pi$	$-\operatorname{acos}\left(\frac{r_c - r_p}{C}\right) + \pi$	$-\operatorname{acos}\left(\frac{r_c + r_p}{C}\right) + \pi$	$-\operatorname{acos}\left(\frac{r_c}{C}\right) + \pi$	$-\operatorname{acos}\left(\frac{r_c - r_p}{C}\right) + \pi$

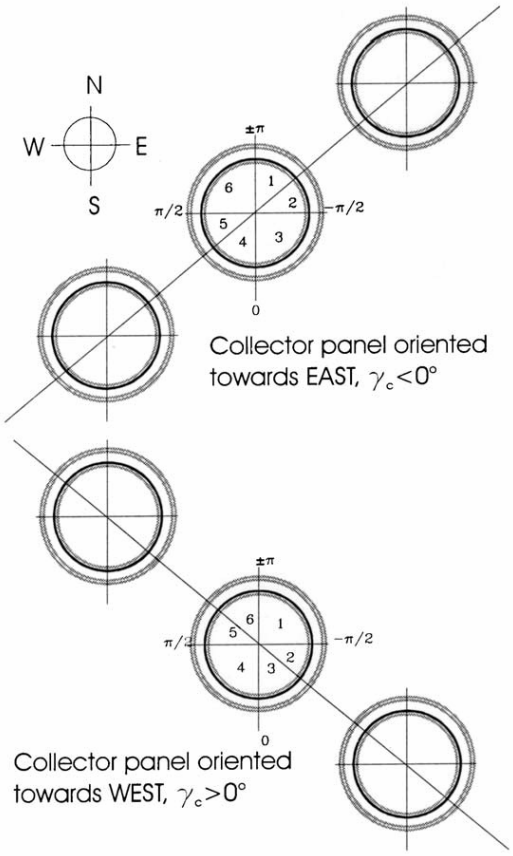

Fig. 6. For analysis purposes, the tubes are divided into six parts.

For a collector panel orientation towards the east, Figs. 7 12 show the angle '$q_{\gamma s}$', which represents the tube area exposed to beam radiation, for different solar azimuths. Further, the angles ξ_{start} and ξ_{stop} used in Eq. (21) are shown.

As a function of the solar azimuth, the angle, $q_{\gamma s}$, and the integration borders, ξ_{start} and ξ_{stop}, are described in Table 3 for a collector-panel orientation towards the east ($\gamma_c \leqslant 0°$) and towards the west ($\gamma_c \geqslant 0°$).

3.5. The incident angle, θ, and the geometric factor, R_b:

In Eq. (21), the incident angle, θ, and the geometric factor, R_b, still need to be addressed. As mentioned earlier, when integrating over the absorber area, both the surface tilt and the surface azimuth change will have an impact on both K_θ and R_b.

The incident angle, θ, can be described as (Duffie and Beckman [7]):

$$\begin{aligned}\cos(\theta) = {} & \sin(\delta)\sin(\phi)\cos(\beta) \\ & - \sin(\delta)\cos(\phi)\sin(\beta)\cos(\xi) \\ & + \cos(\delta)\cos(\phi)\cos(\omega)\cos(\beta) \\ & + \cos(\delta)\sin(\phi)\cos(\omega)\cos(\xi)\sin(\beta) \\ & + \cos(\delta)\sin(\omega)\sin(\xi)\sin(\beta)\end{aligned} \tag{22}$$

The geometric factor, R_b, can be described as (Duffie and Beckman [7]):

$$\begin{aligned}R_b &= \frac{\cos(\theta)}{\cos(\theta_{horizontal})} \\ &= \frac{\cos(\theta)}{\cos(\delta)\cos(\phi)\cos(\omega) + \sin(\delta)\sin(\phi)}\end{aligned} \tag{23}$$

All information needed to calculate the thermal performance is given in the above equations and the collector's outlet temperature $T_{out,hot}$ can finally be calculated from:

$$T_{out,hot} = \frac{P_u - \dfrac{C_{p,col}\left(T_{fm}^{t} - T_{fm}^{t-\Delta t}\right)}{\Delta t}}{\dot{V}\rho C_p} + T_{in,cold} \tag{24}$$

3.6. Solving the performance equation:

All the parameters involved in the performance Eqs. (1) and (2) have been described in Eqs. (3) (23). In order to evaluate the performance of the tubular collector on a yearly basis, the above theory was implemented into a numerical program. All the

Table 3
Angles determining the exposed area, when the pipes are placed vertically

$\gamma_c \leq 0°$				$\gamma_c \geq 0°$			
γ_s is in Part 1	$\lvert q_{ys}\rvert$	ξ_{start}	ξ_{stop}	γ_s is in Part 1	$\lvert q_{ys}\rvert$	ξ_{start}	ξ_{stop}
$\gamma_s \ \gamma_c \leq x_1$	π	$3/2\cdot\pi \ \lvert\gamma_s\rvert$	$3/2\cdot\pi \ \lvert\gamma_s\rvert + \lvert q_{ys}\rvert$	$\gamma_s \ \gamma_c \leq x_1$	π	$\pi/2 \ \lvert\gamma_s\rvert \ \lvert q_{ys}\rvert$	$\pi/2 \ \lvert\gamma_s\rvert$
$x_1 < \gamma_s \ \gamma_c < x_2$	$\pi \ \operatorname{acos}\left(\frac{C\cos(\gamma_s \ \gamma_c + \pi) \ r_c}{r_p}\right)$	$3/2\cdot\pi \ \lvert\gamma_s\rvert$	$3/2\cdot\pi \ \lvert\gamma_s\rvert + \lvert q_{ys}\rvert$	$x_1 < \gamma_s \ \gamma_c < x_2$	$\pi \ \operatorname{acos}\left(\frac{C\cos(\gamma_s \ \gamma_c + \pi) \ r_c}{r_p}\right)$	$\pi/2 \ \lvert\gamma_s\rvert \ \lvert q_{ys}\rvert$	$\pi/2 \ \lvert\gamma_s\rvert$
$\gamma_s \ \gamma_c \ x_2$	$\pi/2$	$3/2\cdot\pi \ \lvert\gamma_s\rvert$	$3/2\cdot\pi \ \lvert\gamma_s\rvert + \lvert q_{ys}\rvert$	$\gamma_s \ \gamma_c \ x_2$	$\pi/2$	$\pi/2 \ \lvert\gamma_s\rvert \ \lvert q_{ys}\rvert$	$\pi/2 \ \lvert\gamma_s\rvert$
$x_2 < \gamma_s \ \gamma_c < x_3$	$\operatorname{acos}\left(\frac{r_c \ C\cos(\gamma_s \ \gamma_c + \pi)}{r_p}\right)$	$3/2\cdot\pi \ \lvert\gamma_s\rvert$	$3/2\cdot\pi \ \lvert\gamma_s\rvert + \lvert q_{ys}\rvert$	$x_2 < \gamma_s \ \gamma_c < x_3$	$\operatorname{acos}\left(\frac{r_c \ C\cos(\gamma_s \ \gamma_c + \pi)}{r_p}\right)$	$\pi/2 \ \lvert\gamma_s\rvert \ \lvert q_{ys}\rvert$	$\pi/2 \ \lvert\gamma_s\rvert$
$\gamma_s \ \gamma_c \geq x_3$	0			$\gamma_s \ \gamma_c \geq x_3$	0		
γ_s is in Part 2	$\lvert q_{ys}\rvert$	ξ_{start}	ξ_{stop}	γ_s is in Part 2	$\lvert q_{ys}\rvert$	ξ_{start}	ξ_{stop}
$\gamma_s \ \gamma_c \leq x_1$	π	$\lvert\gamma_s\rvert \ \pi/2 \ \lvert q_{ys}\rvert$	$\lvert\gamma_s\rvert \ \pi/2$	$\gamma_s \ \gamma_c \leq x_1$	π	$\pi/2 \ \lvert\gamma_s\rvert$	$\pi/2 \ \lvert\gamma_s\rvert + \lvert q_{ys}\rvert$
$x_1 < \gamma_s \ \gamma_c < x_2$	$\pi \ \operatorname{acos}\left(\frac{C\cos(\gamma_s \ \gamma_c + \pi) \ r_c}{r_p}\right)$	$\lvert\gamma_s\rvert \ \pi/2 \ \lvert q_{ys}\rvert$	$\lvert\gamma_s\rvert \ \pi/2$	$x_1 < \gamma_s \ \gamma_c < x_2$	$\pi \ \operatorname{acos}\left(\frac{C\cos(\lvert\gamma_s \ \gamma_c\rvert) \ r_c}{r_p}\right)$	$\pi/2 \ \lvert\gamma_s\rvert$	$\pi/2 \ \lvert\gamma_s\rvert + \lvert q_{ys}\rvert$
$\gamma_s \ \gamma_c \ x_2$	$\pi/2$	$\lvert\gamma_s\rvert \ \pi/2 \ \lvert q_{ys}\rvert$	$\lvert\gamma_s\rvert \ \pi/2$	$\gamma_s \ \gamma_c \ x_2$	$\pi/2$	$\pi/2 \ \lvert\gamma_s\rvert$	$\pi/2 \ \lvert\gamma_s\rvert + \lvert q_{ys}\rvert$
$x_2 < \gamma_s \ \gamma_c < x_3$	$\operatorname{acos}\left(\frac{r_c \ C\cos(\gamma_s \ \gamma_c + \pi)}{r_p}\right)$	$\lvert\gamma_s\rvert \ \pi/2 \ \lvert q_{ys}\rvert$	$\lvert\gamma_s\rvert \ \pi/2$	$x_2 < \gamma_s \ \gamma_c < x_3$	$\operatorname{acos}\left(\frac{r_c \ C\cos(\lvert\gamma_s \ \gamma_c\rvert)}{r_p}\right)$	$\pi/2 \ \lvert\gamma_s\rvert$	$\pi/2 \ \lvert\gamma_s\rvert + \lvert q_{ys}\rvert$
$\gamma_s \ \gamma_c \geq x_3$	0			$\gamma_s \ \gamma_c \geq x_3$	0		
γ_s is in Part 3	$\lvert q_{ys}\rvert$	ξ_{start}	ξ_{stop}	γ_s is in Part 3	$\lvert q_{ys}\rvert$	ξ_{start}	ξ_{stop}
$\gamma_s \ \gamma_c \leq x_1$	π	$\lvert\gamma_s\rvert \ \pi/2$	$\lvert q_{ys}\rvert \ \lvert\gamma_s\rvert \ \pi/2$	$\gamma_s \ \gamma_c \leq x_1$	π	$\pi/2 \ \lvert\gamma_s\rvert \ \lvert q_{ys}\rvert$	$\pi/2 \ \lvert\gamma_s\rvert$
$x_1 < \gamma_s \ \gamma_c < x_2$	$\pi \ \operatorname{acos}\left(\frac{C\cos(\lvert\gamma_s \ \gamma_c\rvert) \ r_c}{r_p}\right)$	$\lvert\gamma_s\rvert \ \pi/2$	$\lvert q_{ys}\rvert \ \lvert\gamma_s\rvert \ \pi/2$	$x_1 < \gamma_s \ \gamma_c < x_2$	$\pi \ \operatorname{acos}\left(\frac{C\cos(\lvert\gamma_s \ \gamma_c\rvert) \ r_c}{r_p}\right)$	$\pi/2 \ \lvert\gamma_s\rvert \ \lvert q_{ys}\rvert$	$\pi/2 \ \lvert\gamma_s\rvert$
$\gamma_s \ \gamma_c \ x_2$	$\pi/2$	$\lvert\gamma_s\rvert \ \pi/2$	$\lvert q_{ys}\rvert \ \lvert\gamma_s\rvert \ \pi/2$	$\gamma_s \ \gamma_c \ x_2$	$\pi/2$	$\pi/2 \ \lvert\gamma_s\rvert \ \lvert q_{ys}\rvert$	$\pi/2 \ \lvert\gamma_s\rvert$
$x_2 < \gamma_s \ \gamma_c < x_3$	$\operatorname{acos}\left(\frac{r_c \ C\cos(\lvert\gamma_s \ \gamma_c\rvert)}{r_p}\right)$	$\lvert\gamma_s\rvert \ \pi/2$	$\lvert q_{ys}\rvert \ \lvert\gamma_s\rvert \ \pi/2$	$x_2 < \gamma_s \ \gamma_c < x_3$	$\operatorname{acos}\left(\frac{r_c \ C\cos(\lvert\gamma_s \ \gamma_c\rvert)}{r_p}\right)$	$\pi/2 \ \lvert\gamma_s\rvert \ \lvert q_{ys}\rvert$	$\pi/2 \ \lvert\gamma_s\rvert$
$\gamma_s \ \gamma_c \geq x_3$	0			$\gamma_s \ \gamma_c \geq x_3$	0		
γ_s is in Part 4	$\lvert q_{ys}\rvert$	ξ_{start}	ξ_{stop}	γ_s is in Part 4	$\lvert q_{ys}\rvert$	ξ_{start}	ξ_{stop}
$\gamma_s \ \gamma_c \leq x_1$	π	$\lvert\gamma_s\rvert \ \pi/2$	$\lvert q_{ys}\rvert + \lvert\gamma_s\rvert \ \pi/2$	$\gamma_s \ \gamma_c \leq x_1$	π	$\pi/2 + \lvert\gamma_s\rvert \ \lvert q_{ys}\rvert$	$\pi/2 + \lvert\gamma_s\rvert$
$x_1 < \gamma_s \ \gamma_c < x_2$	$\pi \ \operatorname{acos}\left(\frac{C\cos(\lvert\gamma_s \ \gamma_c\rvert) \ r_c}{r_p}\right)$	$\lvert\gamma_s\rvert \ \pi/2$	$\lvert q_{ys}\rvert + \lvert\gamma_s\rvert \ \pi/2$	$x_1 < \gamma_s \ \gamma_c < x_2$	$\pi \ \operatorname{acos}\left(\frac{C\cos(\lvert\gamma_s \ \gamma_c\rvert) \ r_c}{r_p}\right)$	$\pi/2 + \lvert\gamma_s\rvert \ \lvert q_{ys}\rvert$	$\pi/2 + \lvert\gamma_s\rvert$
$\gamma_s \ \gamma_c \ x_2$	$\pi/2$	$\lvert\gamma_s\rvert \ \pi/2$	$\lvert q_{ys}\rvert + \lvert\gamma_s\rvert \ \pi/2$	$\gamma_s \ \gamma_c \ x_2$	$\pi/2$	$\pi/2 + \lvert\gamma_s\rvert \ \lvert q_{ys}\rvert$	$\pi/2 + \lvert\gamma_s\rvert$
$x_2 < \gamma_s \ \gamma_c < x_3$	$\operatorname{acos}\left(\frac{r_c \ C\cos(\lvert\gamma_s \ \gamma_c\rvert)}{r_p}\right)$	$\lvert\gamma_s\rvert \ \pi/2$	$\lvert q_{ys}\rvert + \lvert\gamma_s\rvert \ \pi/2$	$x_2 < \gamma_s \ \gamma_c < x_3$	$\operatorname{acos}\left(\frac{r_c \ C\cos(\lvert\gamma_s \ \gamma_c\rvert)}{r_p}\right)$	$\pi/2 + \lvert\gamma_s\rvert \ \lvert q_{ys}\rvert$	$\pi/2 + \lvert\gamma_s\rvert$
$\gamma_s \ \gamma_c \geq x_3$	0			$\gamma_s \ \gamma_c \geq x_3$	0		
γ_s is in Part 5	$\lvert q_{ys}\rvert$	ξ_{start}	ξ_{stop}	γ_s is in Part 5	$\lvert q_{ys}\rvert$	ξ_{start}	ξ_{stop}
$\gamma_s \ \gamma_c \leq x_1$	π	$\lvert\gamma_s\rvert + \pi/2$	$\lvert q_{ys}\rvert + \lvert\gamma_s\rvert + \pi/2$	$\gamma_s \ \gamma_c \leq x_1$	π	$\lvert\gamma_s\rvert \ \pi/2$	$\lvert q_{ys}\rvert + \lvert\gamma_s\rvert \ \pi/2$
$x_1 < \gamma_s \ \gamma_c < x_2$	$\pi \ \operatorname{acos}\left(\frac{C\cos(\lvert\gamma_s \ \gamma_c\rvert) \ r_c}{r_p}\right)$	$\lvert\gamma_s\rvert + \pi/2$	$\lvert q_{ys}\rvert + \lvert\gamma_s\rvert + \pi/2$	$x_1 < \gamma_s \ \gamma_c < x_2$	$\pi \ \operatorname{acos}\left(\frac{C\cos(\gamma_s \ \gamma_c \ \pi) \ r_c}{r_p}\right)$	$\lvert\gamma_s\rvert \ \pi/2$	$\lvert q_{ys}\rvert + \lvert\gamma_s\rvert \ \pi/2$
$\gamma_s \ \gamma_c \ x_2$	$\pi/2$	$\lvert\gamma_s\rvert + \pi/2$	$\lvert q_{ys}\rvert + \lvert\gamma_s\rvert + \pi/2$	$\gamma_s \ \gamma_c \ x_2$	$\pi/2$	$\lvert\gamma_s\rvert \ \pi/2$	$\lvert q_{ys}\rvert + \lvert\gamma_s\rvert \ \pi/2$
$x_2 < \gamma_s \ \gamma_c < x_3$	$\operatorname{acos}\left(\frac{r_c \ C\cos(\lvert\gamma_s \ \gamma_c\rvert)}{r_p}\right)$	$\lvert\gamma_s\rvert + \pi/2$	$\lvert q_{ys}\rvert + \lvert\gamma_s\rvert + \pi/2$	$x_2 < \gamma_s \ \gamma_c < x_3$	$\operatorname{acos}\left(\frac{r_c \ C\cos(\gamma_s \ \gamma_c \ \pi)}{r_p}\right)$	$\lvert\gamma_s\rvert \ \pi/2$	$\lvert q_{ys}\rvert + \lvert\gamma_s\rvert \ \pi/2$
$\gamma_s \ \gamma_c \geq x_3$	0			$\gamma_s \ \gamma_c \geq x_3$	0		
γ_s is in Part 6	$\lvert q_{ys}\rvert$	ξ_{start}	ξ_{stop}	γ_s is in Part 6	$\lvert q_{ys}\rvert$	ξ_{start}	ξ_{stop}
$\gamma_s \ \gamma_c \leq x_1$	π	$\lvert\gamma_s\rvert \ \pi/2$	$\lvert\gamma_s\rvert \ \pi/2 + \lvert q_{ys}\rvert$	$\gamma_s \ \gamma_c \leq x_1$	π	$3/2\cdot\pi + \lvert\gamma_s\rvert \ \lvert q_{ys}\rvert$	$3/2\cdot\pi + \lvert\gamma_s\rvert$
$x_1 < \gamma_s \ \gamma_c < x_2$	$\pi \ \operatorname{acos}\left(\frac{C\cos(\gamma_s \ \gamma_c \ \pi) \ r_c}{r_p}\right)$	$\lvert\gamma_s\rvert \ \pi/2$	$\lvert\gamma_s\rvert \ \pi/2 + \lvert q_{ys}\rvert$	$x_1 < \gamma_s \ \gamma_c < x_2$	$\pi \ \operatorname{acos}\left(\frac{C\cos(\gamma_s \ \gamma_c \ \pi) \ r_c}{r_p}\right)$	$3/2\cdot\pi + \lvert\gamma_s\rvert \ \lvert q_{ys}\rvert$	$3/2\cdot\pi + \lvert\gamma_s\rvert$
$\gamma_s \ \gamma_c \ x_2$	$\pi/2$	$\lvert\gamma_s\rvert \ \pi/2$	$\lvert\gamma_s\rvert \ \pi/2 + \lvert q_{ys}\rvert$	$\gamma_s \ \gamma_c \ x_2$	$\pi/2$	$3/2\cdot\pi + \lvert\gamma_s\rvert \ \lvert q_{ys}\rvert$	$3/2\cdot\pi + \lvert\gamma_s\rvert$
$x_2 < \gamma_s \ \gamma_c < x_3$	$\operatorname{acos}\left(\frac{r_c \ C\cos(\gamma_s \ \gamma_c \ \pi)}{r_p}\right)$	$\lvert\gamma_s\rvert \ \pi/2$	$\lvert\gamma_s\rvert \ \pi/2 + \lvert q_{ys}\rvert$	$x_2 < \gamma_s \ \gamma_c < x_3$	$\operatorname{acos}\left(\frac{r_c \ C\cos(\gamma_s \ \gamma_c \ \pi)}{r_p}\right)$	$3/2\cdot\pi + \lvert\gamma_s\rvert \ \lvert q_{ys}\rvert$	$3/2\cdot\pi + \lvert\gamma_s\rvert$
$\gamma_s \ \gamma_c \geq x_3$	0			$\gamma_s \ \gamma_c \geq x_3$	0		

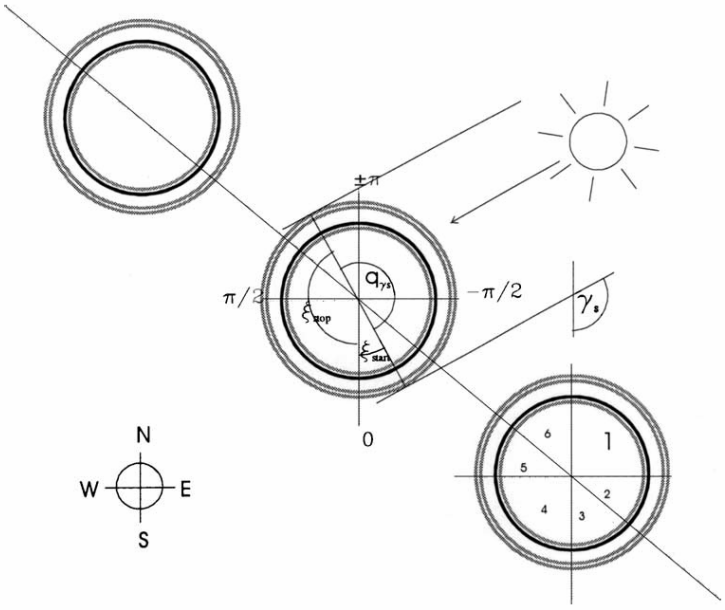

Fig. 7. Relationship between the solar azimuth, γ_s, the beam exposure angle, $q_{\gamma s}$, and the integration borders ξ_{start} and ξ_{stop}, when γ_s is in part 1 and when the pipes are placed vertically.

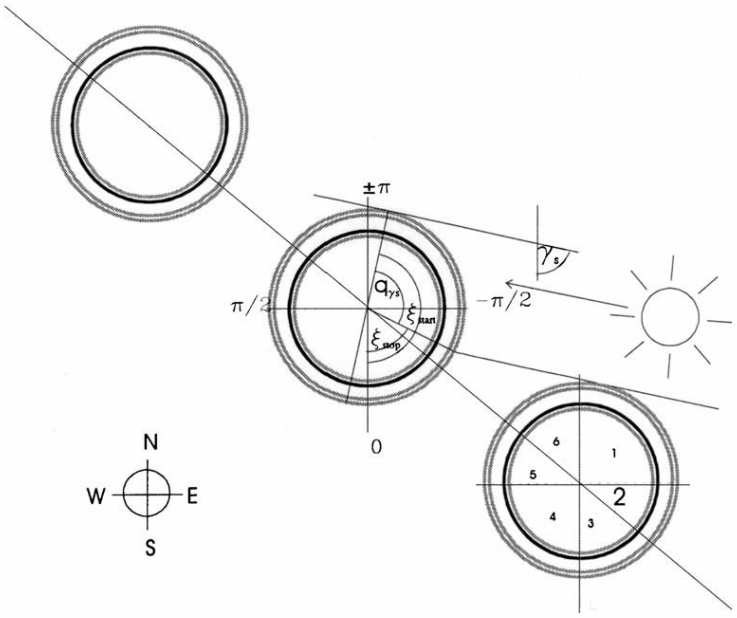

Fig. 8. Relationship between the solar azimuth, γ_s, the beam exposure angle, $q_{\gamma s}$, and the integration borders ξ_{start} and ξ_{stop}, when γ_s is in part 2 and when the pipes are placed vertically.

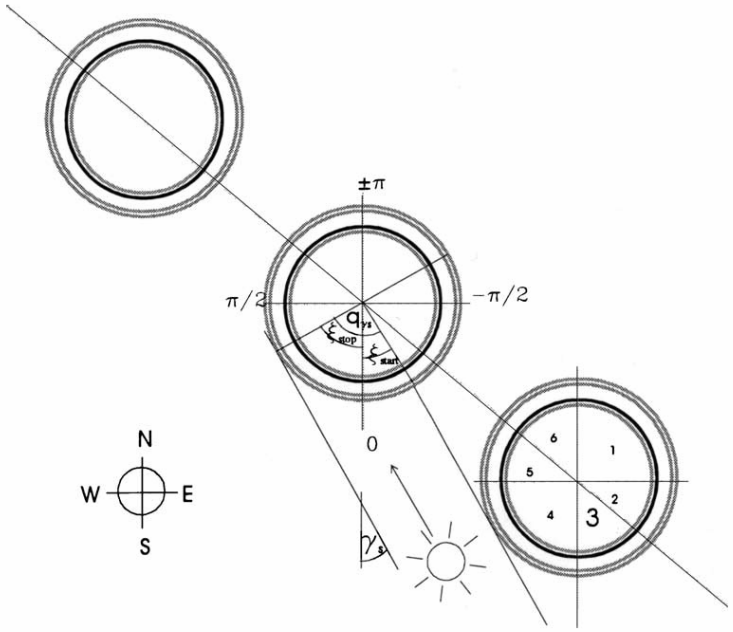

Fig. 9. Relationship between the solar azimuth, γ_s, the beam exposure angle, $q_{\gamma s}$, and the integration borders ξ_{start} and ξ_{stop}, when γ_s is in part 3 and when the pipes are placed vertically.

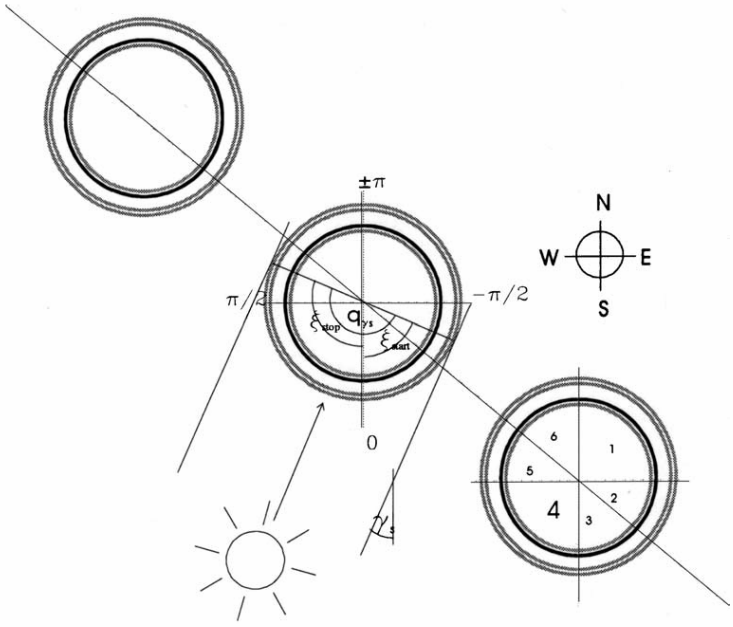

Fig. 10. Relationship between the solar azimuth, γ_s, the beam exposure angle, $q_{\gamma s}$, and the integration borders ξ_{start} and ξ_{stop}, when γ_s is in part 4 and when the pipes are placed vertically.

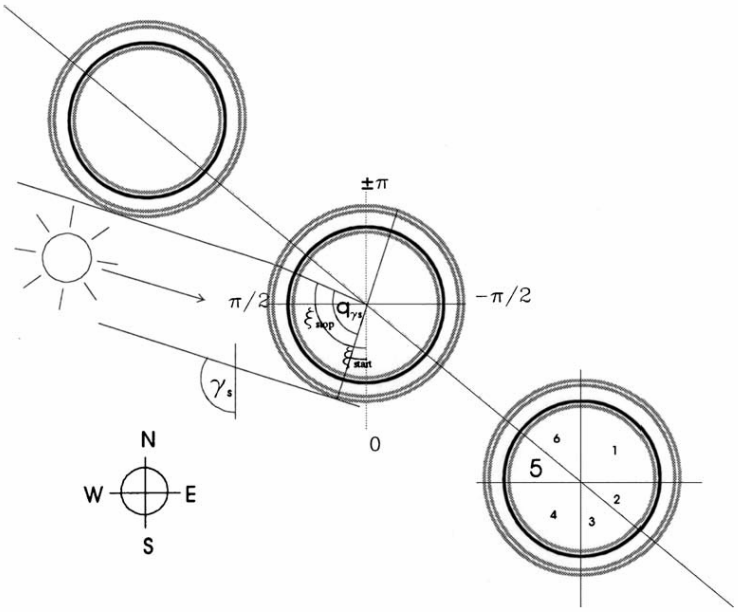

Fig. 11. Relationship between the solar azimuth, γ_s, the beam exposure angle, $q_{\gamma s}$, and the integration borders ξ_{start} and ξ_{stop}, when γ_s is in part 5 and when the pipes are placed vertically.

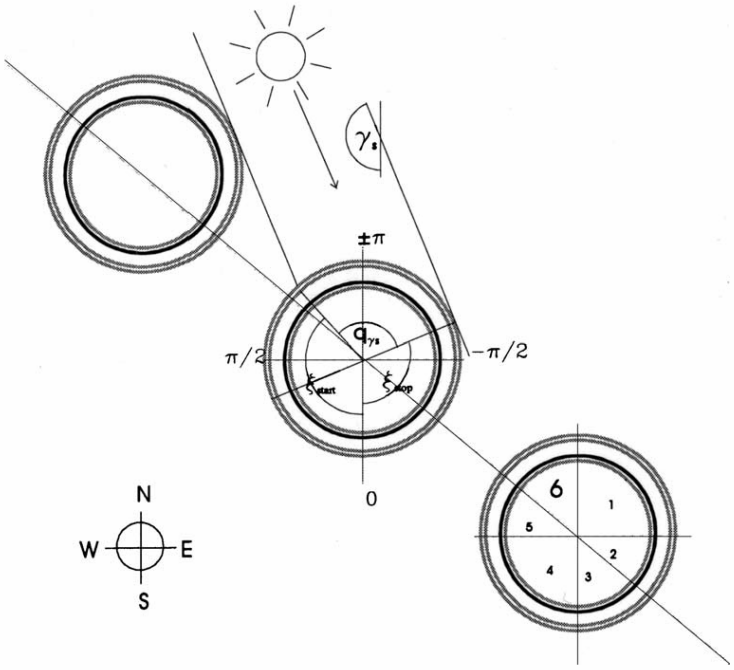

Fig. 12. Relationship between the solar azimuth, γ_s, the beam exposure angle, $q_{\gamma s}$, and the integration borders ξ_{start} and ξ_{stop}, when γ_s is in part 6 and when the pipes are placed vertically.

integrals could be solved analytically, except the integral in Eq. (21), which was solved by using the trapezoidal formula for solving integrals numerically. Three hundred and sixty integration steps were used in the numerical integration.

The program is based on weather data with hourly data for global radiation, diffuse radiation on horizontal and outdoor temperature. However, the incident angle and thus the collector performance were calculated every half hour.

4. Measurements

The performance of the collector was measured in an outdoor test facility where the inlet temperature, the outlet temperature and the volume flow-rate were measured. The temperatures were measured with copper-constantan thermocouples (Type TT) and the volume flow rate was measured with a HGQ1 flow meter. A 31% glycol/water mixture was used in the solar-collector loop. Further, the global radiation and the diffuse radiation on the horizontal were measured with two Kipp&Zonen CM11 pyranometers.

The power from the solar collector was determined from the measurements by:

$$P_u = \dot{V}\rho C_p\left(T_{out,hot} - T_{in,cold}\right) + \frac{C_{p,col}\left(T_{fm}^{t} - T_{fm}^{t-\Delta t}\right)}{\Delta t} \tag{25}$$

5. Comparing the model predictions with measurements

Two periods of 6 days (25/7 30/7 2003 and 12/8 7/8 2003) have been selected for validating the computer model of the collector. In Fig. 13, the global irradiance, the ambient temperature, the inlet temperature to the collector and the volume-flow rate in the collector are shown. These values are used as input data to the model.

The necessary data for describing the collector are shown in Table 4. The heat loss coefficient, k_0, was determined from efficiency measurements and split into two parts for the evacuated tubes and the manifold pipes respectively (Shah et al. [5]). F' was calculated from theory (Duffie and Beckman [7], Incropera and de Witt [8]) and $\tau\alpha_e$ and a were calculated with a simulation program for determining optical properties (Svendsen and Jensen [9]). The collector's heat-capacity was calculated from the geometrical information.

Table 4
Data describing the collector in the model

No. of pipes	L (m)	r_c (m)	r_p (m)	C (m)	k_0 (W/m^{2}K)	F' ( )	$\tau\alpha_e$ ( )	$C_{p,col}$ (J/K)	a ( )
14	1.47	0.0235	0.0185	0.067	2.09	0.98	0.856	27614	3.8

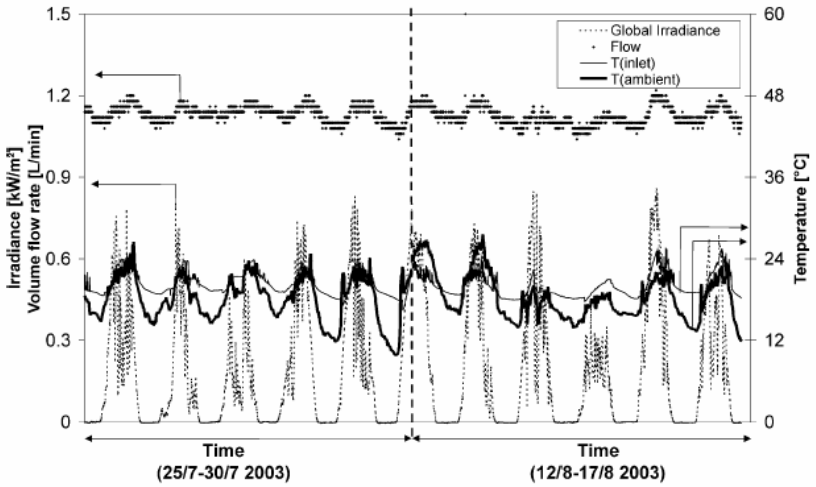

Fig. 13. Total solar irradiance on the collector plane, ambient temperature, collector's inlet temperature and collector's volume flow rate during the test periods.

In Fig. 14 the measured and calculated collector outlet temperatures are compared. It can be seen that there is a good degree of similarity between the measured and calculated temperatures.

6. Theoretical investigations

In this section, the model will be used for theoretical investigations. Only vertically-placed pipes will be analysed, as the model is yet unfit to calculate for tilted pipes. The collector's performance is investigated for two locations:

- Copenhagen, Denmark, lat. 56°N, yearly average ambient-temperature: 7.8 °C. Weather data: DRY (Lund [10]).
- Uummannaq, Greenland, lat. 71°N, yearly average ambient-temperature: −4.2 °C. Weather data: TRY (Kragh [11]).

Fig. 15 shows the sum of the solar radiation on the front and the back of vertical planes with different orientations. For Copenhagen, there is symmetry around 0° (south) whereas for Uummannaq the minimum solar radiation on the plane is around −30° (towards the east). The reason for this asymmetrical behaviour is that there is a mountain east of Uummannaq, which reduces the radiation coming from the east.

As a function of the collector's azimuth, Fig. 16 shows the utilized solar energy per tube in a panel assuming a tube centre distance of 0.067 m and a constant solar-collector's fluid temperature throughout the year of 50 °C. For both Uummannaq and Copenhagen, there is an optimum at a collector azimuth of about 45° 60°. The

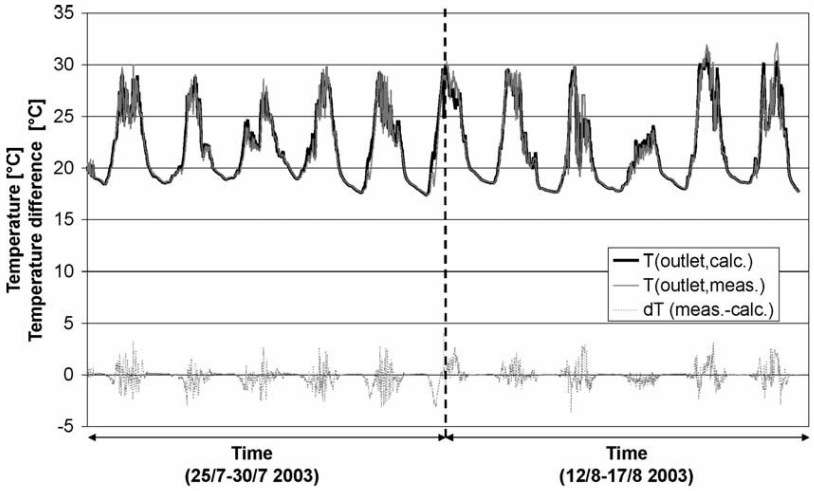

Fig. 14. Measured and calculated outlet temperatures for the test periods.

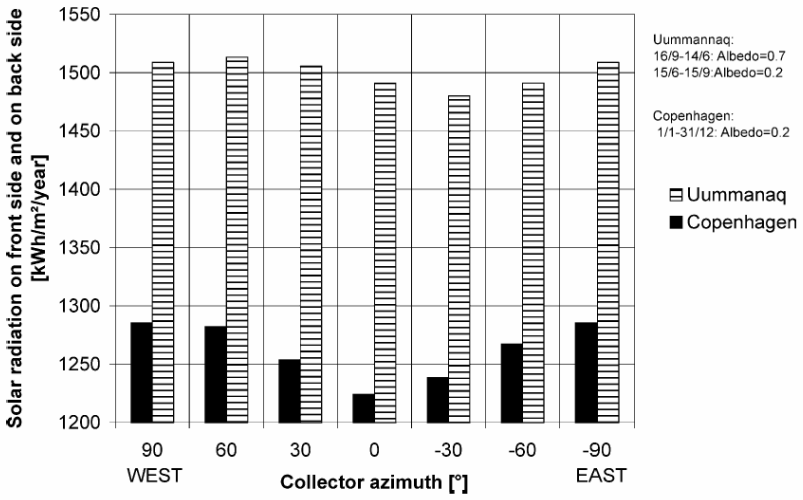

Fig. 15. Solar radiations on the front and the back of vertical planes with different orientations.

results are caused both by the distribution of solar radiation and by the higher afternoon temperatures.

Fig. 17 shows the utilized solar-energy per tube as a function of the tube centre distance for a collector fluid temperature of 50 °C. For both locations, the utilized energy increases for tube centre distances up to 0.2 m, which is due to the reduced shaded areas. For larger distances, the utilized energy decreases again, due to the increasing heat loss from the manifold pipes.

For the two locations, Figs. 18 and 19 show the utilized solar-energy per tube as a function of the collector azimuth and the tube centre distance for a collector fluid

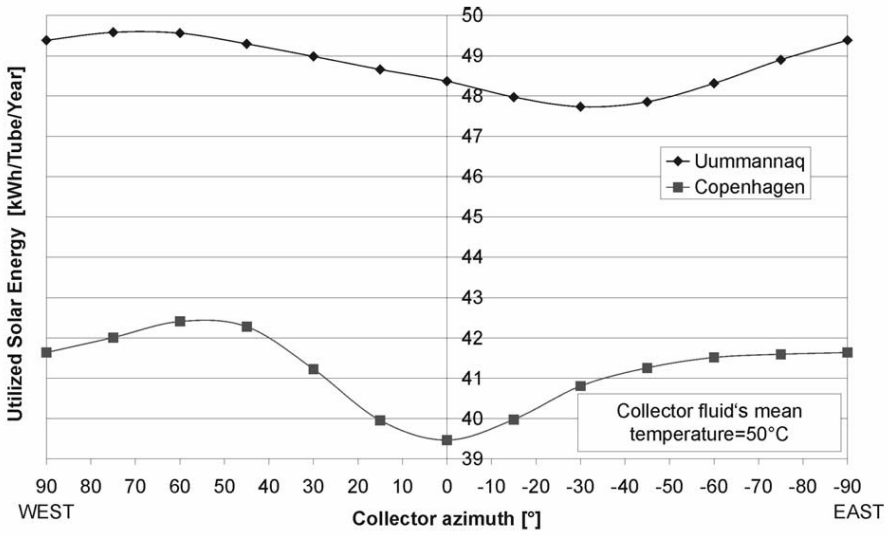

Fig. 16. Utilized solar-energy per tube as a function of the collector's azimuth. Tube centre distance = 0.067 m.

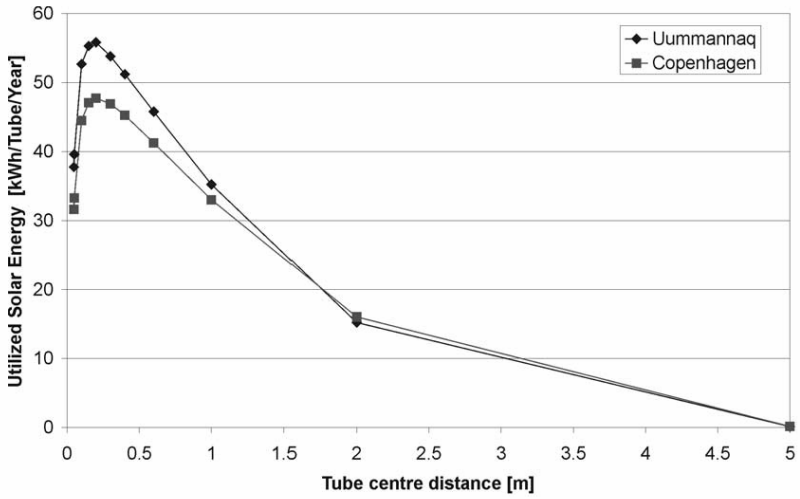

Fig. 17. Utilized solar-energy per tube as a function of the tube centre distance for a collector fluid mean-temperature of 50 °C.

mean temperature of 50 °C. Here it can be seen that the tendencies in Fig. 16 are true for tube distances in the range of 0.047 0.3 m.

Finally Figs. 20 and 21 show the utilized solar-energy per m^2 as a function of the collector-fluid's mean temperature assuming a tube centre distance of 0.047 m and a collector azimuth of 50°. Further, the thermal performance of the newest (Vejen et al. [12]) Arcon HT flat-plate collector is shown. This collector represents the state of the art of collectors for solar-heating plants. The Arcon HT flat-plate collector is

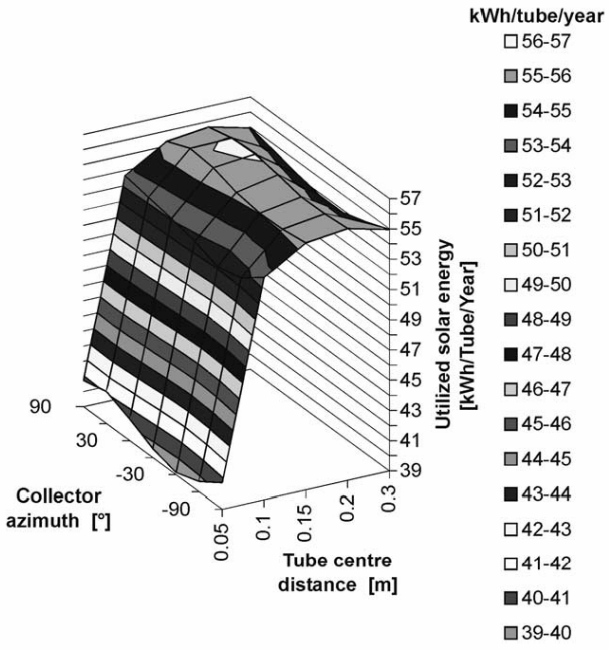

Fig. 18. Uummannaq: Utilized solar-energy per tube as a function of the collector's azimuth and the tube centre distance. Collector's fluid mean-temperature: 50 °C.

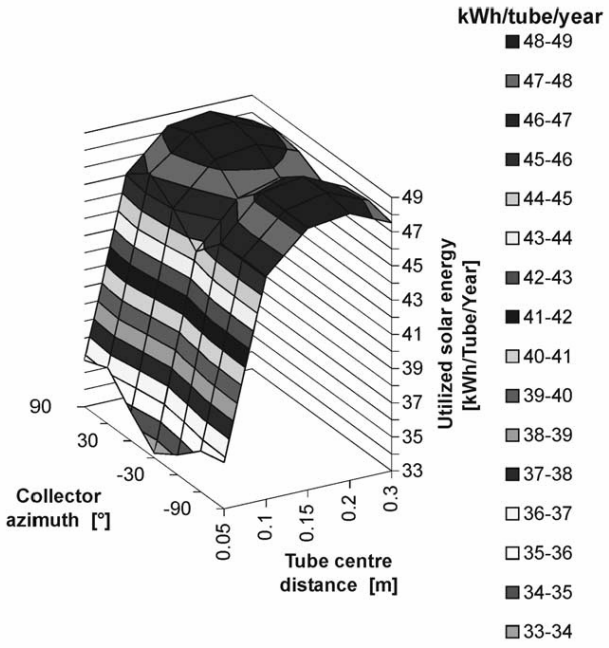

Fig. 19. Copenhagen: Utilized solar-energy per tube as a function of the collector's azimuth and the tube centre distance. Collector's fluid mean-temperature: 50 °C.

facing south and tilted at 45° in Copenhagen. In Uummannaq the Arcon HT flat-plate collector is facing south and tilted at 60°.

It can be difficult to compare the thermal performances of flat-plate collectors and tubular collectors as the effective area of a flat plate collector typically is defined as the transparent area of the glass cover and the effective area of a tubular collector can be defined in many ways. In the present comparison, having a tube centre distance of 0.047 m eliminates this problem. This means that there is no air-gap between the tubes and the outer tube cross-section area ($=L\cdot 2\cdot r_c\cdot N$) directly corresponds to the transparent area of a flat-plate collector.

In Figs. 20 and 21, it is interesting that the Arcon collector is the best performing collector under Copenhagen conditions, whereas the thermal performance of the evacuated tubular collector based on the outer tube cross-section area, is the highest under the Uummannaq conditions. The reason for the change in the ranking of the

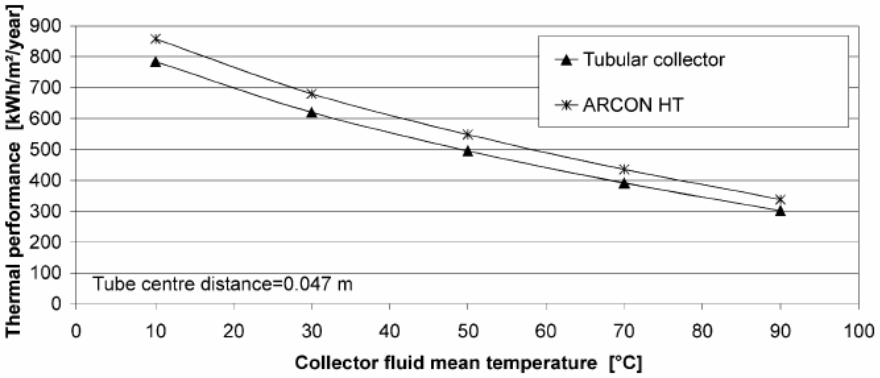

Fig. 20. Copenhagen: Utilized solar-energy per m^2 as a function of the collector's fluid mean-temperature. For the ARCON HT flat-plate collector, the area in consideration is defined as the transparent area of the cover plate and, for the tubular collector, the considered area is the outer-tube's cross section area

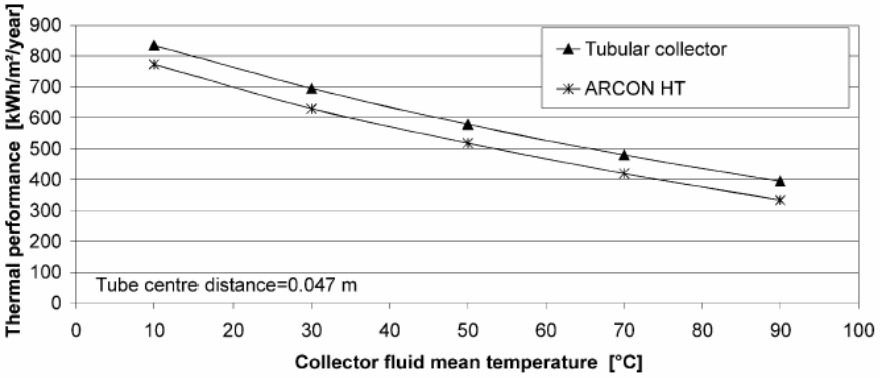

Fig. 21. Uummannaq: Utilized solar-energy per m^2 as a function of the collector's fluid mean-temperature. For the ARCON HT flat-plate collector, the area in consideration is defined as the transparent area of the cover plate and, for the tubular collector, the considered area is the outer-tube's cross section area

collectors is that the tubular collector is not optimally tilted in Copenhagen but also that there is much more solar radiation "from all directions" in Uummannaq and this radiation can be utilized with the tubular collector.

7. Discussion and conclusion

A prototype collector with parallel-connected evacuated double glass tubes is investigated theoretically and experimentally. The collector has a tubular absorber and can thus utilize solar radiation coming from all directions. The collector performance is measured in an outdoor test facility.

Further, a theoretical model for calculating the thermal performance is developed. In the model, the flat-plate collector performance equations have been integrated over the whole absorber circumference. In this way, the transverse incident-angle modifier is eliminated. Also, the model determines the shading of the tubes as a function of the solar azimuth in order to calculate the energy from the beam radiation correctly. The calculation of the energy from the diffuse and ground-reflected radiation is based on an isotropic diffuse sky model.

The calculations with the model are compared with measured results and there is a good degree of similarity between the measured and calculated results.

The model is used for theoretical investigations on vertically-placed pipes placed in Copenhagen, Denmark and in Uummannaq, Greenland. For both locations, the results show that to achieve the highest thermal performance the tube distance should be about 0.2 m and the collector azimuth should be about 45 60° towards the west. The thermal performance of the evacuated solar collector is also compared to the thermal performance of the Arcon HT flat-plate solar collector. These results show that the Arcon collector is the best performing collector under Copenhagen conditions, whereas the performance of the evacuated tubular collector is the highest under the Uummannaq conditions. The reason is that the tubular collector is not optimally tilted in Copenhagen but also that there is much more solar radiation "from all directions" in Uummannaq and this radiation can be utilized with the tubular collector. It is therefore concluded that the collector design is very promising especially for high latitudes.

The theoretical results presented in this paper are based on a collector model, which needs to be further developed. First of all, the model must be able to calculate for tilted pipes. The reflections between the pipes must be included in the model and also an anisotropic diffuse-sky model should be included. This extended model must of course be thoroughly validated with measurements.

Finally, though the collector design seems very promising the collector reliability and durability must be examined before any final conclusions can be drawn.

Acknowledgements

The study is financed by the VILLUM KANN RASMUSSEN FOUNDATION.

References

[1] Barrett AL, et al. Thermal modelling of evacuated tubular solar-collectors. Solar 88, Proceedings of the 1988 annual meeting of the American Solar Energy Society, 1986. 505 510.
[2] Qin L, Furbo S. Evaluation of evacuated tubular solar-collectors for large SDHW systems and combined space-heating systems. Proceedings of NorthSun99, Edmonton, Alberta, Canada, 11 14 August 1999.
[3] Perez R, et al. Calculating solar radiation received by tubular solar-energy collectors. Solar Engineering 1995;I:699 704.
[4] Lart S. (2000) Development of a thermal performance test for an Integrated Collector-Storage Solar Water-Heating System. pp. 90 100. PhD thesis. Division of Mechanical Engineering and Energy Studies. University of Wales Cardiff.
[5] Shah LJ, et al. Thermal performance of evacuated tubular collectors utilizing solar radiation from all directions. Proceedings of ISES Solar World Congress, Gothenburg, Sweden, 16 19 June (in press).
[6] Pyrko J. A model of the average solar radiation for the tubular collector. Int J Solar Energy 1984;32: 563 5.
[7] Duffie JA, Beckman WA. Solar engineering of thermal processes, 2nd ed. New York: Wiley Interscience; 1991.
[8] Incropera FP, de Witt DP. Introduction to heat transfer. Singapore: John Wiley & Sons; 1990.
[9] Svendsen S, Jensen FF. Soltransmittans. Lecture note. Technical University of Denmark: Thermal Insulation Laboratory; 1994.
[10] Lund H. The Design Reference Year User Manual. Report of IEA-SHC Task 9. Report 274. Technical University of Denmark: Thermal Insulation Laboratory; 1995.
[11] Kragh J, et al. Grønlandske vejrdata. Nuuk. Uummannaq. Technical University of Denmark: Department of Civil Engineering; 2002 (November 2002).
[12] Vejen NK, Furbo S, Shah LJ. Development of 12.5 m^2 solar-collector panel for solar heating plants. Proceedings of ISES Solar World Congress, Gothenburg, Sweden, 16 19 June 2003.

Bilag 4: Artikel optaget i Sletten. Avisen ved DTU. Nr. 7/2003.

Solvarme i Grønland

Stort potentiale for udnyttelse af solvarme i Grønland

Solenergi er den reneste og naturligste energiform, vi overhovedet har. Solindfaldet er så stort på kloden – og i Grønland – at der er mulighed for at udnytte solenergi i stort omfang.

Solenergi kan udnyttes til at reducere brugen af fossile brændsler, f. eks. ved at anvende solvarmeanlæg til boliger. Solvarmeanlæg kan for eksempel benyttes til brugsvandsopvarmning eller til kombineret rumopvarmning og brugsvandsopvarmning.

Det årlige antal timer med mulighed for solskin er stort set det samme, uanset hvor på kloden vi befinder os.

Fordelingen af solstrålingen over årets måneder afhænger stærkt af breddegraden: Jo højere mod nord vi befinder os, des større del af solindfaldet finder sted i sommermånederne. Solens bane over himlen er også stærkt afhængig af breddegraden. Jo højere mod nord vi befinder os, des lavere står solen på himlen, og des større er dagsvariationen af retningen til solen. Nord for polarcirklen er solen således om sommeren på himlen 24 timer i døgnet, og retningen til solen gennemløber i løbet af 24 timer alle kompassets retninger.

Solindfaldet på en flade afhænger stærkt af fladens lokalitet, orientering og hældning. I København (breddegrad 56°) er solindfaldet størst på en sydvendt 40° hældende flade, mens solindfaldet i Sisimiut i Grønland (breddegrad 67°) er størst på en sydvendt 60° hældende flade. Solindfaldet i København og i Sisimiut er stort set ens på de optimalt hældende flader, ca. 1160 kWh/m²/år.

Solvarmeanlæg

Anvendelsen af solvarmeanlæg varierer stærkt fra land til land. I Europa er Østrig og Grækenland, efterfulgt af Danmark, Tyskland og Schweiz, de lande hvor der er installeret flest kvadratmeter solfangere pr. indbygger. Der er ingen entydig sammenhæng mellem disse landes (relative) succes inden for solvarmeområdet, solindfald og energiprisniveau. Der er eller har været en aktiv solvarmeindustri og politisk opbakning til solvarmeanlæg i form af støtte til forskning, udvikling og demonstrationsprojekter i alle de nævnte lande. Derudover er der, eller har der været, økonomisk støtte til opførelse af solvarmeanlæg.

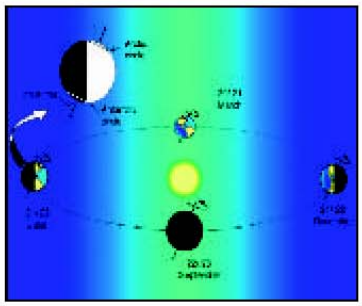

Jordens bane i forhold til solen.

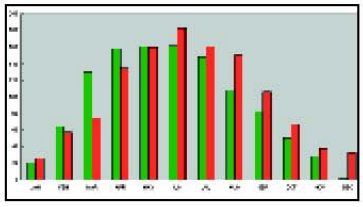

Solindfald (kWh/m²) på optimalt hældende flader i Sisimiut (grøn) og i København (rød) januar - december.

Et vakuumrør bestående af et dobbeltglasrør

Testsolfanger baseret på vakuumglasrør.

Solvarmeanlægs rentabilitet afhænger stærkt af energiprisniveauet og energiprisudviklingen. I Danmark har typiske solvarmeanlæg økonomiske tilbagebetalingstider på ca. 10 år og energimæssige tilbagebetalingstider på ca. et år, og der er inden for en forholdsvis kort tidshorisont mulighed for teknologisk udvikling så den økonomiske tilbagebetalingstid når ned på ca. fem år.

Solvarme i Grønland

Der er et antal barrierer for udnyttelse af solvarme i Grønland. Blandt andet kan det nævnes at:

- energipriserne for fossilt brændsel er lavere i Grønland end i Danmark.
- der ikke er en solvarmeindustri i Grønland.
- der ikke er solvarmeuddannede VVS-installatører i Grønland (eller kun få).
- der ikke er udviklet solvarmeanlæg, som er specielt velegnede til Grønland.

Der er dog også en række forhold, som gør, at solvarmeanlæg er mere velegnede i Grønland end i Danmark. Blandt andet kan nævnes at:

- sne reflekterer en meget stor del af solstrålingen. Derfor er solindfaldet på tagflader i perioder med sne på jorden meget stort i Grønland.
- der er rumopvarmningsbehov i sommerperioden med meget sol i Grønland.
- temperaturen af det kolde brugsvand, der tilføres boligerne, er lavere i Grønland end i Danmark.
- den optimale solfangerhældning fra vandret er større i Grønland end i Danmark. Det bevirker, at solfangereffektiviteten for den samme solfanger er højere i Grønland end i Danmark.
- der er mere solindstråling fra "alle retninger" i Grønland end i Danmark. I denne forbindelse kan det nævnes, at de forholdsvis billige kinesiske masseproducerede vakuumglasrør sandsynligvis er specielt velegnede til grønlandske forhold, da de kan udnytte solstråling fra alle retninger, dvs. de kan udnytte solstrålingen i alle døgnets lyse timer, hvis blot rørene placeres lodret med frit udsyn til alle sider.

Vakuumrørsolfangere

Vakuumrørsolfangere har i mange år været markedsført i Europa og i USA. Da der er vakuum i glasrørene, er varmeta-

DTU udstiller i lufthavnen

Fra 1. april - 5. maj deltager DTU i udstillingen Future & Technology i Københavns Lufthavn. Fra DTU vil man bl.a. kunne blive klogere på den seneste forskning inden for laserteknologi og micromanufacturing på IPL, telekommunikation på COM, ansigtsmodellering og ansigtsgenkendelse på IMM og satellitnavigation, solfangere mv. på Center for Arktisk Teknologi/BYG/Ørsted.

Ud over DTU deltager bl.a. Intel, Center for Avanceret Teknologi (CAT), Symbion, Alexandra Instituttet og Instituttet for Fremtidsforskning.

Udstillingen er delt op i tre zoner, og DTU kan opleves i Zone 1 over for den store Tax Free butik mellem Finger B og C - også kaldet Nytorv. Så for at se udstillingen kræves det altså, at man skal ud at flyve i løbet af den næste måneds tid. Ca. 40.000 passagerer rejser hver dag igennem lufthavnen, så der er tale om en ganske pæn eksponering af nogle af DTU's forskningsområder.

Studerende fra DTU bemander udstillingen, som er åben hver dag fra kl. 6.30 - 19.00. Løn til de studerende samt øvrige udgifter til plancher osv. betales af lufthavnen og Intel, som sponserer udstillingen. *amd*

Udviklingen af solvarme er en af de temaer, der er så interessante, at det blev fundet værdigt til at repræsentere DTU på udstillingen Future & Technology i lufthavnen. Her fortæller centerleder Arne Villumsen om et af de andre projekter, som Center for Arktisk Teknologi samarbejder med Ørsted•DTU om, nemlig at levere information om havisen til skibe, der sejler i de nordlige farvande. Nina Holmboe er en af de 23 studerende, der bemander standene. (Foto: Tine Kortenbach)

bet fra absorberne på grund af konvektion og varmeledning meget lille. Varmetabskoefficienten for vakuumrørsolfangere er derfor meget mindre end varmetabskoefficienten for almindelige plane solfangere.

I modsætning til almindelige plane solfangere kan vakuumrørsolfangere udnytte solstråling specielt godt, når indfaldsvinklen er stor. Årsagen til dette forhold er dels refleksionsforholdene mellem glasrørene, dels glasrørenes cylinderformede overflade, som tillader, at solstråler transmitteres gennem glasset selv ved store indfaldsvinkler på tværs af glasrørene.

Vakuumrørsolfangere udnytter solens stråler specielt godt ved høje solfangervæsketemperaturer, ved lave udelufttemperaturer, ved små bestrålingsstyrker og ved store indfaldsvinkler.

Billige solfangere fra Østen

For nylig har en række kinesiske firmaer startet masseproduktion af forholdsvis billige vakuumrørsolfangere. I Asien har vakuumrørsolfangere derfor nået så lavt et prisniveau og så høj en effektivitet, at det er blevet attraktivt at benytte disse højeffektive solfangere i stedet for almindelige plane solfangere.

De mest anvendte kinesiske solfangere er baseret på dobbeltglasrør med vakuum i mellemrummet mellem glassene. De udvendige overflader af de inderste glasrør har en høj absorptans og en lav emittans. Når solen skinner på glasrøret, bliver det indvendige glasrør derfor meget varmt. Varmen fra det indvendige glasrør kan overføres til solfangervæsken på forskellige måder: Enten kan solfangervæsken strømme igennem det indvendige glasrør i direkte kontakt med glasvæggen, eller solfangervæsken kan strømme igennem et metalrør, som er i god termisk kontakt med det indvendige glas. Der er forskellige muligheder for at sammenkoble sådanne vakuumrør til et solfangerpanel og dermed også forskellige muligheder for solfangervæskens passage gennem solfangerpanelet.

Studenterprojekter

I forbindelse med kurset Arktisk Teknologi (Kursus nr. 11422) begyndte undersøgelserne vedrørende solvarme i Grønland. I 1999 tog et hold studerende op til Sisimiut og opførte et solvarmeanlæg med plane solfangere ved Bygge- og Anlægsskolen, og allerede året efter, også i forbindelse med Arktisk Teknologi, blev endnu et solvarmeanlæg opført. Man kan læse om anlæggene på hjemmesiden http://www.byg.dtu.dk/greenland/. Her ligger der også informationer og præsentationer fra Arktisk Solenergi Symposium, som blev afholdt i efteråret 2001.

For nylig er et eksamensprojekt ved BYG-DTU med titlen Design and Analysis of an Evacuated Tubular Collector afsluttet, hvor en første forsøgssolfanger baseret på de kinesiske vakuumrør blev opbygget (se foto), og i et igangværende eksamensprojekt, "Vakuumrørsolfangere til Grønland", undersøges grønlandske solstrålingsforhold samt forventede ydelser for vakuumrørsolfangere under grønlandske forhold.

Yderligere er tre studerende i gang med et midtvejsprojekt, "Vakuumrørsolfangere og Sæsonvarmelagring under Arktiske Forhold", som de har kombineret med kurset Arktisk Teknologi. Under deres feltstudier i Grønland til sommer skal de tre midtvejsstuderende bl.a. undersøge installationsforhold med fokus på optimal hældning og orientering af vakuumrørsolfangerne.

Vakuumrørskonceptet er ikke kun interessant for arktiske forhold. Det er interessant for alle klimaforhold og for de fleste typer af solvarmeanlæg. Det er bl.a., fordi der med optimalt designede vakuumrørsolfangere er mulighed for at forbedre solvarmeanlægs rentabilitet mærkbart. Det kræver grundig forskning, før det er muligt at udforme solfangerne på denne måde.

Der er mange andre muligheder for teknologiske forbedringer af solvarmeanlæg, og vi håber derfor på at kunne fortsætte de mange studenterprojekter og videreføre forskningen vedrørende vakuumrørsolfangere og solvarmeanlæg.

Louise Jivan Shah, forskningsadjunkt og Simon Furbo, lektor BYG•DTU

Bilag 5: Overheads til foredraget “Thermal Performance of Evacuated Tubular Collectors utilizing Solar Radiation from all Directions”.

ISES Solar World Congress, June 14-19, 2003.

BYG·DTU
Department of Civil Engineering
DTU

Thermal Performance of Evacuated Tubular Collectors utilizing Solar Radiation from all directions

L. J. Shah, S. Furbo & S. Antvorskov
Department of Civil Engineering
Technical University of Denmark
Building 118, DK-2800 Kgs. Lyngby
DENMARK
E-mail: ljs@byg.dtu.dk

BYG·DTU
DTU

The Evacuated Tubular Collector

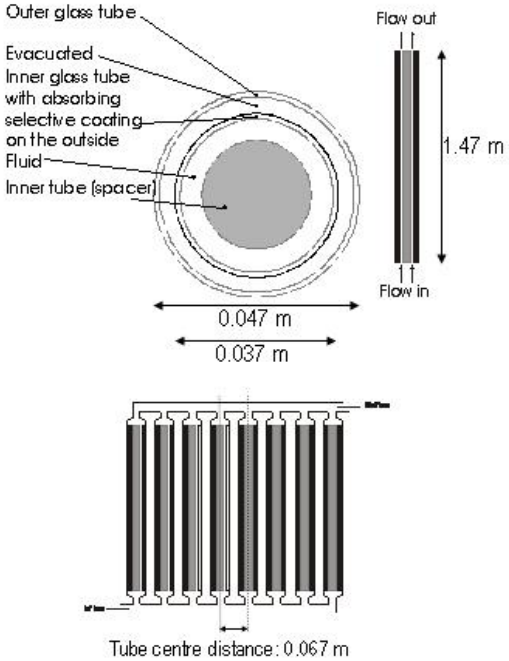

Prototype collector. Tilt: 45°

Investigations

- **Theoretical:**
  - Developed collector performance theory that include:
    - Treatment of solar radiation from all directions (also from the "back" of the collector)
    - Shadow effects from neighbouring tubes
    - Treatment of tubular geometry and incident angle modifiers

- **Experimental:**
  - Thermal performance
  - Efficiency expression

Theory

The collector performance equation is integrated over the pipe circumference:

$$P_u = \int_{-\pi}^{\pi} \left(P_b + P_d + P_{gr} - P_{loss} \right) \cdot d\xi$$

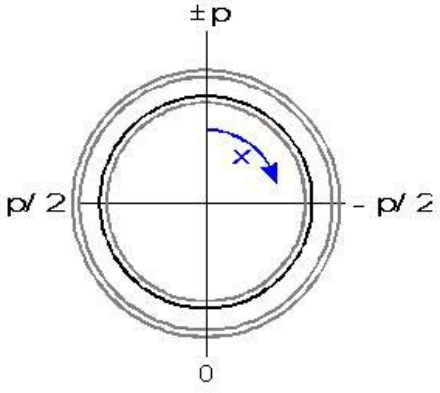

$$P_b = A_b \cdot F' \cdot (\tau\alpha)_e \cdot K_\theta \cdot R_b \cdot G_b$$
$$P_d = A_a \cdot F' \cdot (\tau\alpha)_e \cdot K_{\theta,d} \cdot F_{c-s} \cdot G_d$$
$$P_{gr} = A_a \cdot F' \cdot (\tau\alpha)_e \cdot K_{\theta,gr} \cdot F_{c-gr} \cdot G_{gr}$$
$$P_{loss} = A_a \cdot U_L \cdot (T_{fm} - T_a)$$

The Model

- View factor between tubes
  - depending on tube geometry and distance
- View factors to sky and ground
  - integrating over the tube circumference
  - minus view factor to adjacent tubes
- The energy from beam radiation
  - size and position of the non shaded area as a function of solar azimuth
  - integrating over this area
- The energy from diffuse radiation
  - isotropic model
- The energy from ground reflected radiation
  - albedo
- Heat loss
  - based on a heat loss coefficient for the total absorber area

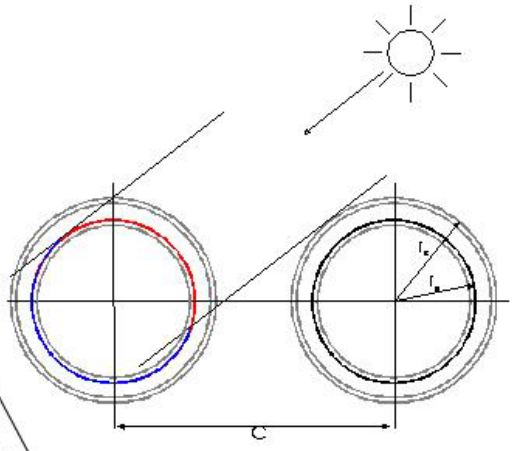

All included in a simulation program that can calculate the thermal performance of the tubular collector on a yearly basis.

Measurements

Efficiency expression:

- G_{tot} > 800 W/m²
- Incidence angle on collector aperture < 20°
- $G_{dif} < 0.22 \cdot G_{tot}$
- Stationary conditions during at least 15 min.
- Based on outer tube cross area (0.97 m²)

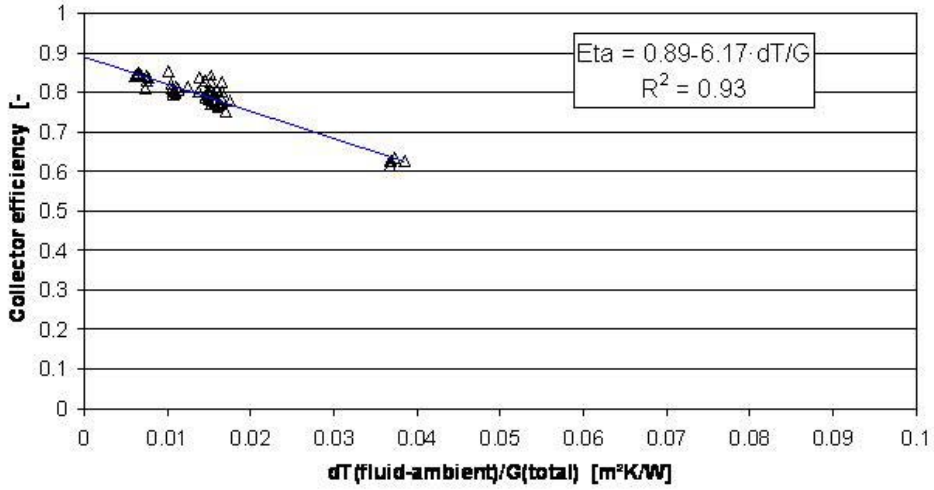

Comparison of measured and calculated results

- **Model input:**
  - Global irradiance, diffuse irradiance and ambient temperature
  - Inlet temperature and volume flow rate
  - Geometry, F' and $\tau\alpha_e$
- **Model output:**
  - Outlet temperature

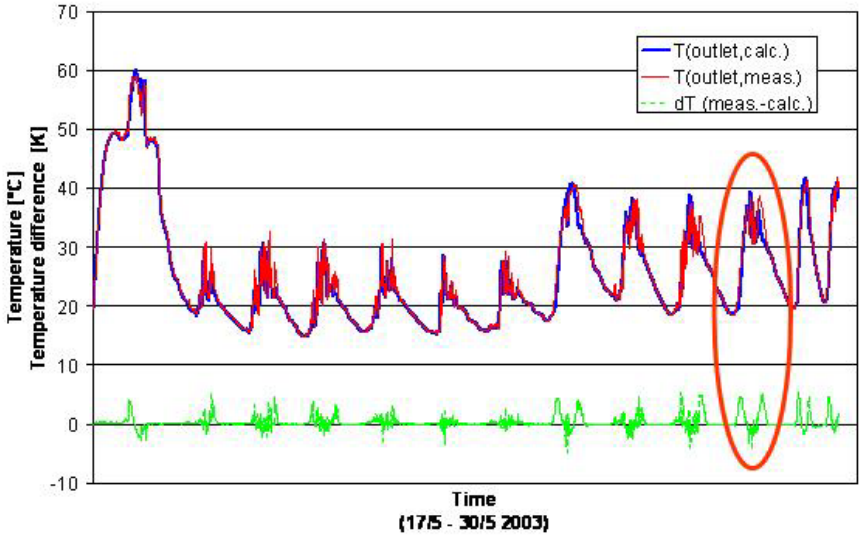

Comparison of measured and calculated results

- Problem:
  - Systematic error in the mornings/evenings
- Reason:
  - Shadow model not developed for tilted pipes

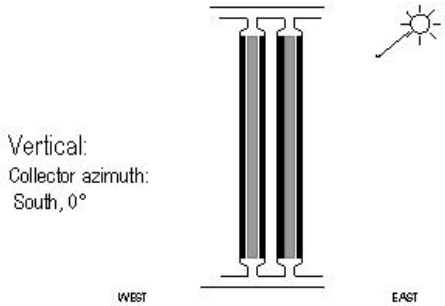

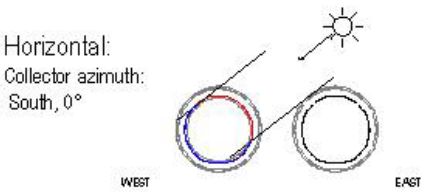

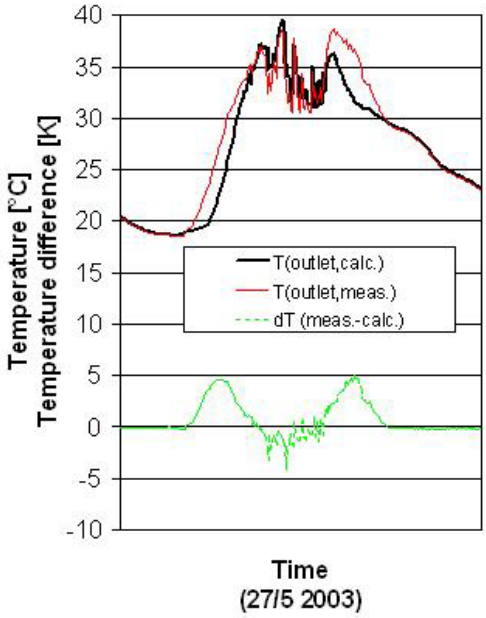

Investigations with the model

- **Vertical pipes**
- **Two locations:**
  - Ummannaq (GL, 71°N)
  - Copenhagen (DK, 56°N)
- **Expected yearly thermal performance:**
  - Optimal pipe distance
  - Optimal collector azimuth
  - Yearly thermal performance
  - Comparison with Arcon HT

Pipe distance/Collector azimuth

Copenhagen:

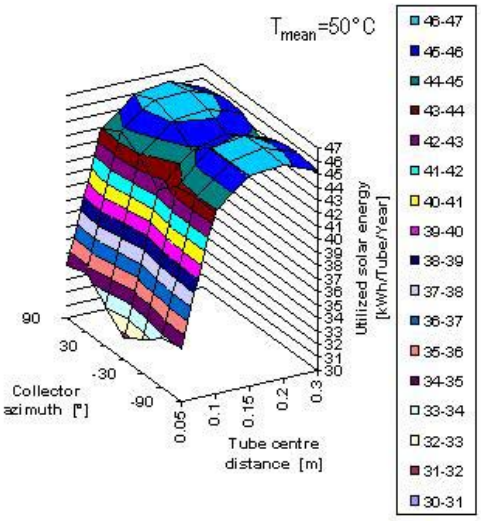

Ummannaq:

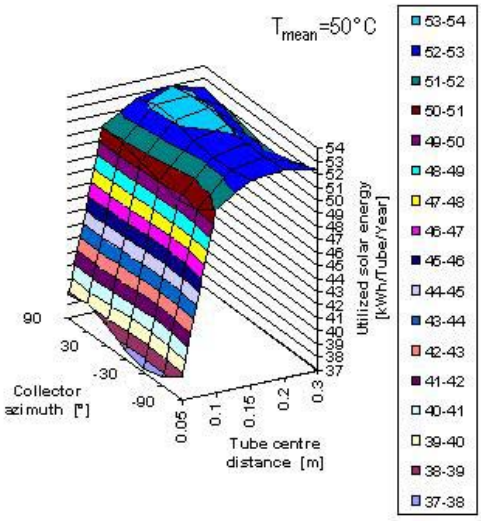

(Outer tube diameter=0.047 m)

Yearly thermal performance

based on the transparent area

Tubular collector:
Orientation: 50° west
Tilt: 0°

Arcon HT:
Orientation: 0° south
Tilt: 45°

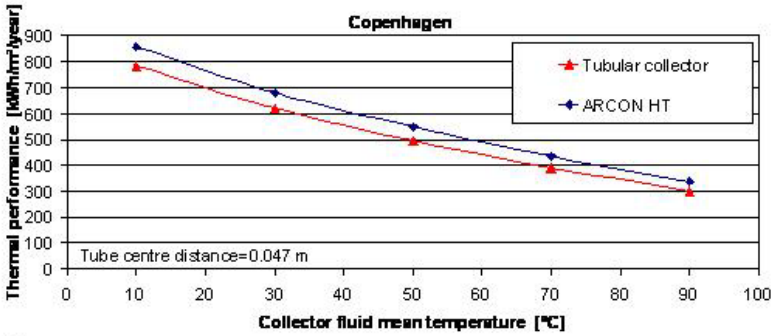

Tubular collector:
Orientation: 50° west
Tilt: 0°

Arcon HT:
Orientation: 0° south
Tilt: 60°

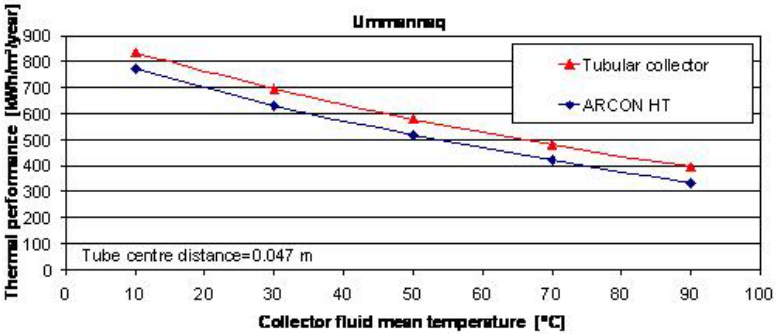

Conclusion

- **A prototype collector utilizing solar radiation from all directions has been investigated**
- **Vertical placed tubes in Copenhagen and Ummannaq have the highest thermal performance with:**
  - a tube distance of 0.2 m.
  - a collector azimuth of 45°-60° towards west.
- **Calculated yearly thermal performance:**
  - **Copenhagen:** Arcon HT best performing.
  - **Ummannaq:** Tubular collector best performing.
  - **Reason:** The tubular collector is not optimally tilted in Copenhagen and there is much more solar radiation "from all directions" in Ummannaq .
- **The collector design is very promising – especially for high latitudes.**
- **Further work:**
  - the model must be able to calculate on tilted pipes
  - the reflections between the pipes must be included in the model
  - an anisotropic diffuse sky model should be included
  - the model must be thoroughly validated with measurements.
  - more measurements
  - durability and reliability tests

Bilag 6: Overheads til foredraget ”Vakuumrørsolfangere”.

DANVAK møde: ”Solvarmeforskning på DTU”, 18/9 2003.

Vakuumrørsolfangere der udnytter solstrålingen fra alle retninger

L. J. Shah
BYG·DTU
Technical University of Denmark
Bygning 118, DK-2800 Kgs. Lyngby
DANMARK
E-mail: ljs@byg.dtu.dk

Vakuumrørsolfanger som kan udnytte solstråling fra alle retninger

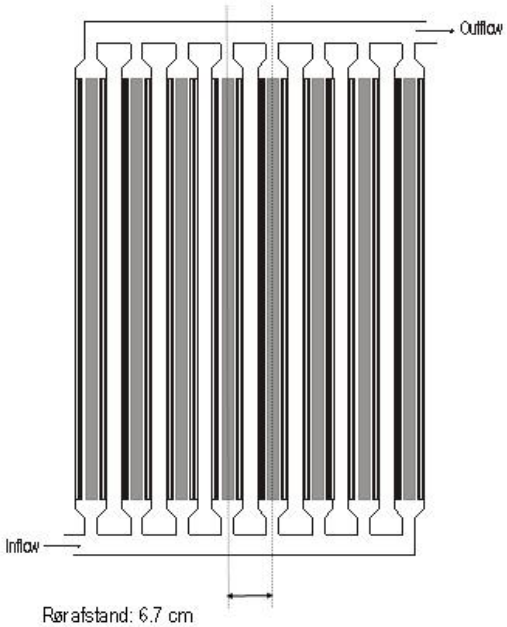

Rørafstand: 6.7 cm

Prototype solfanger

Rørets opbygning

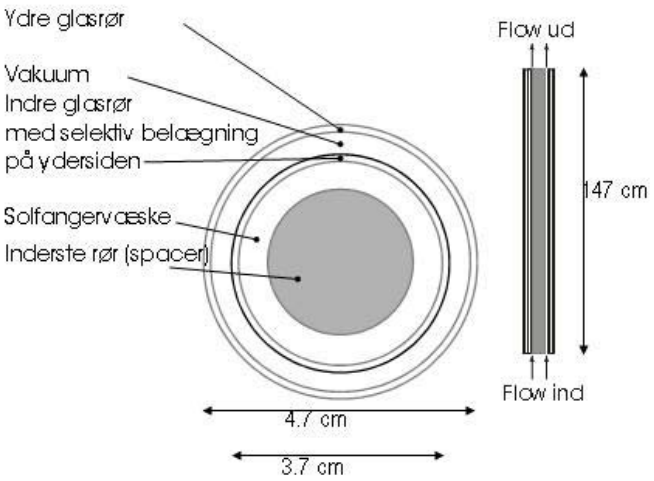

Undersøgelser

- **Teoretisk:**
  - Udvikling af en solfanger teori som kan behandle:
    - Solstråling fra alle retninger (også bag fra solfangeren)
    - Skyggeeffekter fra naborørene
    - Cylindrisk geometri i forbindelse med indfaldsvinkelkorrektioner
- **Eksperimentelt:**
  - Solfangerydelse

Teorien inkluderer:

- Vinkelforhold mellem rørene
  - som afhænger af rør diametre og rør afstand
- Vinkelforhold til himmel og jord
  - som afhænger af rørafstanden
- Udnyttet energi fra direkte stråling
  - som afhænger af skyggerne fra naborørene
- Udnyttet energi fra diffus himmelstråling
  - som afhænger af vinkelforholdet til himlen
- Udnyttet energi fra jordreflekteret stråling
  - som afhænger af vinkelforholdet til jorden og af refleksionskoefficienten
- Varmetab
  - som afhænger af varmetab fra glasrørene, manifoldrørene m.m.

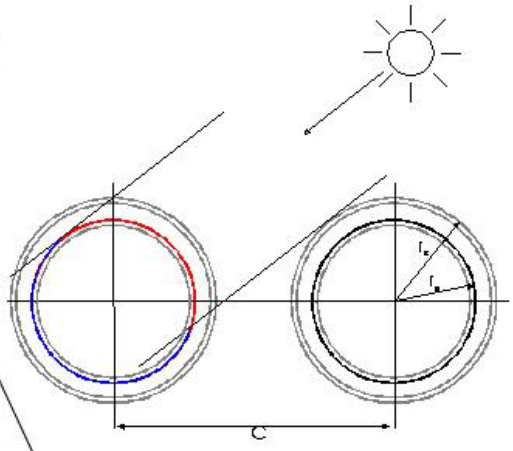

Al teorien samles i et simuleringsprogram således at den årlige termiske ydelse af vakuumrørsolfangerne kan bestemmes

Ingen teori uden målinger ...

- Solfangerydelsen blev bestemt i en udendørs prøvestand hvor følgende blev målt:
  - indløbstemperatur
  - udløbstemperatur
  - volumenstrøm
  - solstråling
  - omgivelsestemperatur

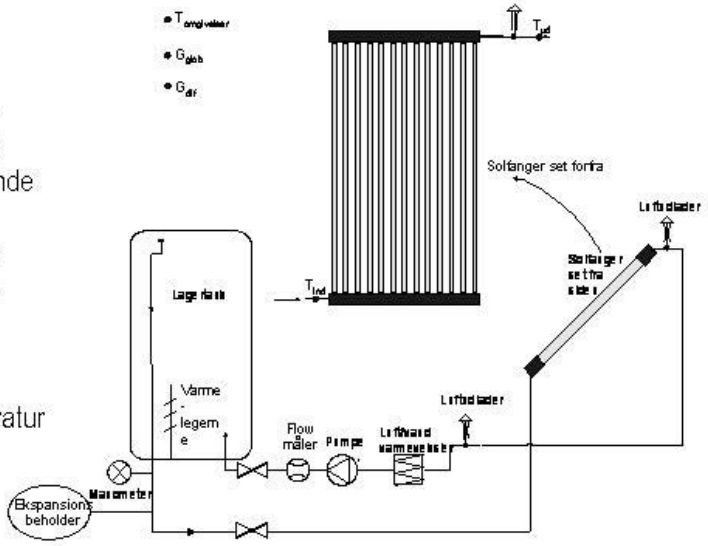

$$P_u = \dot{V} \cdot \rho \cdot C_{p,væske} \cdot \left(T_{ud,varm} - T_{ind,kold} \right) + \frac{C_{solfanger} \cdot \left(T^{t}_{middel} - T^{t-\Delta t}_{middel} \right)}{\Delta t}$$

Målinger

- Forsøgsbetingelser:
  - 2 perioder (11 dage)

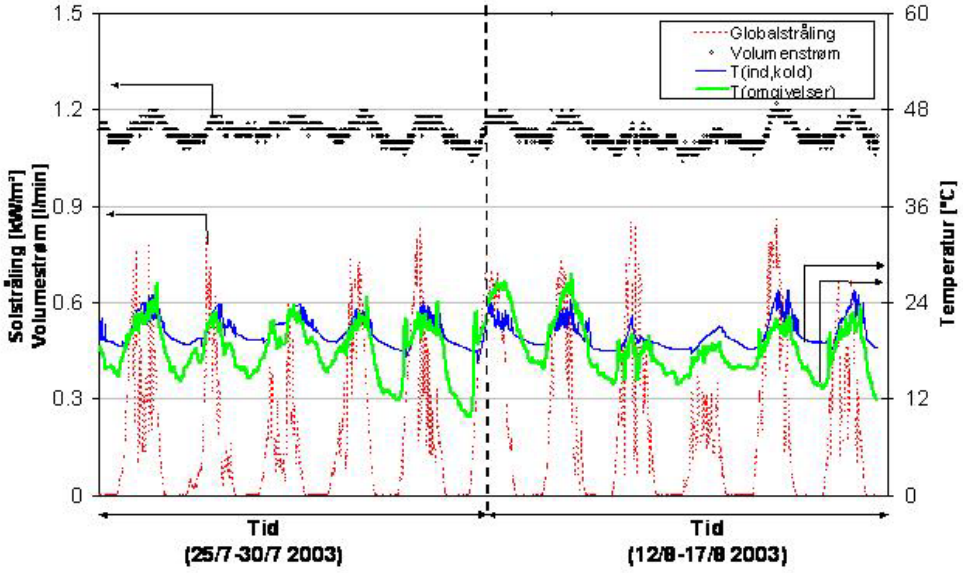

Sammenligning mellem målinger og beregninger

- **Model input:**
  - Globalstråling, diffus stråling og omgivelsestemperatur
  - Indløbstemperatur og volumenstrøm
  - Geometri, F' and $\tau\alpha_e$

Antal rør	L [m]	r_c [cm]	r_p [cm]	C [cm]	k_0 [W/m²K]	F' [-]	$\tau\alpha_e$ [-]	a [-]
14	1.47	2.35	1.85	6.7	2.09	0.98	0.856	3.6

- **Model output:**
  - Udløbstemperatur
  - Ydelse

Sammenligning mellem målinger og beregninger

- Der er en god overensstemmelse mellem målt og beregnet udløbstemperatur (og dermed også mellem målte og beregnede ydelser – mindre end 2% afvigelse)

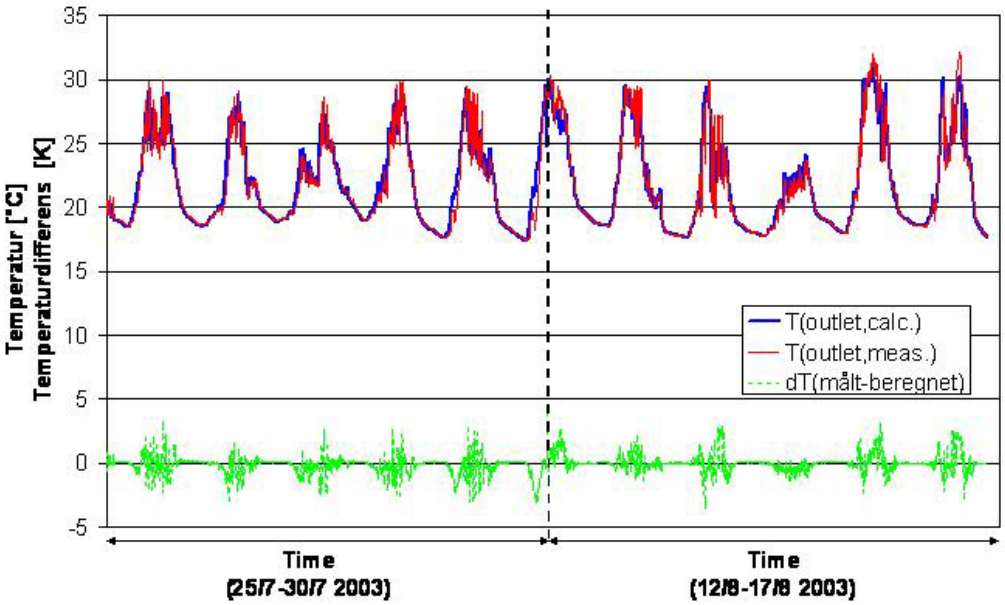

Årsberegninger med den nye teori

- **Lodrette rør**
  - Teorien gælder kun for lodrette rør
- **To lokationer:**
  - Uummannaq (GL, 71°N)
  - København (DK, 56°N)
- **Forventede årsydelser:**
  - Rør afstand
  - Solfanger azimut
  - Sammenligning med Arcon HT

Først lidt om solstråling i København og i Uummannaq

- Figuren viser summen af solstråling på forsiden og bagsiden af en lodret flade for forskellige orienteringer.
- For København er der (næsten) symmetri omkring 0° (syd).
- I Uummannaq er der et minimum omkring –30° (mod øst).
- Årsagen er at der er et bjerg øst for Uummannaq, som reducerer solstrålingen som kommer fra øst.
- Solstrålingsværdierne er højst i Uummannaq fordi det er et solrigt sted, fordi fladen er lodret og fordi der er meget sne.

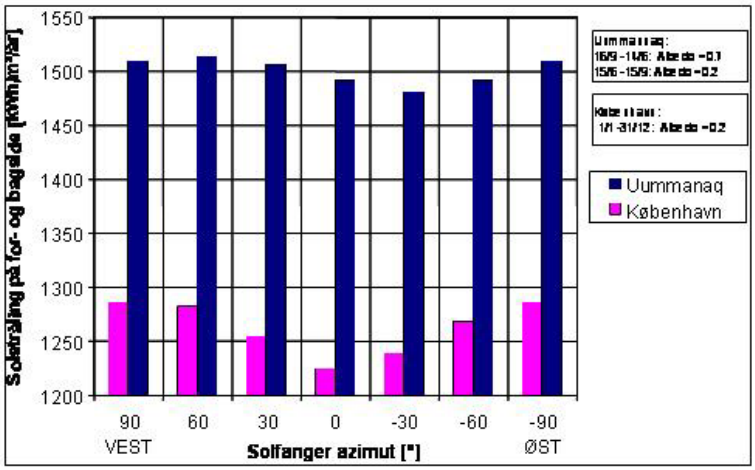

- **København: Årlig middeltemperatur: 7.8°C**
- **Uummannaq: Årlig middeltemperatur : -4.2°C**

Solfangerazimut

- **Figuren viser ydelsen pr. rør i et solfangerpanel, hvor rørafstanden er 6.7 cm (≈ 2 cm luft mellem rørene) og solfangermiddeltemperaturen er 50°C.**
- **I Uummannaq og i København, er den optimale solfangerorientering (azimut) omkring 45°-60°.**
- **Resultaterne skyldes både solstrålingsfordelingen (jf. forrige figur) og at temperaturerne er højst om eftermiddagen.**

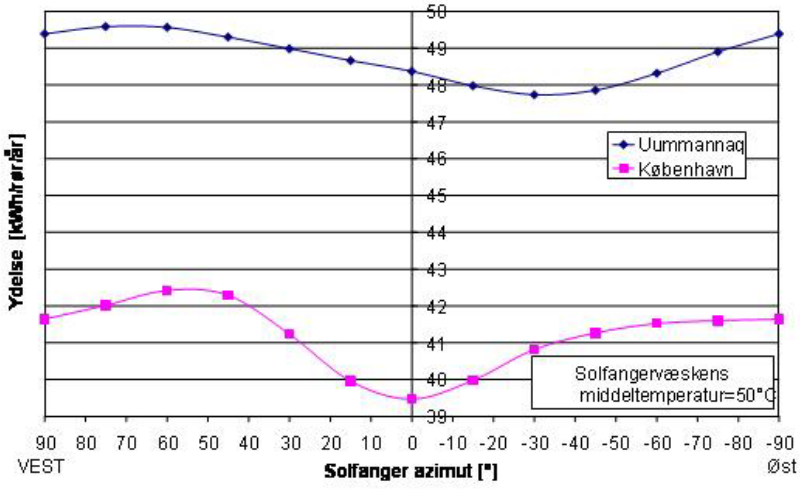

Rørafstand

- Figuren viser ydelsen pr. rør i et solfangerpanel der vender mod syd, hvor rørafstanden varieres og solfangermiddeltemperaturen er 50°C.
- Ydelsen stiger når centerafstanden øges op til 0.2 m (≈ 15 cm luft mellem rørene), hvilket skyldes at skyggerne fra naborørene mindskes.
- For endnu større afstande falder nettoydelsen igen hvilket skyldes et stigende varmetab fra manifoldrørene.

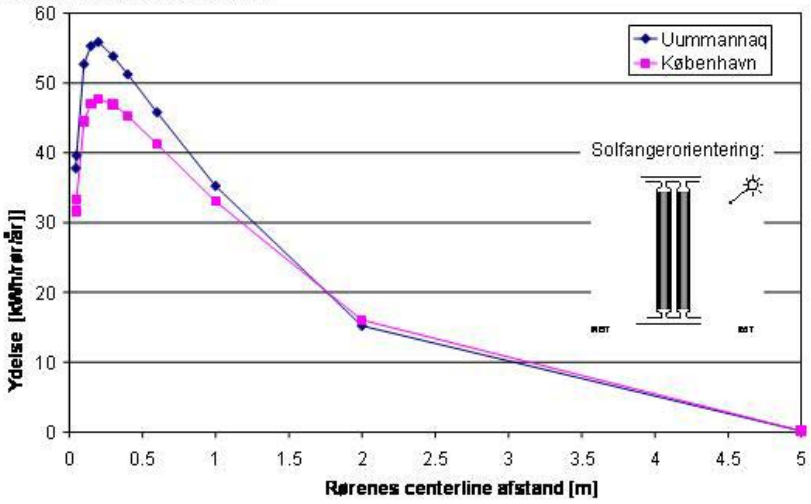

Årsydelser sml. med Arcon HT

- Figurerne viser solfangerydelsen pr. m² transparent areal som funktion af solfanger middeltemperaturen
- Vakuumrørene er placeret helt tæt op ad hinanden så det transparente areal for vakuumrørsolfangeren kan sammenlignes med det transparente areal for Arcon HT
- Arcon HT er bedst ydende i København
- Vakuumrørsolfangeren er bedst ydende i Uummannaq.
- Årsagen er at vakuumrørsolfangeren ikke er optimalt hældende i København
- Årsagen er også at der er meget mere solstråling fra "alle retninger" i Uummannaq og den stråling kan udnyttes af vakuumrørsolfangeren.

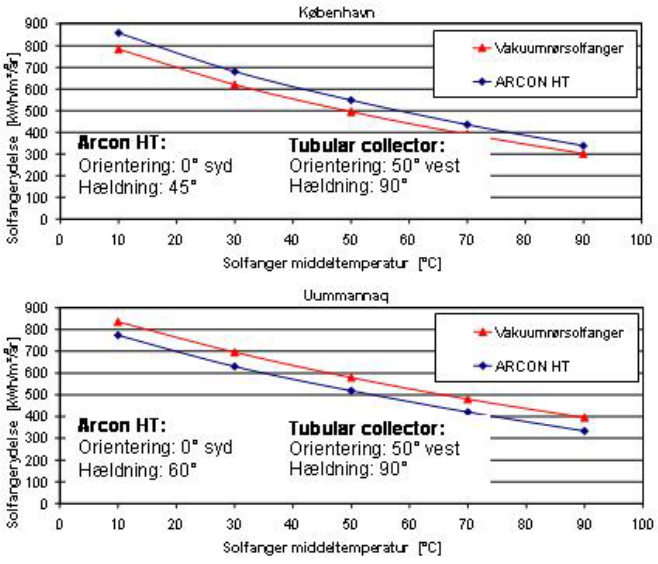

Konklusion

- **Undersøgelserne drejer sig om vakuumrørsolfangere som kan udnytte solstråling fra "alle retninger"**
- **Dertil har vi udviklet en teori for beregning af vakuumrørsolfangernes ydelse:**
  - rørafstand = 0.2 m
  - solfangerazimut = 45°-60° mod vest
- **Beregnede årsydelser viste:**
  - **København:** Arcon HT højstydende
  - **Uummannaq:** Vakuumrørsolfanger højstydende
  - **Årsag:** Årsagen er at vakuumrørsolfangeren ikke er optimalt hældende i København, og atder er meget mere solstråling fra "alle retninger" i Uummannaq og den stråling kan udnyttes af vakuumrørsolfangeren
- **Solfangerdesignet er lovende – især for nordlige breddegrader**
- **Fortsat arbejde:**
  - teorien skal udvides til at kunne tage ikke-lodrette rør i beregning
  - refleksioner mellem rørenes skal inkluderes i teorien
  - flere diffuse strålingsmodeller skal inkluderes i teorien
  - flere design skal undersøges (rørtyper, koblingsprincipper, varmevekslingsprincipper m.m.)
  - flere målinger (både i Danmark og i Grønland)
  - undersøgelser af holdbarhed og pålidelighed